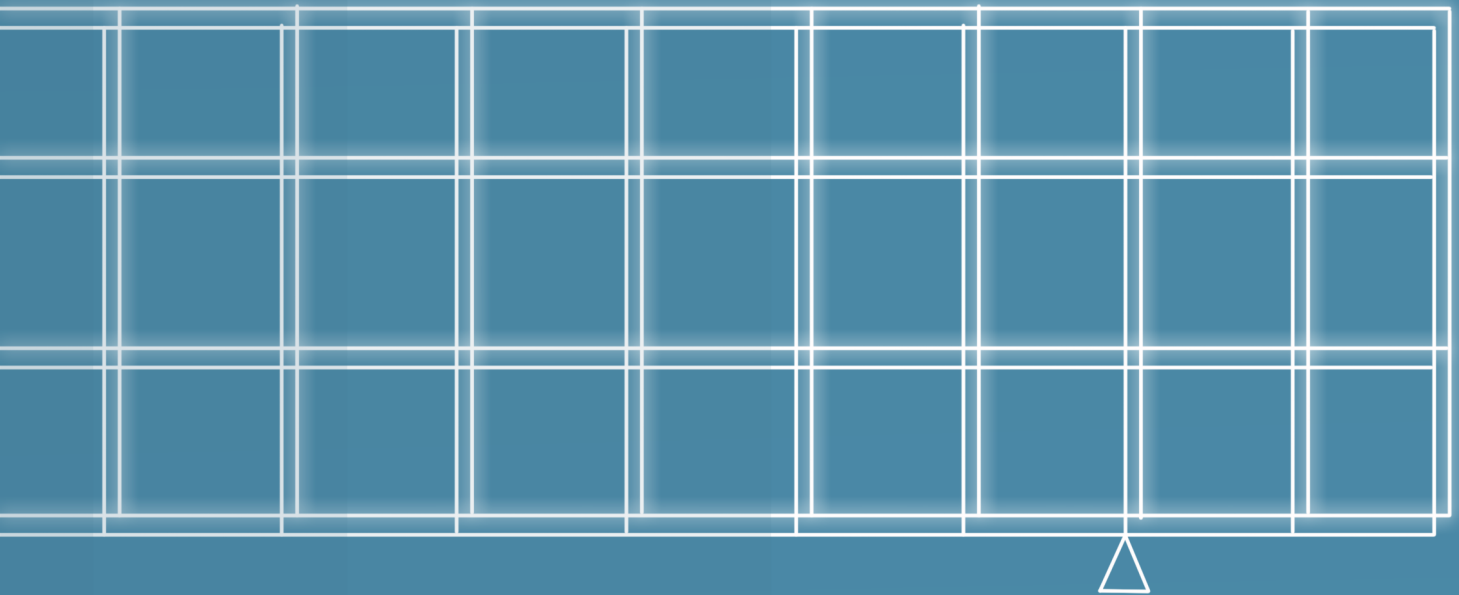# Finite Element Modelling of ASR Affected Reinforced Concrete Beams Based on Realistic Pre-damage

Xin Chen

Finite Element Modelling of ASR Affected Reinforced Concrete Beams Based on Realistic Pre-damage

Master of Science Thesis

For the Degree of Master of Science in Structural Engineering, Concrete Structures at Delft University of Technology

TUDelft

Xin Chen

October 5, 2018

Delft University of Technology
Department of
Structural and Building Engineering, Concrete Structures

The Undersigned Hereby Certify That They Have Read and Recommend to the Faculty of
Civil Engineering and Geosciences for Acceptance a Thesis Entitled

Finite Element Modelling of ASR Affected
Reinforced Concrete Beams
Based on Realistic Pre-damage

by

Xin Chen

In Partial Fulfillment of the Requirements for the Degree of
Master of Science in Structural Engineering, Concrete Structures

Dated: _____

Supervisors:

Prof. dr. ir. D.A. Hordijk

Dr. ir. M.A.N Hendriks

Dr. ir. Y.G. Yang

Ir. N.W. Kostense

Acknowledgements

First of all, I would like to express my sincere gratitude to my daily supervisor Ir. N.W. Kostense, the most humble and objective person that I have ever seen, for his patient guidance and enthusiastic encouragement.

Further, I would like to thank Dr. ir. M.A.N. Hendirks and Dr. ir. Y.G. Yang for illuminating the path whenever I was stucked in the darkness. Also, I would like to thank Prof. dr. ir. D.A. Hordijk, it is my honor to have you in my committee.

I would like to thank Dr. ir. Y.G. Yang and Ir. C. van der Vliet, who informed and introduced me about this topic so that I can work on this challenging but fantastic project.

The last but the most important, I would like to thank my friends. The time and happiness we shared is the biggest motivation on the road of my life.

Finally, I want to give the deepest love to my parents, for being my shield, so I can be the sword.

陈鑫

Rotterdam,
October 5, 2018

Abstract

A new type of finite element model, called the double mesh model is proposed in this thesis. With the level of free expansion as the input, the model is able to simulate the restrained ASR expansion by taking into account the effects of physical restraints. The retrained ASR expansion in reinforced concrete cubes and beams are simulated. Numerical expansion obtained from this new model showed a good agreement with the experiments. Then, the expanded beams are loaded in shear to simulate the shear behaviour of ASR affected concrete beams. In this new model, ASR damage is embedded through a realistic simulation of ASR expansion. Whereas, in the traditional method, ASR damage is taken into account by a direct reduction of the input material properties and the expansions are not simulated. According to the data obtained from experiments, even though the mechanical properties of concrete are reduced due to ASR, but this not necessarily leading to the decrease in the capacity of the beams. In some experiments the change of failure mode is observed where the unaffected beam failed in shear but the ASR affected one failed in bending. This is because in ASR affected beams, the increase in shear load results in the enlargement of the existing ASR cracks instead of generating new diagonal shear cracks, and thus the shear failure is prevented. In the precracking method, the effects of ASR cracks on the capacity and the failure mode are taken into account in the model since the ASR cracks are simulated. Whereas, in the traditional method, where the ASR damage is included through the reduction of the input properties, the effects of ASR cracks are not able to be reflected in the model.

Keywords: ASR, Non-linear Finite Element Method, Concrete Crack, Shear Behaviour

Contents

Chapter 1

Introduction

1.1 Background

Alkali-silica reaction (ASR) is a materials related distress that has resulted in the premature deterioration of concrete structures throughout the world.

ASR is caused by the reaction of **alkali** hydroxyl ions in cement paste and certain **siliceous** minerals found in some aggregates, together with **water** from pores. The formed alkali-silica gel tends to swell when exposed to moisture. The expansion will be confined in pore structure of concrete thus leading to internal pressures and the formation of cracks. As a consequence, the concrete will expand and its mechanical properties will degrade.

From the standpoint of structural performance, ASR is one of the major causes of deterioration in concrete structures around the world. The structures at high risk of ASR problems are those exposed to wet environments because one requirement for expansive ASR to occur is moisture. The deterioration, including expansion, cracking and reduction in engineering properties, of concrete causes premature distress in concrete structures such as dams, bridges and nuclear reactors.

ASR induced expansion is confined by internal and external restraints. Reinforcement is a typical internal restraint. The externally applied stresses are categorized as external restraints. For a typical reinforced concrete beam, the reinforcement is placed longitudinally at the bottom part of the beam. In this longitudinally reinforced beam, the ASR expansion in the longitudinal direction is less than in the transverse direction since the longitudinal expansion is restrained by the reinforcement. The external restraints have a similar effect. For instance, a plain concrete beam is loaded in compression in one direction. The ASR expansion in the compressed direction is less than in the other directions since the expansion is confined by the compressive stresses.

Due to the effects of the restraints, the ASR induced expansion is not uniformly distributed in the volume of the structure. Since the ASR damage is associated with the expansion: the larger the expansion, the more severe the damage, the residual properties in ASR affected concrete beams are therefore not uniform either, and it is actually more accurate to describe the material properties as anisotropic.

Mechanical properties such as tensile strength, compressive strength, and Young's modulus are reduced due to ASR. The reduction of mechanical properties result in a decrease in the structural performance of concrete members, in terms of both capacity and durability. However, this is not always the case. For instance, experiments found that in some reinforced concrete beams, the shear capacity increases when the beam is suffered by ASR. Apart from the degradation on mechanical properties of ASR affected concrete. Some papers also reported that the presence of ASR cracks may change the crack pattern and failure mode in a reinforced concrete beam.

The effects of ASR on reinforced concrete beams are complicated. To achieve a comprehensive simulation, accurate capture of anisotropic residual properties and the effects of ASR cracks are of

great importance. Traditionally, the finite element modelling of ASR affected structures uses isotropic material models and the ASR damage is taken into account by directly using the residual material properties as the input properties. In this way, the anisotropic residual properties in ASR affected structures are not correctly reflected, and the change of crack pattern and failure mode are not able to be presented either. In this thesis work, a new finite element model, namely the double mesh model, is proposed. In the double mesh model, ASR damage in concrete elements are embedded through the expansion of the fictitious elements. The expansion takes into account the effects of reinforcement. Therefore, the anisotropic residual properties are achieved and the change of crack pattern and failure mode due to the presence of ASR cracks are able to be simulated.

1.2 Research Questions

Research questions are distinguished into two parts, as shown in Figure 1.1. One part of the questions are related to the effects of ASR to concrete structures observed from experimental research. The questions will be answered through a literature study. The other part of the questions are related to the FE-modelling of ASR. This part focus on how to take the effects of ASR observed in experiments into account in the FE-model.

Research Questions related to ASR facts:

- What are the effects of restraints on ASR expansion?
- What are the effects of ASR on the mechanical properties of concrete?
- What are the effects of ASR on the structural behaviour of reinforced concrete beams?

Research Questions related to FE-modelling of ASR:

- How can the model take into account the effects of restraints on ASR expansion?
- How can the model take into account the effects of ASR on mechanical properties?
- How can the model take into account the effects of ASR on structural behaviours?
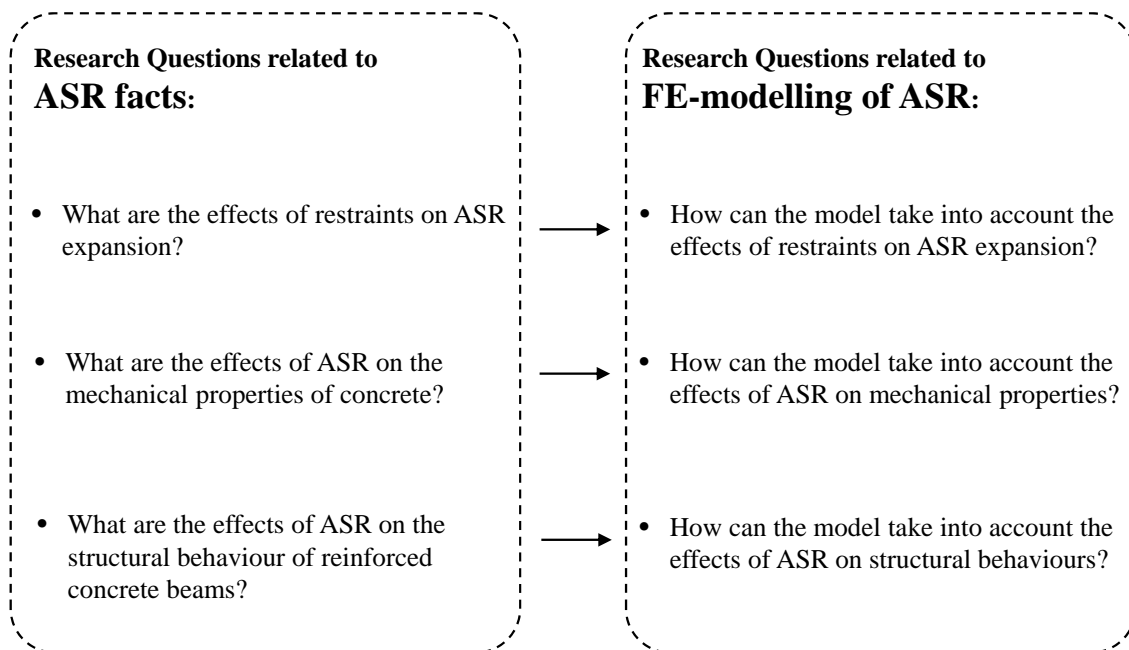
Figure 1.1: Research questions

1.3   Research Methodology

Depending on the manner of taking into account the ASR damage in the FE-model, two methods are investigated in this thesis, namely the precracking method and the traditional method. A brief introduction of these two methods are illustrated below.

The precracking method

In the precracking method, the restrained ASR expansion and concrete degradation are simulated through a so-call double mesh model. As its name described, there are two sets of mesh in the double mesh model: structural mesh and shadow mesh. Shadow mesh is a fictitious mesh used to simulate the ASR expansion. Strain at the level of free expansion is applied on the shadow mesh. The expansion of shadow mesh results in the expansion of structural mesh. By including the effects of restraints from the structural mesh, the input expansion in shadow mesh is a uniform free expansion, but the final deformation in structural mesh is a non-uniform restrained expansion. The structural mesh has the nonlinear material properties of concrete. Consequently, the expansion in structural mesh will result in the reduction of mechanical properties because of the cracking of concrete. In the precracking method, the ASR damage is embedded through a realistic simulation of ASR expansion. Due to the fact that ASR expansion is not uniform across the structure, this method is able to achieve anisotropic residual material properties.

The expansion in the structural mesh is dominated by the properties of the shadow mesh. The properties of shadow mesh need to be decided for simulating ASR expansions. For the practical reason, shadow mesh is assigned with elastic material model in this thesis work.

The traditional method

In the traditional method, ASR damage is taken into account by directly applying the residual material properties that measured from ASR affected concrete as the input. ASR expansion and cracks are not simulated in this method. Due to the used concrete material model is an isotropic material model, the resulted residual material properties are isotropic as well. Table 1.1 shows a comparison of the traditional method and the precracking method.

Table 1.1: A comparison of the traditional method and the precracking method

	Traditional method	Precracking method
FE-models	The normal FE-model	The double mesh model
ASR damage	ASR damage is taken into account by a direct reduction of the input material properties	ASR damage is taken into account by simulating the ASR expansion and deterioration of concrete
ASR induced expansion	Not simulated	Simulated
ASR induced cracks	Not simulated	Simulated
Material properties after inducing ASR damage	Isotropic	Anisotropic

About material properties used for FE-modelling

Depending on the degree of damage, three levels of material properties are distinguished. Material properties of level I represents the virgin properties measured from ASR unaffected concrete. Level II represents the residual properties measured from ASR affected concrete. Level III represents the residual properties that estimated based on the lower bond curve provided by ISE (1992). This curve describes the relation between the lower bond value of the residual properties of ASR affected concrete and its expansion. The residual properties can be estimated once the expansion is known. Since the residual properties estimated based on this curve is a lower bond value, the residual properties obtained from level III is usually lower than level II.

The use of level I, II and III has different purposes. Level I representing the virgin properties, it is used for simulating of ASR unaffected concrete beams. Level II and level III represent the residual properties of ASR affected beams. They are used for simulating ASR affected concrete beams. The difference is that, the residual properties of level II represents the real reduction in that specific case, so that the numerical results obtained from level II are compared with the experimental results.

However, the residual properties of level III are estimated based on the expansion. The use of level III is to study the possibility of simulating the ASR affected concrete beams when the expansion is known but the residual properties are unknown. Because in practice, measuring expansion is much easier than testing the residual concrete properties. Also, the residual properties of level III are the lower bond values,so it gives a more conservative prediction. Table 1.2 briefly concludes the different levels of the material properties used for FE-modelling.

Table 1.2: The different levels of material properties used for FE-modelling

Material properties	Description	Purpose
Level I	Measured from ASR unaffected concrete	To simulate ASR unaffected concrete beam
Level II	Measured from ASR affected concrete	To simulate ASR affected concrete beam when the residual properties are known
Level III	Estimated based on the expansion according to lower bond curve	To simulate ASR affected concrete beam when the residual properties are unknown

The degree of damage:
Level I (Virgin, No damage) > Level II > Level III

1.4 Thesis Layout

As shown in Figure 1.2, this thesis report includes 7 chapters. As a guide for the readers, a brief introduction of each chapter is provided here.
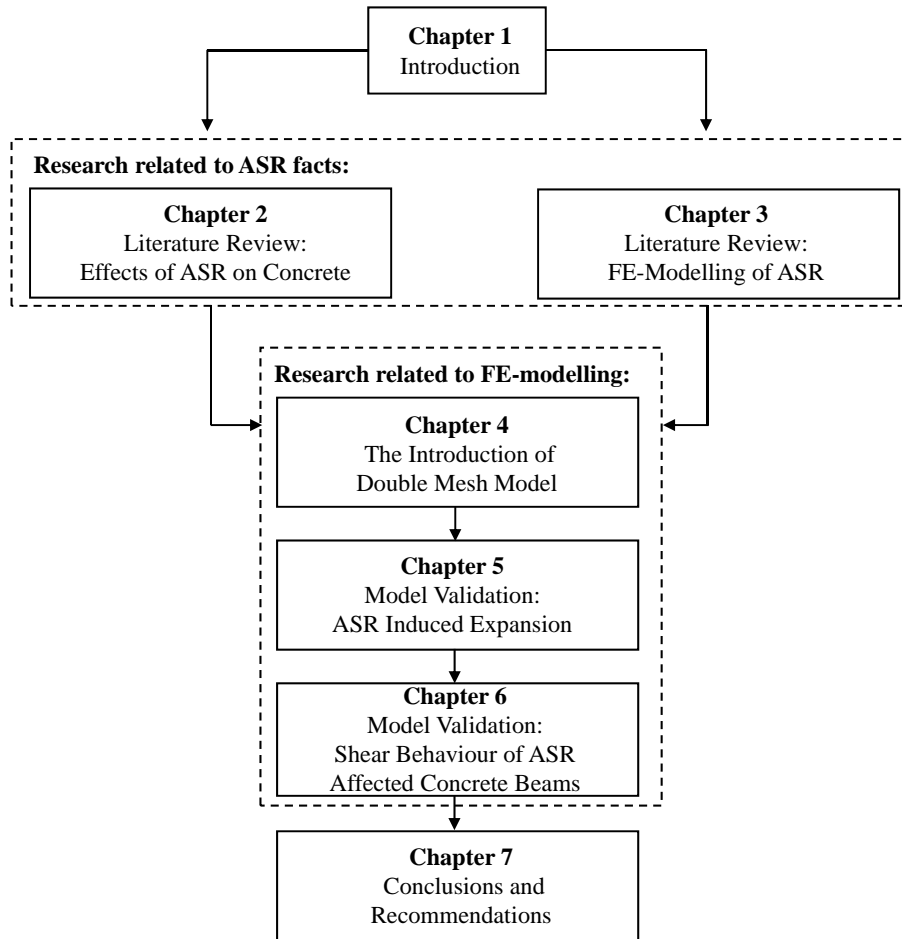

Figure 1.2: Thesis layout

Chapter 1 gives an overview of this thesis work.

Chapter 2 and 3 are related to the state of the art of the effects of ASR on the reinforced concrete beams. Chapter 2 focus on the effects of ASR from an experimental point of view. Chapter 3 concentrates on the finite element modelling of ASR affected concrete structures.

Chapter 4, 5 and 6 are related to the numerical research. In chapter 4, a new FE-model, namely the double mesh model, is proposed. The theory of this model is stated and an elementary test is performed in this chapter. Chapter 5 is about the simulation of ASR expansion. Chapter 6 utilize the conclusions obtained from chapter 5 to further link the ASR expansion to property reduction . In this chapter, the ASR-damaged beam is loaded in shear to analyse the shear behaviour. The numerical results are compared with experimental results. Also, the results obtained from the proposed FE-model are compared with the results calculated form the traditional FE-model.

Chapter 7 gives the final conclusions and recommendations of this thesis work.

Chapter 2

Literature Review: The effects of ASR on concrete

In this chapter, the effects of ASR on concrete expansion and the resulting degradation is reviewed. ASR induced expansion, from a physical point of view, can be distinguished as free expansion and restrained expansion. Free expansion (also referred as unrestrained expansion or swelling) of concrete means a concrete member expands without restraints, otherwise, it is called restrained expansion. Restraints can be divided into internal restraints and external restraints. Reinforcement is a typical internal restraint and the applied stress is categorized as external restraints. Whenever discussing the ASR induced degradation, one should distinguish the difference between the mechanical properties of concrete and the structural behaviours of concrete members. Studies indicated that when a concrete member is suffer by ASR, the mechanical properties of concrete, such as tensile strength, compressive strength and Young's modulus always decreases. However, the structural behaviours, such as the flexural and shear strength are not necessarily reduced. Figure 2.1 shows the layout of this chapter.
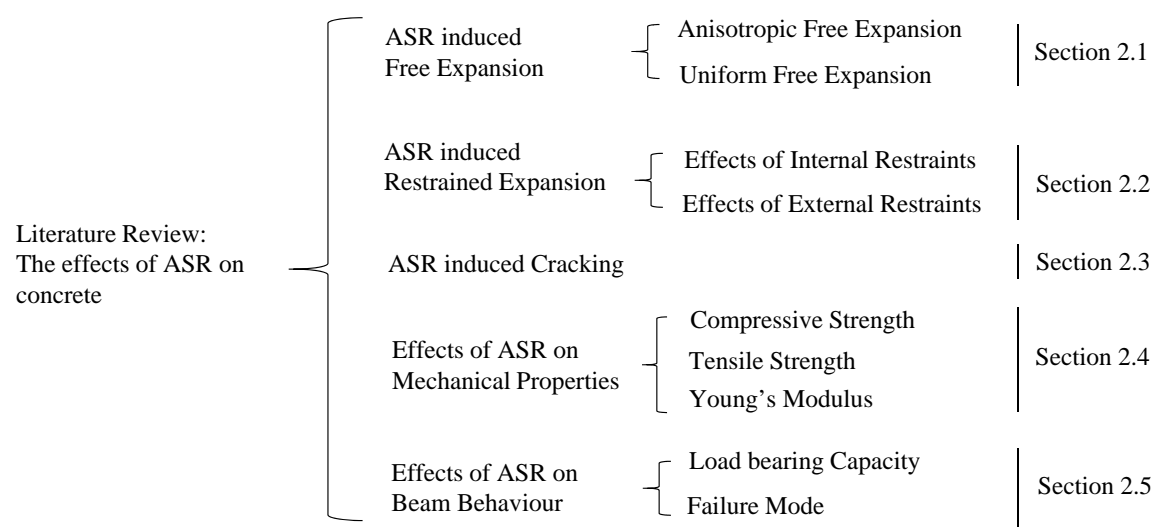
Figure 2.1: Layout of this chapter.

2.1 ASR Induced Free Expansion

2.1.1 Anisotropic Free Expansion

Smaoui et al. (2004) studied the behaviour of the free expansion induced by ASR. The studies demonstrate that the ASR expansion is always higher in the direction perpendicular to the casting plane. A part of the experiment is shown in Figure 2.2. The experiment consists of cylinders cast vertically, prisms cast vertically and prisms cast horizontally. As can be seen from Figure 2.2, it clearly shows that ASR expansion is much higher in the direction perpendicular to the casting plane, and this holds for all three cases.
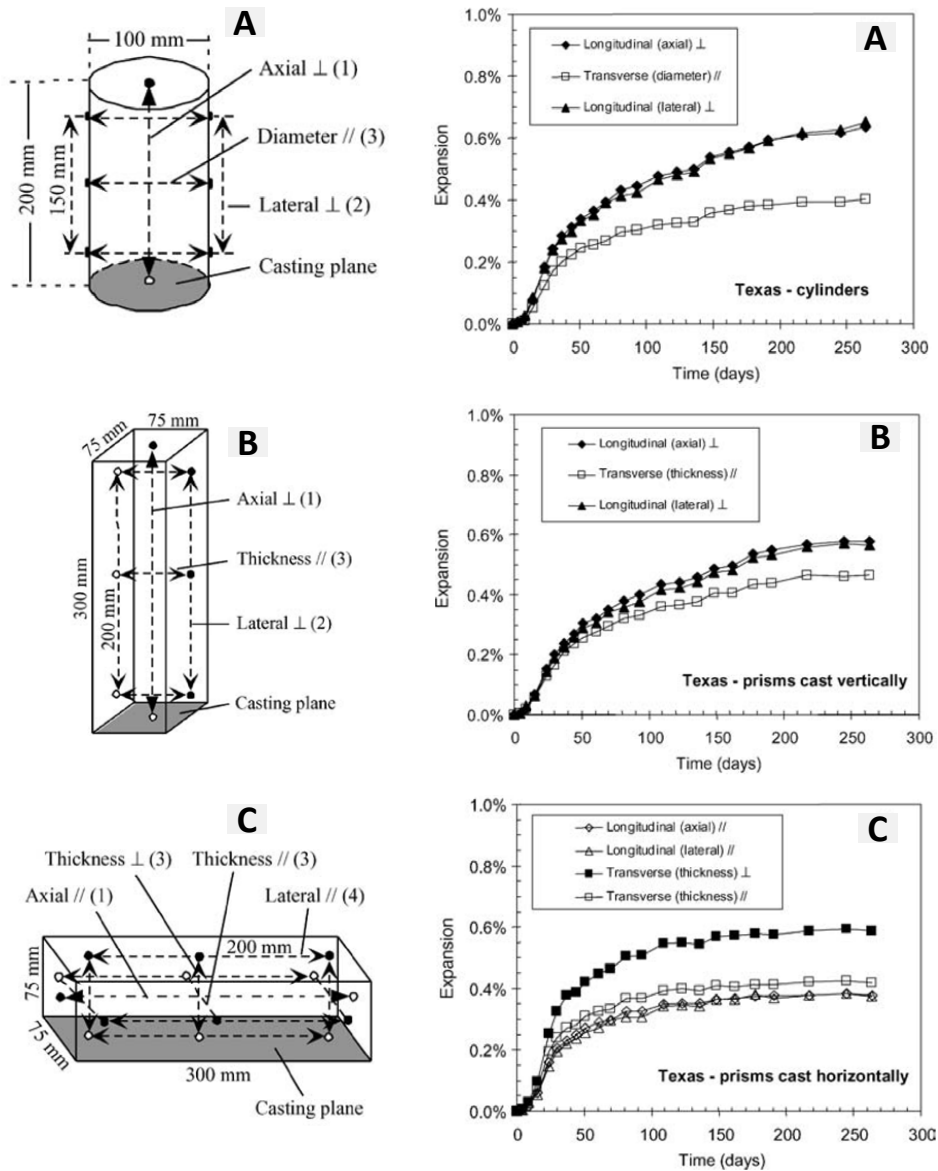

Figure 2.2: Experiment layouts and the corresponding results collected from Smaoui et al. (2004). Cylinders and prisms made with the Texas sand and consolidated using a vibrating table. A) Cylinders cast vertically. B) Prisms cast vertically. C) Prisms cast horizontally. (//: measurement parallel to the casting plane; ⊥: measurement perpendicular to the casting plane).

According to Larive et al. (2000), such behaviour could be related to the presence of a water film under the aggregate particles along the casting plane, and this behaviour would be increased in the presence of flat or elongated aggregate particles. This assumption has been validated by Smaoui et al. (2004), who explained that flat and elongated particles are more likely to orient themselves parallel

to the casting plane and to trap a relatively larger quantity of water under them. They also concluded this behaviour as the intrinsic anisotropy of ASR expansion.

2.1.2 Uniform Free Expansion

Recent experiment performed by Wald et al. (2017) and experiments conducted by Fan and Hanson (1998), and Mohammed et al. (2003) did not observe this intrinsic anisotropy. Even though one of the case from Wald et al. (2017) shows a higher expansion in the direction perpendicular to the casting plane, the authors stated that the casting direction does not play any major role in the measured differences, but no further explanation was given. A possible reason for the contradictory conclusion could be the high variability of this type of experiment due to the Heterogeneity of concrete.

2.2 ASR Induced Restrained Expansion

2.2.1 Influence of Internal Restraints

According to ISE (1992), the effects of reinforcement restraint in terms of expansion and induced stresses are:

- The restrained expansion is reduced from the free (unrestrained) value.

- The reinforcement is stressed in tension.

- The concrete is stressed in compression parallel to the reinforcement.

2.2.1.1 Restrained Expansion in Concrete

The available test data collected from Hobbs (1988), Hanshin (1986), Kobayashi et al. (2013), Cope (1993), Koyanagi et al. (1992), Takemura et al. (1989) is shown in Figure 2.3. Vertical axis is the ratio between restrained expansion and free expansion. Horizontal axis represents reinforcement ratio. It can be seen from Figure 2.3 that the presence of reinforcement can effectively reduce ASR expansion, and the more the reinforcement, the greater the reduction. The restrained expansion is very sensitive to the reinforcement ratio when the amount of reinforcement is small. Even a small percent of reinforcement significantly reduces the ASR expansion. However, the scatter of data is wide. For instance, for a reinforcement ratio of 0.5%, the ratio between restrained and free expansion varies from 0.2 to 0.8 from one study to another. A possible reason for this highly variable data could be that the nature and degree of reactivity of the aggregates can also strongly affect this ratio, as explained by Smaoui et al. (2007).

However, there are still some exceptions. Wald et al. (2017) observed approximatly the same amount of reduction when the reinforcement ratio changes from 0.5% to 1.1% and 1.5%, and concluded that the reinforcement ratio did not significantly influence expansion behavior. Mohammed et al. (2003) declared that it is not the reinforcement ratio that affects the expansion, but the degree of restraints. (The degree of restraints here means the extent of bond between concrete and steel.)

Wald et al. (2017) and Mohammed et al. (2003) also measured the expansion that perpendicular to the restrained direction. Test data indicate that the expansion perpendicular to the restrained direction is always larger than the free expansion, and the free expansion is always larger than the restrained expansion.
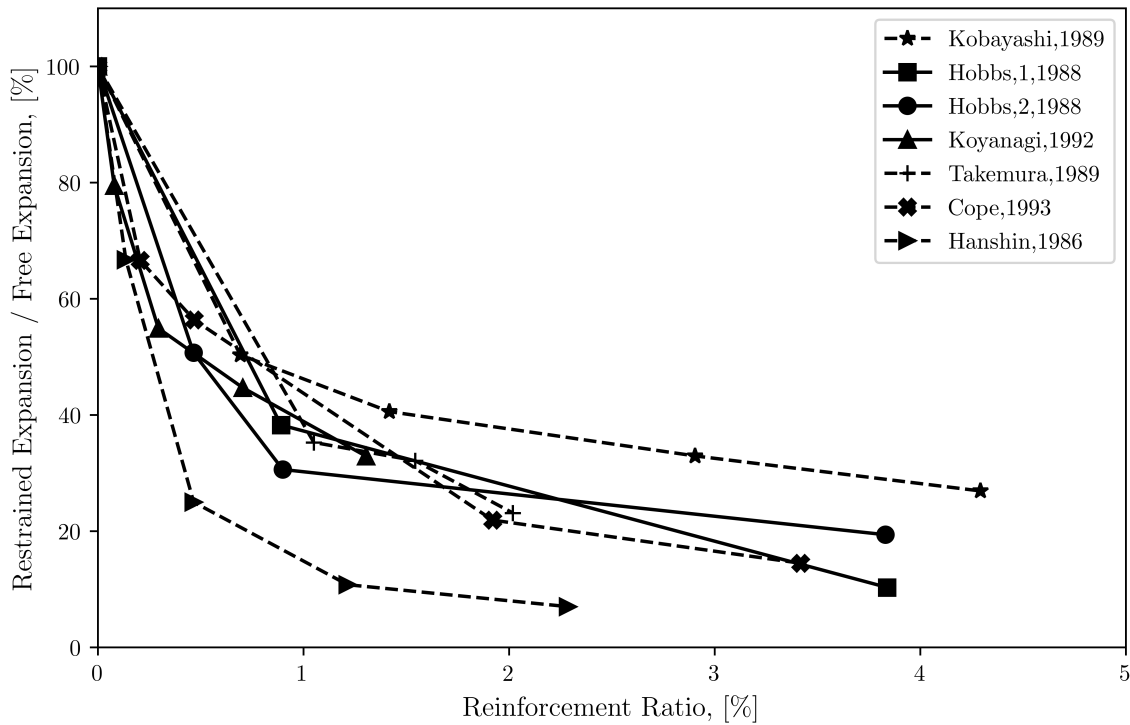
Figure 2.3: Relation of reinforcement restraint and expansion

2.2.1.2 Induced Tension in Reinforcement, Bonding

ASR loads reinforcement in tension, and the higher the percentage of reinforcement, the lower the deformation in the rebars. ISE (1992) indicated that the steel is likely to yield when the steel percentage is less than about 1.6% and 0.9% for mild and high yield steel respectively. Smaoui et al. (2007) and Mohammed et al. (2003) observed the yielding of steel in ASR affected concrete.

The debonding might take place when the expansion reaches a significant level. Experiment from Smaoui et al. (2007), for seven concrete blocks out of 15 in total, the deformation measured from reinforcement is lower than that measured from concrete, thus indicating the debonding between the rebars and concrete. Such debonding also observed by Mohammed et al. (2003) and Fan and Hanson (1998). However, it should be noted that in all those three papers, the expansion of concrete is measured from the surface, instead of the surrounding area of the reinforcement.

2.2.1.3 Induced Compression in Concrete

In reinforced concrete, ASR induces tensile stresses in the reinforcement, accompanied by the compressive stresses in the surrounding concrete. This prestress is highly variable but generally limited to 4 MPa as suggested by ISE (1992). Several studies indicated the positive effects of this so-call "chemical prestress" induce by ASR. Further details about this will be discussed in chapter 3.

2.2.2 Influence of External Restraints

External restraints arising from applied stress has a similar effect to internal reinforcement restraint. Available data collected from Cope (1993), Chana and Korobokis (1991), Ng (1991), and Clayton et al. (1990) is shown in 2.4. The data are obtained from specimens under uniaxial constant compressive stress. It clearly shows that the applied stress dose have a significant influence on ASR expansion. The higher the applied stress, the more the expansion is reduced.

It should be noted that Figure 2.4 only indicates that compressive stress reduces expansion in the direction of the stress. Will the compressive stress affect the expansion in other directions, the test
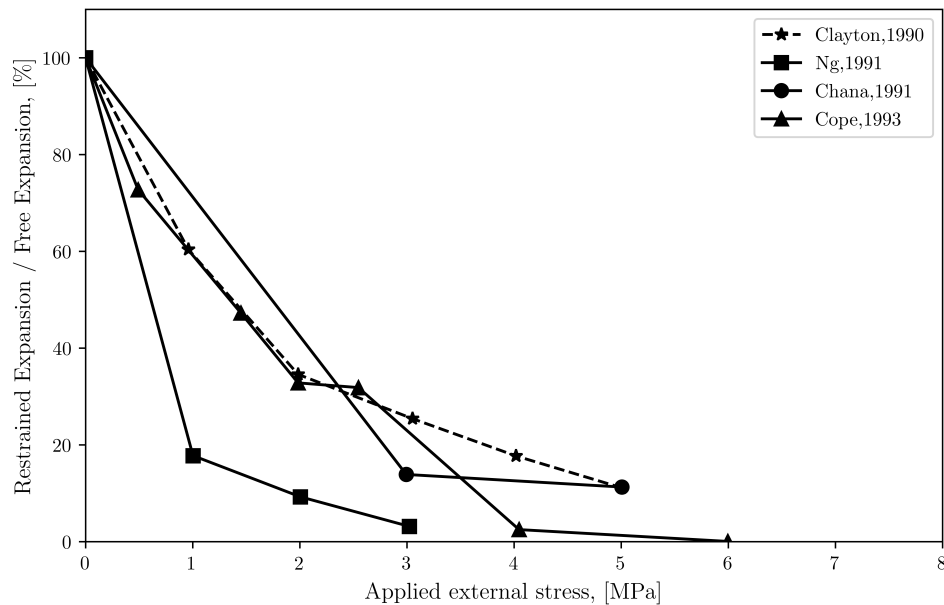
Figure 2.4: Relation of applied stress and expansion

data does not give a clear indication. Also, contrary to compressive stress, a tensile stress increases expansion, but few data are available.

2.3 ASR Induced Cracking

According to ISE (1992), ASR induces **micro-cracks** inside of the concrete and **macro-cracks** at the surface. The micro-cracks within a mass of unrestrained concrete are orientated randomly. The combination of variability of expansion and greater expansion of interior concrete results in tensile strain at the surface, which can develop into macro-cracks.

- In unrestrained concrete, the pattern of macro-cracks is irregular with intersecting and bifurcating cracks which often referred to "map cracking".

- In restrained concrete, the macro-crack tends to be parallel to the direction of the restraint.

Typical cracking patterns obtained by Fan and Hanson (1998) is collected in Figure 2.5. It shows the cracking patterns of plain concrete (left) and horizontally reinforced concrete (right) after 4, 5, 6, 12 months in alkali solution. The patterns on the left side, representing cracking patterns of plain concrete, illustrate the map cracking that usually can be seen in unrestrained concrete members. The right four concrete members are restrained by longitudinal reinforcement on both top and bottom side, and it can be seen that most of the cracks are orientated parallel to the reinforcement.

Another example is given by ISE (1992), shown in Figure 2.6. The upper beam has only bottom reinforcement, and the map cracking can be seen in the unreinforced top region of the beam. In contrast, the lower beam has equal top and bottom reinforcement and the cracks are parallel to the main reinforcement. It also observed that, a hogging curvature can be observed when the reinforcement on the top and bottom side is not equal.
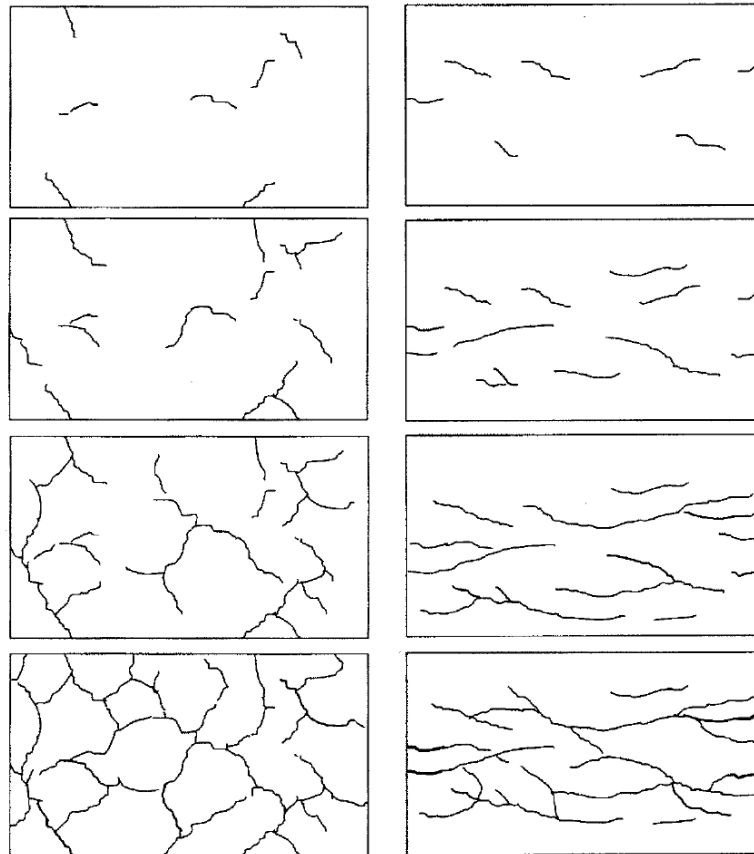
Figure 2.5: Cracking patterns of plain concrete (left) and horizontally reinforced concrete (right) after 4, 5, 6, 12 months in alkali solution, adopted from Fan and Hanson (1998)
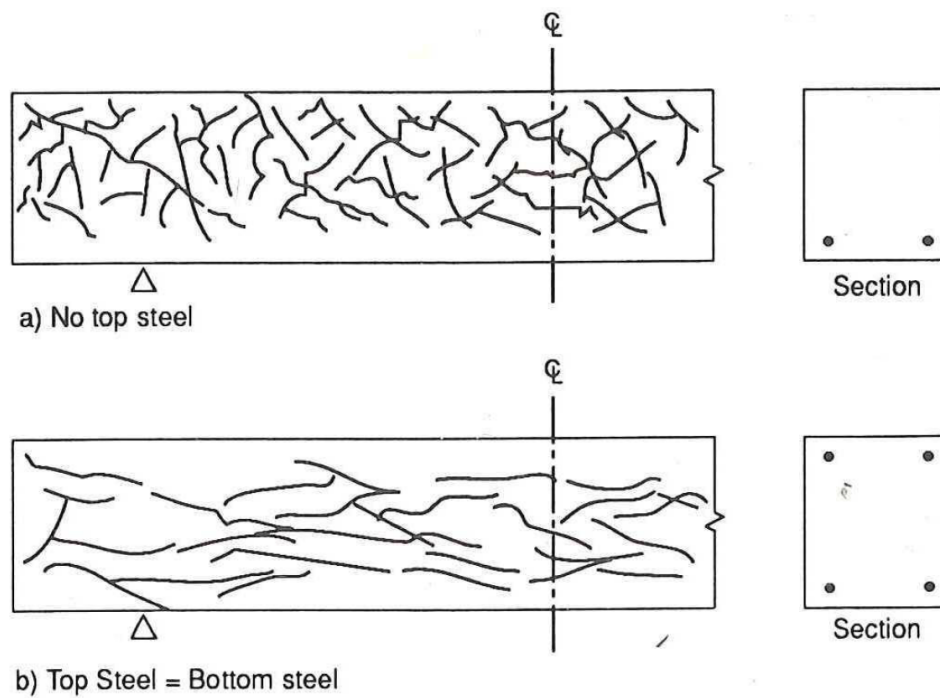

Figure 2.6: Influence of reinforcement on ASR cracking, adopted from ISE (1992)

2.4 Effects of ASR on Mechanical Properties

Mechanical properties measured on unrestrained concrete specimens generally show a reduction in compressive strength, tensile strength, and Young's modulus in ASR affected concrete. The degree of reduction depends on the the degree of expansion. Generally, studies found that the reduction in Young's modulus is the most severe one, followed by the tensile strength, and the compressive strength has the least reduction. Whereas, it should be noted that due to the randomness of ASR expansion, the measured residual mechanical properties in ASR affected concrete usually accompanied by high variabilities.

As for the tensile strength, Den Uijl and Kaptijn (2002) stated that the direct tensile strength in ASR affected beam is smaller than the splitting tensile strength. The reason comes from the difference between the direct tensile strength, which reflects the strength of the weakest section, and the splitting tensile strength, which gives the strength at the section where the splitting force is applied. However, based on the data collected by Esposito et al. (2016), such difference between direct tensile strength and splitting tensile strength in ASR affected concrete is not observed.

Experiments also found that the uniaxial compressive strength as obtained from a long cylinder or core test is reduced by ASR to a greater extent than is the cube strength. It is the uniaxial compressive strength which is required for structural assessment.

Figure 2.7 demonstrates the residual mechanical properties of unrestrained ASR affected concrete as percentages of the properties of unaffected concrete. Lines with two categories are indicated in Figure 2.7. One is the lower bond value of residual mechanical property obtained from ISE (1992), and the other one is the curve fitting value obtained from Esposito et al. (2016).

It is emphasised that the residual strengths and stiffnesses in actual structures will be modified from the values shown in Figure 2.7. This is because the concrete in actual structures is generally restrained by adjacent material and is in a biaxial or teiaxial stress state. These effects will tend to reduce the damage to the concrete and increase its residual mechanical properties.
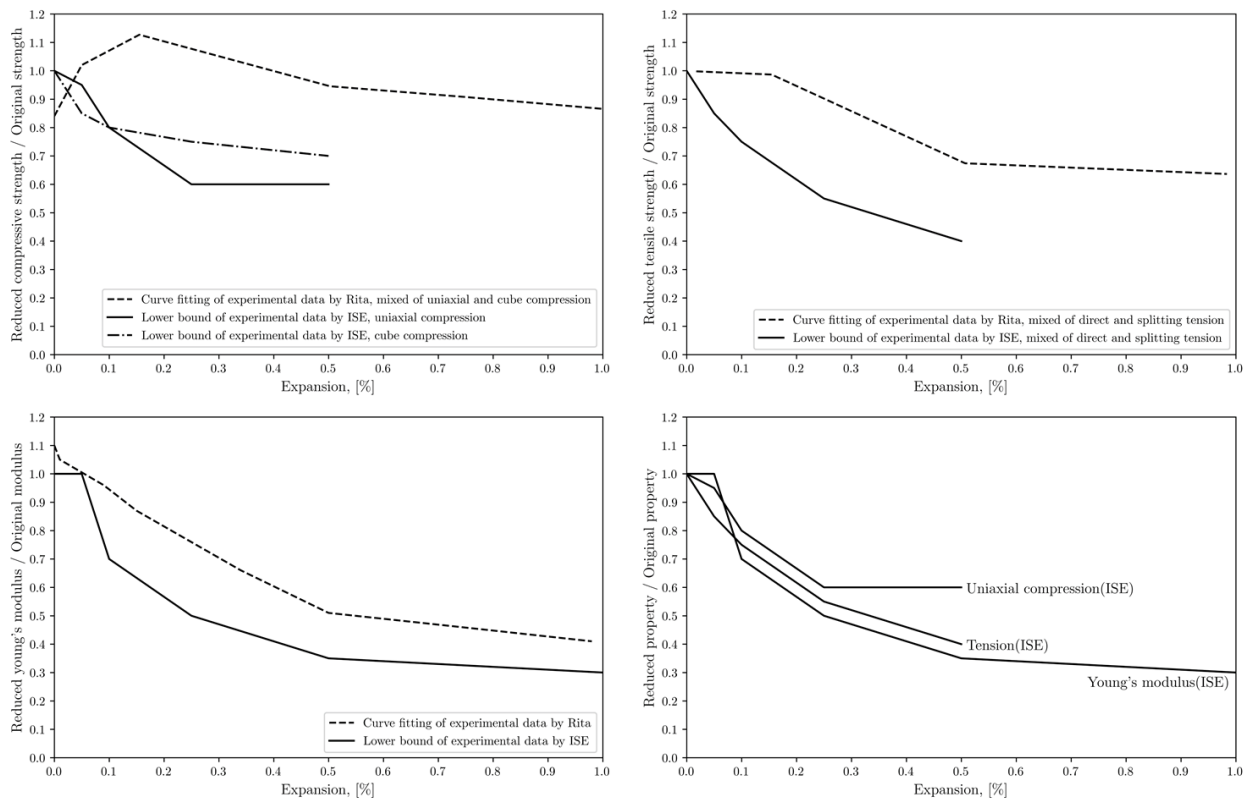

Figure 2.7: Reduction of mechanical properties, adapted from Esposito et al. (2016) and ISE (1992).

13

2.5 Effects of ASR on Beam Behaviour

Literatures related to the ASR affected concrete beams are reviewed in this section. The attention is paid on the change of loading capacity, failure mode and crack pattern due to ASR. A brief description of each reviewed literature is given below, followed by table 2.1 which gives a collection of all the reviewed papers and a discussion cross these papers.

Abe et al. (1989) investigated the influence of ASR on the flexural yield strength and the ultimate shear strength of reinforced concrete beams. The parameters in this experimental study are the tension reinforcement ratio and the degree of deterioration due to ASR. It is found that, as the longitudinal expansion increases, the yield strength was slightly reduced and the deflection at yield strength decreased dramatically. According to their experimental results, the ultimate shear strength of affected specimens was slightly higher than that of unaffected specimen, and the affected specimens failed in shear showed a better deformability. The change of failure mode was observed in Series AIII, as shown in Figure 2.8. In Series AIII, the failure mode of unaffected beams was the diagonal shear tension failure after flexural yield, while some of the affected beams failed in horizontal slip failure which occurred connecting the horizontal cracks generated by ASR.
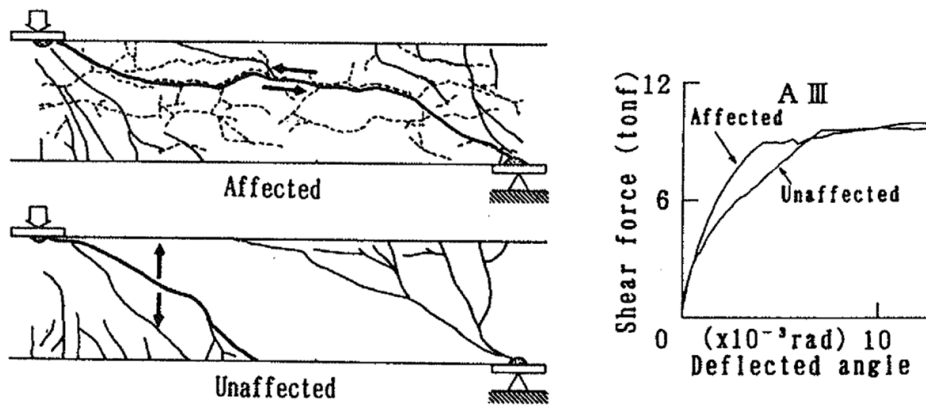

Figure 2.8: The failure mode changed from diagonal shear tension in unaffected beams to horizontal slip failure in affected beams, adopted from Abe et al. (1989).

Ohno et al. (1989) studied the effects of ASR on the flexural capacity in reinforced concrete beams. The ultimate flexural strength of the beams damaged by ASR was almost the same as that of the unaffected beams. The deflection at the yield strength, however, was reduced. The crack pattern was different as well. In unaffected specimens, the flexural cracks distributed evenly along the bottom part of the beam, and in affected specimens, the flecural cracks are more concentrated at the mid span.

Inoue et al. (1989) investigated the long-term (two years) structural behaviour of ASR affected reinforced concrete beams. Beams with reactive and non-reactive mixtures are reinforced with different amount of tension reinforcement resulting a tension reinforcement ratio of 0.77%, 1.2% and 1.74% respectively. All the beams have the same web reinforcement ratio of 0.3%. It is found that the flexural cracking strength of the affected beams was larger than that of the unaffected beams because of the induced chemical prestress. The chemical prestress also acted effectively to improve the shear resistance of concrete. The reduction in the yield strength and the maximum ultimate strength of affected beams was approximately 10% compared with those of unaffected beams. The overall deformation behaviour of affected beams was similar to that of unaffected beams except for the case of reinforcement ratio is 1.74%, in which the ASR affected beam failed in flexural with enough ductility while the unaffected one failed in shear and in a brittle manner. The crack pattern and load-deflection curve of this case is shown in Figure 2.9.
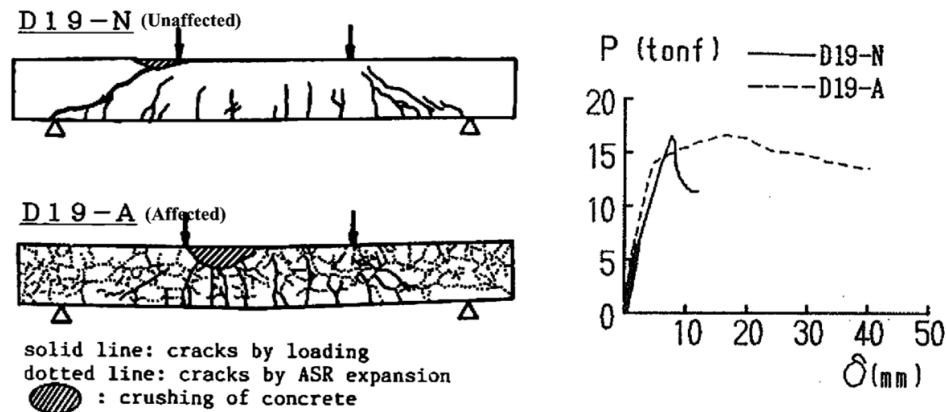
Figure 2.9: The unaffected beams failed in shear while the affected ones failed in bending, adopted from Inoue et al. (1989).

Ahmed et al. (1998) studied the effects of ASR on the shear capacity of reinforced concrete beams. The parameters in this experiment are the presence of links and the degree of anchorage. Concrete beams with or without links (shear reinforcement), with good and poor anchorage were cast with reactive and non-reactive mixtures. In beams with and without links, good anchorage reduced expansion and increased the ultimate shear strength of ASR concrete beams. The shear capacity in affected beams was higher than the unaffected beams, and this held for beams with or without shear reinforcement. The provision of links increased the shear resistance of both affected and unaffected beams, and in the case of affected beams, to a sufficient extent the change of failure mode from shear to bending was observed.

Fan and Hanson (1998) researched the effects of ASR on the flexural capacity of reinforced concrete beams. Different from the experiments performed by Ohno that discussed above, in this experiment, one series of the beams are loaded in bending from the start of the expansion stage. The experiment found that the flexural capacity in the affected beams was nearly the same compared with the unaffected beams, which means the load applied at the expansion stage did not influence the final flexural capacity of the ASR affected beams.

Kobayashi et al. (2013) studied the effects of ASR on beam strength. The parameters in this experiment are shear reinforcement ratio and the presence of hooks. With a relatively large shear reinforcement ratio, beam failed in bending due to the crush of concrete, and no apparent difference was observed between beam with and without hooks. Beams with less shear reinforcement failed in shear, and in case without hooks, beams failed in shear with a light degree of bond splitting. The change of failure mode from shear to bending was also observed. The author attributed the reason to the chemical prestress and the presence of ASR cracks. The ASR cracks enlarged as the shear strain increased and thereby prevented the formation of new cracks that could lead to a sudden shear failure.

Chana and Korobokis (1991) performed a systematic study to investigate the shear behaviour of ASR affected reinforced concrete beams. A lot of variables were taken into account, such as medium or high expansion, good or poor anchorage, smooth or ribbed rebars, with or without links and small-scale or full-scale beam. The strength of beams tested at a medium expansion level is not significantly different from the strength at a high expansion level. In beams with and without links affected by ASR, the poor anchorage performed as well as the good anchorage, and this applies to both smooth and ribbed rebars. In beams with links, ASR did not have a significant detrimental effect on the shear strength. It appears that the loss in the tensile strength is compensated by the compressive stress induced by restrained ASR expansion. In beams without links affected by ASR, shear strength reduced 20% to 30% for ribbed rebars and 15%-25% for smooth rebars. Data obtained from full-scale test are not enough to give conclusive comments. However, it is likely that any detrimental effects of ASR will be exaggerated in small-scale specimens since the depth of ASR cracks is relatively greater.

Table 2.1: The effects of ASR on structural behaviour and mechanical properties. (S represents shear failure and B represents bending failure. Data are collected from Abe et al. (1989), Ohno et al. (1989), Inoue et al. (1989), Ahmed et al. (1998), Fan and Hanson (1998), Kobayashi et al. (2013) and Chana and Korobokis (1991))

Reference	Specimen Label	Specimens Description	Tensile Strength	Compressive Strength	Young's Modulus	Failure Mode (unaffected → affected)	Load Bearing Capacity
Abe	AI	Tension reinforcement ratio in AI, AII and AIII are 0.75%, 1.17% and 1.76% repectively. Stirrups are the same, D6@100mm.	Not measured	-6.40%	-29%	S → S	+5%
	AII					S → B	-4%
	AIII					S → S	-8%
Ohno	R1	R1 and R2 are the same. Tension reinforcement ratio=0.8%. Shear reinforcement ratio = 0.3%.	Not measured	-13.50%	-58%	B → B	+5%
	R2					B → B	+6%
Inoue	D13-A	Tension reinforcement ratio in D13, D16 and D19 are 0.77%, 1.2% and 1.74% repectively. Shear reinforcement ratio=0.3%.	-40%	-36%	-52%	B → B	-11%
	D16-A					B → B	-10%
	D19-A					S → B	-12%
Ahmed	S1-A	S1 to S4 have the same tension reinforcement ratio 0.1%.Shear reinforcement (links): Φ3.2@50mm (If appliable). S1 = Beam with no links and poor anchorage S2 = Beam with no links and good anchorage S3 = Beam with links and poor anchorage S4 = Beam with links and good anchorage	-5%	-11%	-20%	S → S	+9.8%
	S2-A					S → S	+7.4%
	S3-A					S → B	+11.1%
	S4-A					S → B	+11.8%
Fan	3R	Tension reinforcement ratio in 3R and 5R1 are 0.04%, 1% repectively. Stirrups are the same, D-5 wire@75mm.	-40%	-28%	-32%	B → B	+3.2%
	5R1					B → B	+3.9%
Kobayashi	D6-with hook-1	Tension reinforcement ratio=2%. Shear span is reinforced with D6 stirrups @100mm.	Not measured	-20%	-64%	B → B	+8.3%
	D6-with hook-2					B → B	+11.1%
	D6-w/o hook-1					B → B	+9.2%
	D6-w/o hook-2					B → B	+17.7%
	Φ3-with hook-1	Tension reinforcement ratio=2%. Shear span is reinforced with Φ3 stirrups @100mm.				S → B	-26.7%
	Φ3-with hook-2					S → B	-37.8%
	Φ3-w/o hook-1					S → S	-8.0%
	Φ3-w/o hook-2					S → S	-22.8%
	0-with hook-1	Tension reinforcement ratio=2%. Shear span is not reinforced.				S → S	-12.0%
	0-with hook-2					S → S	-35.6%
	0-w/o hook-1					S → S	-9.7%
	0-w/o hook-2					S → S	+16.1%
Chana	M-1A	Tension reinforcement ratio=2%. M represents medium expansion. H represents high expansion. A represents good anchorage. B represents poor anchorage. 1 represents smooth rebar without links. 2 represents smooth rebar with links. 3 represents ribbed rebar without links. 4 represents ribbed rebar with links.	-44%	-19%	-31%	S → S	-25%
	M-1B					S → S	+8%
	M-2A					S → S	+0%
	M-2B					S → S	+20%
	M-3A					S → S	-30%
	M-3B					S → S	-26%
	M-4A					S → S	+8%
	M-4B					S → S	+6%
	H-1A		-46%	-20%	-66%	S → S	-15%
	H-1B					S → S	-18%
	H-2A					S → S	-1%
	H-2B					S → S	+2%
	H-3A					S → S	-19%
	H-3B					S → S	-21%
	H-4A					S → S	+2%
	H-4B					S → S	-10%
	SM-ST	This is a full-scale beam test. SM represents smooth rebar RB represents ribbed rebar ST represents straight rebar end BT represents bent rebar end	-40%	-21%	-64%	S → debonding	-46%
	SM-BT					S → S	–
	RB-ST					S → S	-22%
	RB-BT					S → S	-14%

Informations of the reviewed literatures are collected in table 2.1. The effects of ASR are discussed and compared crossing these papers from different aspects.

The stiffness in ASR affected beams not always decreases even though a large reduction in elastic modulus is observed. The change of stiffness cannot be predicted based on the reduction in elastic modulus. For instance, in Ohno's case, the stiffness increased with a reduction of 52% in elastic modulus, while in Ahmed's case, the stiffness remains the same even with a reduction of 64% in elastic modulus. The chemical prestress induced by the restrained ASR expansion and the arched shape of the beams that is formed due to uneven rebar arrangement act positively for increase of beam stiffness. Therefore, the assessment of the stiffness in affected beam should also take these two factors into account.

In some of the experiments the change of failure mode is observed: the unaffected beams failed in shear but the affected ones failed in bending. Two reasons are mentioned by the authors who observed this change. One is the chemical prestress induced by the restrained ASR expansion. It is believed that the chemical prestress has a positive effects on the shear resistance of the affected beams. Another reason is the presence of ASR cracks. When the affected beam is loaded in shear, the increase of shear load results in the widening of the existing ASR cracks so that the formation of shear cracks, which could lead to a sudden shear failure, are prevented. From the reviewed literatures, it seems that the change of failure mode tends to happen in beams with shear reinforcement. However, the change from bending to shear never happens.

In all the experiments, the reductions in the mechanical properties of concrete due to ASR are much larger than the reductions in the flexural or shear strength of reinforced concrete beams. Two reasons to explain this. One is that the mechanical properties are measured from plain concrete cylinders and cubes where the expansion is not confined. The expansion in reinforced concrete beams are confined so that the real properties reduction in reinforced beams is less than plain concrete. Another reason is that the chemical prestress and the presencs of ASR cracks have positive effects on the structural behaviour in affected beams, which make the flexural and shear strength less reduced compared with the mechanical properties.

As observed from the table, the maximum reduction in flexural strength is 11%, but maximum reduction in shear strength can go up to 40%, which means that ASR has a more detrimental effect on beams failed in shear than in bending. This is because the reduction of tensile strength is more than the reduction of compressive strength in ASR affected concrete. The shear capacity is more sensitive to the tensile strength, and the flexure capacity is more dominated by the compressive strength of concrete.

It is also worthy to mention the difference between ASR cracks and the cracks induced by mechanical loads. As described in some literatures, the presence of mechanical cracks result in a stiffness reduction in the beams at the early loading stage. However, this stiffness reduction is not observed in ASR affected beams. A possible explanation is, the generation of ASR cracks is due to gel expansion, but the gel also fills in those cracks and eventually leave some cracks that only is visible on the outer zone of the concrete member. In other words, the ASR cracks are not "hollow". The stiffness reduction is related to crack closure, but the ASR cracks are already filled with ASR gel so that the reduction cannot happen.

Chapter 3

Literature Review: Finite Element Modelling of ASR Affected Concrete Structures

In this chapter, literatures related to the finite element modelling of ASR affected concrete structures are reviewed. Depending on the purpose of these papers, the FE-models usually consists of different input and output parameters. Two types of the models are distinguished in this chapter based on their input and output. One type of the model attempts to simulate the effects of environment conditions on ASR expansion. The input of the model are environment related parameters such as temperature and moisture, and the output is the strain and stress distribution. Another type of the model focus on the effects of ASR on the structural behaviour. The ASR expansion usually is known and treated as the input. The output is structure related parameters such as the load-deflection response and crack pattern. These two different types of models are reviewed in different sections as shown in Figure 3.1.
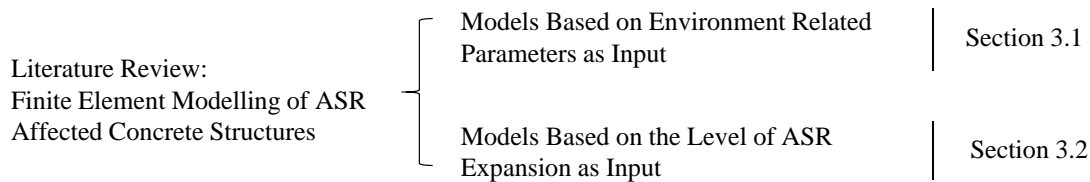
Literature Review:
Finite Element Modelling of ASR
Affected Concrete Structures

Models Based on Environment Related Parameters as Input — Section 3.1

Models Based on the Level of ASR Expansion as Input — Section 3.2

Figure 3.1: layout of this chapter

3.1 Models Based on Environment Related Parameters as Input

Ulm et al. (2000) developed a chemoelastic model that quantitatively analyses the coupled heat diffusion and ASR kinetics. This research belongs to the scope of linking the environment conditions to ASR expansion. The 1D form of the chemoelastic model is shown in Figure 3.2. It is a parallel spring system. σ is the macroscopic stress due to external forces, and ε is the corresponding overall strain. E_μ is the elastic modulus of concrete and E_g is the elastic modulus of gel. ξ represents the extent of the chemical reaction. It is assumed that the expansion is proportional to the reaction extent. The ASR expansion is thus related to the chemical reaction. The chemoelastic approach is a first-order structural engineering approach to predict the effects of ASR in the time-space scale of concrete structures. The model is validated through a 2D dam and a 2D bridge box girder. Only the effects of temperature on ASR kinetics are considered. The effects of moisture is not considered. The stress induced anisotropic expansion is not considered in this study.

Farage et al. (2004) modified the chemoelastic model proposed by Ulm by adding a cohesive joint element for modeling crack opening in tension. The one-dimensional form of the model is demon-
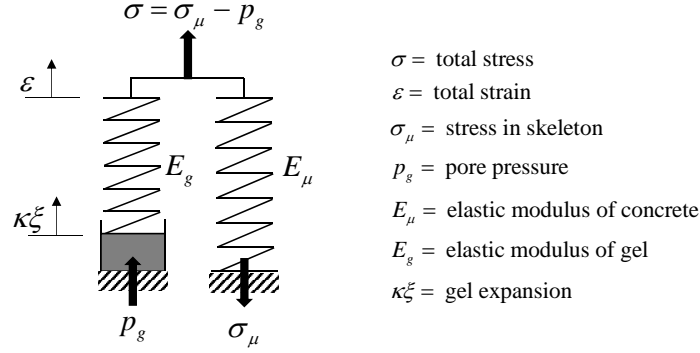
$$\sigma = \sigma_\mu - p_g$$

Figure 3.2: 1D chemoelastic model

σ = total stress
ε = total strain
σ_μ = stress in skeleton
p_g = pore pressure
E_μ = elastic modulus of concrete
E_g = elastic modulus of gel
$\kappa\xi$ = gel expansion

strated in Figure 3.3. Cracking is modeled within the framework of the classic theory of smeared crack finite element approach. The input of the model are gel and concrete properties, characteristic parameters for gel kinetics, and the output are displacements, stresses and cracking pattern. The model is validated through a ASR affected cylindrical concrete specimen loaded in uniaxial compression and to loading-unloading conditions. Numerical results indicates that the model is able to reproduce ASR effects in concrete structures under certain loading and boundary conditions. Further researches about the coupling of stresses and ASR expansion are needed to extend the model application to structures under more complicated loading and boundary conditions.
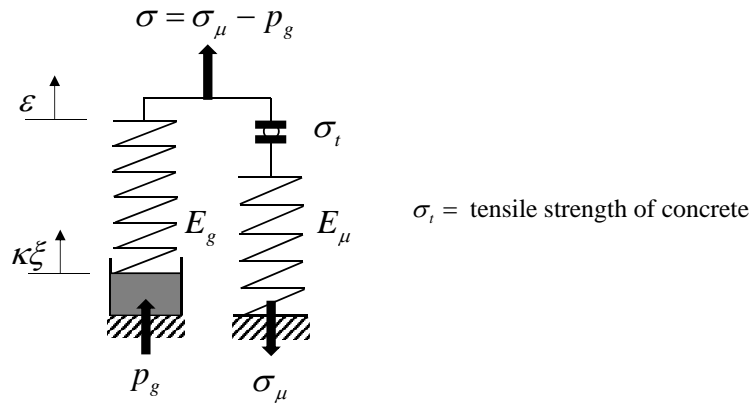
$$\sigma = \sigma_\mu - p_g$$

σ_t

σ_t = tensile strength of concrete

Figure 3.3: The modified 1D chemoelastic model

The modified 1D chemoelastic model is improved in Fairbairn et al. (2005). The improved model considers the expansion as a function of temperature and humidity, and it considers cracking as the factor to achieve the anisotropic behaviour of the structures. The model is validated through a real ASR affected dam. The ASR induced pressure and displacement of the dam is simulated. A good agreement is observed for the displacement comparing with recorded data.

Followed the path of 1D chemoelastic model, Li and Coussy (2002) proposed a so-called 1D equivalent chemoplastic model. This model is shown in Figure 3.4. In 1D equivalent chemoplastic model, the ASR expansion can generate a elastic material deformation by chemical pot 1 and an irreversible deformation by chemical pot 2. E_h is the equivalent elastic modulus of the gel E_g and the skeleton E_μ. Depending on the relation between E_g and E_μ, this model is further distinguished as the imposed chemoplastic model and the coupled chemoplastic model. According to the imposed chemoplastic model, the concrete degradation at a structure level is induced and only induced by the structure effects, for instance, the boundary conditions. However, in the coupled chemoplastic model, in addition to the plastic deformation induced by the structural effects, this model does account for possible material plastic deformation due to the chemical expansion. Therefore, the coupled chemoplastic model can be used to examine the degradation at a structure level as well as a material level. The validations are performed at a material level with the coupled chemoplastic model and at

a structural level with the imposed chemoplastic model. The applications of these two models are encouraging since the numerical results, to some extent, reflected the ASR phenomenon.
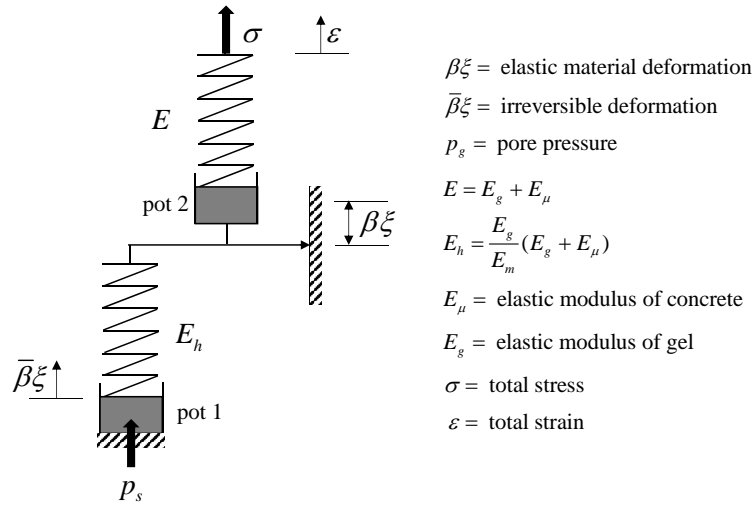

$\beta\xi$ = elastic material deformation

$\overline{\beta}\xi$ = irreversible deformation

p_g = pore pressure

$E = E_g + E_\mu$

$E_h = \dfrac{E_g}{E_m}(E_g + E_\mu)$

E_μ = elastic modulus of concrete

E_g = elastic modulus of gel

σ = total stress

ε = total strain

Figure 3.4: The 1D chemoplastic model

Capra and Sellier (2002) proposed a new method which can achieve an orthotropic ASR expansion based on the a probabilistic description of the main physical parameters of the concrete. In this method, concrete is modelled by a material model with elastic and inelastic properties so that the concrete degradation can be included. ASR gel is modelled by a global kinetics taking into account the effects of temperature and humidity. The coupling between mechanics and ASR makes the model capable to simulate the experiments performed on ASR affected concrete specimens. The validation is performed through two types of specimens. One is a concrete cylinder uniaxially loaded in compression. The expansion along the axial and transverse directions are simulated. The other specimen is a reinforced concrete beam. The beam is only reinforced in the longitudinal direction, and the expansion along longitudinal and transverse direction are simulated. The obtained numerical results a good agreement with the experiments.

3.2 Models Based on the Level of ASR Expansion as Input

Ferche et al. (2017) performed a macro-modelling of ASR affected structures. The theoretical frame is constructed based on The Modified Compression Field Theory and the Disturbed Stress Field Model developed by Vecchio. The behaviour and magnitude of ASR induced expansion and resulting degradation on the mechanical properties are considered during the implementation of ASR effects on the smeared rotating crack model. ASR expansion is treated as an offset strain. This offset strain does not induce any stress, but is rigorously included in the finite element formulation to determine the stiffness factors. The reduction of mechanical properties are taken into account through two methods. One is directly using the value of the ASR affected material properties. The other method evaluates the residual material properties as a function of free expansion base on ISE prescriptions. The model validation is performed at material level and structural level. At material level, the stress-strain behaviour of a ASR affected plain concrete cylinder are simulated, and at the structural level, the load-deflection response of a reinforced concrete beam are simulated. The Validations achieved reasonably well estimations but also revealed some of limitations and deficiencies. The model is not able to capture the ASR induced anisotropic material properties. The bond degradation which may occur as a result of ASR in not addressed. Most importantly, the confinement effects due to the chemical prestress in reinforced concrete members is not able to include.

A collection of all the reviewed papers in this chapter are collected in Table 3.1.

Table 3.1: A collection of the reviewed papers.

References	Model Input Parameters	Model validations	Simulation of Anisotropic Expansion	Simulation of ASR Cracks
Ulm et al. (2000)	Temperature related	Expansion of 2D dam and bridge box girder	No	No
Farage at al. (2004)	Temperature amd moisture related	Expansion of 2D uniaxial loaded concrete cylinder	No	–
Fairbairn et al. (2005)	Temperature amd moisture related	Expansion of 2D dam	Yes	No
Li and Coussy (2002)	Temperature amd moisture related	Expansion of 2D bridge pier	–	No
Capra and Sellier (2002)	Temperature amd moisture related	Expansion of 2D uniaxial loaded concrete cylinder and reinforced concrete beam	Yes	No
Feeche et al. (2017)	The level of free expansion	Load-deflection response of reinforced concrete beam	No	Yes

Chapter 4

The Double Mesh Model

In this chapter, the mechanism of the proposed double mesh model is demonstrated. With the level of free expansion as the input, the model is able to simulate the restrained ASR expansion by taking into account the effects of physical restraints. In the first section, the mechanism of double mesh model is illustrated. Analytical solution for calculating ASR expansion is illustrated in 1D and 2D froms within the scope of elastic behaviour. Then, a single-element test is performed to study the non-linear expansion simulated in double mesh model. A parametric study is also performed in this single-element test to investigate the effects of material properties on ASR expansion. The layout of this chapter is shown in Figure 4.1.
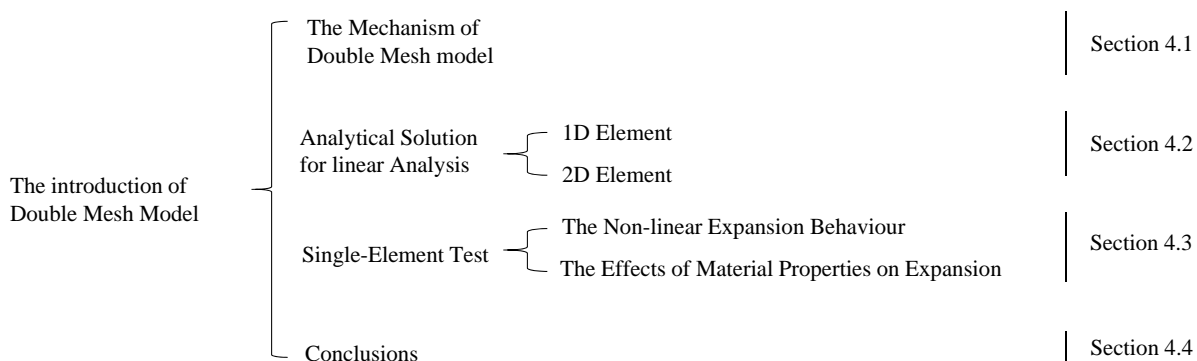
Figure 4.1: Layout of this chapter

4.1 The Introduction of Double Mesh Model

A so-called double mesh model (DMM) is developed to simulate ASR expansion. Different from the normal finite element model that contains only one set of mesh, DMM consists of two overlapped meshes, namely structural mesh and shadow mesh. Shadow mesh is an extra mesh attached to the structural mesh. It shares the same nodes with structural mesh but composed by different elements. Figure 4.2 illustrates an example of the simplest 2D DMM.

Shadow mesh and structural mesh use different elements so that different material properties can be assigned to the two meshes. Generally, non-linear material properties of concrete is assigned to structural mesh to simulate the non-linear behaviour of concrete and linear properties is assigned to shadow mesh to simulate the behaviour of ASR gel.

Shadow mesh and structural mesh will always have the same deformation due to the fact that they share the same nodes. However, the deformation is not a result of shadow mesh or structural mesh only, but is a combined result of both meshes. In the normal model that only has structural mesh,

23

deformation is determined by the stiffness of structural mesh, loads, and boundary conditions. When shadow mesh is added, the stiffness of shadow mesh also need to be taken into account.
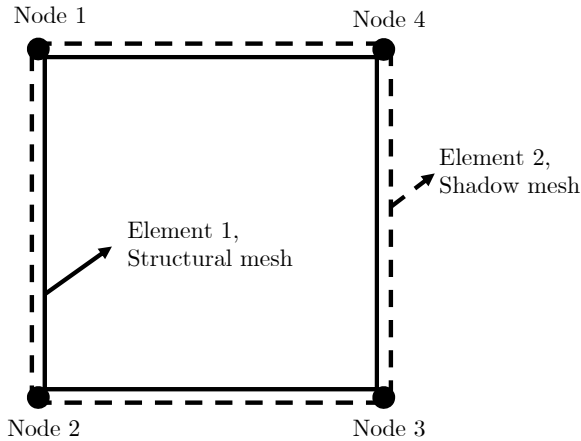

Figure 4.2: The simplest 2D DMM: A 4-node single-element shadow mesh attached to a 4-node single-element structural mesh. The nodes are shared by two elements, so 4 nodes and 2 elements in total.(Here, shadow mesh is larger and placed outside of the structural mesh so that it is visible, the truth is two meshes are overlapped and of the same size.)

Strain is applied on shadow mesh to simulate the expansion of alkali-silica gel. The applied strain will be confined by structural mesh. As a consequence, shadow mesh will be loaded in compression and structural mesh will be loaded in tension, resulting in cracks in structural mesh.

4.2 Analytical Solution for Linear Analysis

4.2.1 1D Element

Figure 4.3 shows the simplest 1D double mesh model with two elements in total, one is for structural mesh and the other one is for shadow mesh. One-dimensional element can be seen as spring. The stiffness of structural mesh and shadow mesh are denoted as K_{st} and K_{sh}. The interaction between two meshes is explained stepwise as follow.

- Stage 1. Structural mesh and shadow mesh stay at their original place, no load applied.

- Stage 2. Initial strain is applied to shadow mesh, leading to a initial displacement Δ_0 as shown in Figure 4.3. It should be noted that applying initial strain is different from applying strain. The mechanism of initial strain considers the deformation after applying initial strain as its original situation. Thus, applying initial strain will not result in stress in the element. However, the model at this stage is still not in equilibrium, not in terms of force, but in terms of deformation compatibility. The fact that both meshes share the same nodes, so they should deform together. Nevertheless, initial strain is only applied on shadow mesh, which breaks the compatibility. This stage is transient and the dissatisfaction of deformation compatibility will result in a further deformation, bringing the model to stage 3.

- Stage 3. It should be noted that deformation at this stage does generate stresses considering that it no longer belongs to initial strain. Structural mesh and shadow mesh will deform towards each other because that is the only way to meet the force equilibrium and the deformation compatibility. The final displacement is at a location between stage 1 and stage 2, and it depends on the magnitudes of K_{st} and K_{sh}.
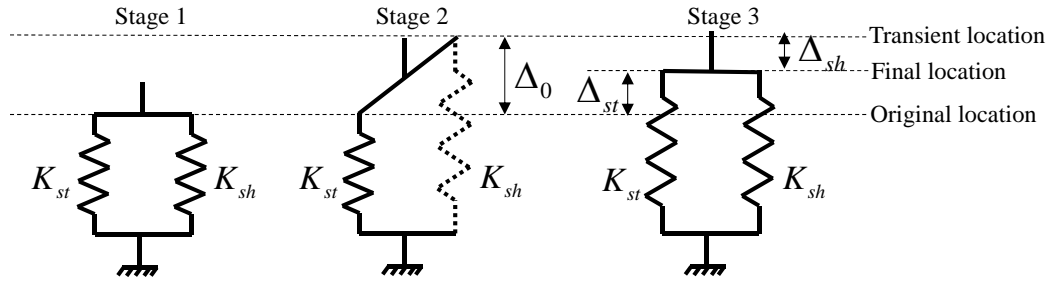
Figure 4.3: The interaction between structural mesh and shadow mesh in 1D model.

The final displacement can be derived as follow, where Δ_{sh} is the displacement of shadow mesh and Δ_{st} is the displacement of structural mesh, also representing the final displacement.

Force equilibrium and deformation compatibility:

$$K_{st}\Delta_{st} = K_{sh}\Delta_{sh} \tag{4.1}$$

$$\Delta_{st} + \Delta_{sh} = \Delta_0 \tag{4.2}$$

Combining equation 4.1 and 4.2, the final displacement can be expressed as a function of initial displacement.

$$\Delta_{st} = \frac{K_{sh}}{K_{sh} + K_{st}}\Delta_0 \tag{4.3}$$

As can be seen from equation 4.3, the final displacement depends on the relative magnitude between K_{st} and K_{sh}. For a certain value of K_{st}, the increase of K_{sh} makes the final deformation infinitely approaching to initial displacement, and the decrease of K_{sh} makes the final deformation infinitely approaching to zero.

4.2.2   2D Element

4.2.2.1   Poisson Ratio Induced Iterations

The final displacement derived from previous section is extended for 2D element. The presence of 2D element induces a new property, poisson ratio, which results in iterations of deformation between x and y direction. Figure 4.4 shows a detailed iteration procedure in case of applying initial strain in y direction. In case of applying initial strain in both x and y direction, the result is a superposition of applying initial strain in x and y direction, and the superposition holds as long as the material properties keep constant.

Remark: displacement Δ, δ used here are direction-dependent. Positive value of Δ, δ leads to expansion and negative value results in contraction.

① Initial strain is applied on shadow mesh

② Using equation 1.3, $\Delta_{st,y0} = \dfrac{K_{sh}}{K_{sh}+K_{st}}\Delta_{y0}$
$\Delta_{sh,y0} = -\dfrac{K_{st}}{K_{sh}+K_{st}}\Delta_{y0}$

Δ_{y0}

$\Delta_{sh,y0}$
$\Delta_{st,y0}$

① ②

③ Deformation in y direction results in deformation in x direction due to poisson ratio.
$\delta_{st,x0} = -\Delta_{st,y0}\upsilon_{st}$
$\delta_{sh,x0} = -\Delta_{sh,y0}\upsilon_{sh}$

③

$\Delta_{st,y1}$ and $\Delta_{sh,y1}$ are the input of next iteration !

$\delta_{st,x0}$ $\delta_{sh,x0}$

⑤ Deformation in x direction results in deformation in y direction due to poisson ratio.
$\delta_{st,y0} = -\Delta_{st,x0}\upsilon_{st}$
$\delta_{sh,y0} = -\Delta_{sh,x0}\upsilon_{sh}$

$\delta_{sh,y0}$
$\delta_{st,y0}$

$\Delta_{sh,y1}$
Δ_{y0}
$\Delta_{st,y1}$

⑥ ⑤ ④

⑥ The same process with stage 4.
$\Delta_{y0} = \dfrac{K_{st}\delta_{st,y0} + K_{sh}\delta_{sh,y0}}{K_{sh}+K_{st}}$
$\Delta_{st,y1} = \Delta_{yo} - \delta_{st,y0}$
$\Delta_{sh,y1} = \Delta_{yo} - \delta_{sh,y0}$

④ Δ_{x0} is the distance between the new and old equilibrium position
$\Delta_{st,x0}$ and $\Delta_{sh,x0}$ are the movements of structural mesh and shadow mesh.

$\Delta_{x0} = \dfrac{K_{st}\delta_{st,x0} + K_{sh}\delta_{sh,x0}}{K_{sh}+K_{st}}$
$\Delta_{st,x0} = \Delta_{xo} - \delta_{st,x0}$
$\Delta_{sh,x0} = \Delta_{xo} - \delta_{sh,x0}$

Δ_{x0}

$\Delta_{st,x0}$ $\Delta_{sh,x0}$

Figure 4.4: An example of iterations of applying initial strain to shadow mesh in y direction.

4.2.2.2 Steel Induced Increase in Stiffness

When concrete is reinforced, the existence of steel increases the stiffness along its own direction. For instance, a 2D element shown in Figure 4.5 is reinforced in x direction, resulting in the stiffness of structural mesh in x direction is higher than y direction. Equation 4.3 now is expressed as:

$$\begin{bmatrix} \Delta_{st,x} \\ \Delta_{st,y} \end{bmatrix} = \begin{bmatrix} \frac{K_{sh}}{K_{sh}+K_{st,x}} & 0 \\ 0 & \frac{K_{sh}}{K_{sh}+K_{st,y}} \end{bmatrix} \begin{bmatrix} \Delta_{0,x} \\ \Delta_{0,y} \end{bmatrix} \tag{4.4}$$

$$K_{st,x} = K_c + K_s, K_{st,y} = K_c \tag{4.5}$$

Where subscript "c" stands for concrete, and "s" stands for steel.
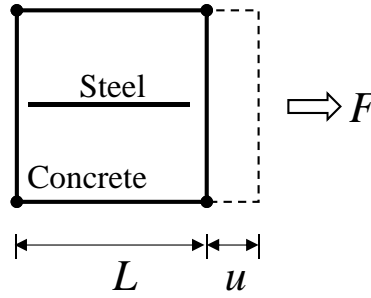
Figure 4.5: A 2D element is reinforced in x direction

Assuming a full bond between concrete and steel, the increase of stiffness (presented by the increase of Young's modulus) can be calculated as follow. Concrete and steel experience the same strain:

$$\varepsilon_L = \frac{u}{L} \tag{4.6}$$

$$\sigma_s = E_s \varepsilon_L, \sigma_c = E_c \varepsilon_L \tag{4.7}$$

If the total cross-sectional area of reinforced concrete is A, then the cross-sectional area of steel and concrete are given by the total area multiplied by the volume fraction (V) of steel or concrete.

$$F = V_s A E_s \varepsilon_L + (1 - V_s) A E_c \varepsilon_L \tag{4.8}$$

Both sides divided by cross-sectional area A:

$$\sigma_L = (V_s E_s + (1 - V_s) E_c) \varepsilon_L \tag{4.9}$$

$$E_L = (V_s E_s + (1 - V_s) E_c) = E_{st,x} \tag{4.10}$$

For instance, if $E_s = 210 GPa$, $E_c = 35 GPa$, $A_s = 1\%$:

$$\frac{E_{st,x}}{E_{st,y}} = \frac{V_s E_s + (1 - V_s) E_c}{E_c} = \frac{210 \times 0.01 + 35 \times (1 - 0.01)}{35} = 1.05 \tag{4.11}$$

Every 1% of reinforcement ratio increases stiffness by 5%.

4.3 Single-Element Test

From the last section, it is known that the deformation is a result of interaction between shadow mesh and structural mesh. The stiffness and poisson raio of both meshes influence the deformation. However, this is the conclusion from linear aspect of view. In non-linear analysis, the induced cracks in structural mesh reduces the stiffness and poisson ratio, which means the interaction between shadow mesh and structural mesh is now a dynamic process. The interaction changes along with the extent of cracks in structural mesh.

There are two purposes of performing single-element test:

- to investigate the non-linear expansion behaviour. See results in section 4.3.1.

- to study the effects of material properties on expansion. See results in section **??**.

It is call single-element test but actually the model contains two elements, one belongs to shadow mesh and another one belongs to structural mesh. Figure 4.6 shows the finite element model. General information of the model is listed below:
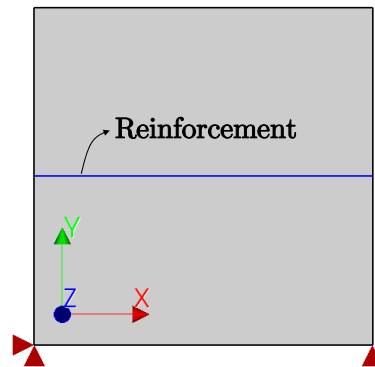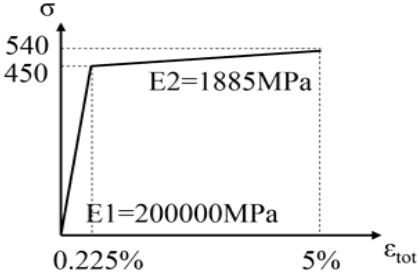
Figure 4.6: Model for single-element test

- Elements: two 4-node plane stress elements.

- Nodes: 6 nodes in total, 4 nodes shred by two meshes and 2 nodes belongs to reinforcement.

- Bond: reinforcement is assumed to be fully bonded to surrounding concrete.

- Boundary conditions: only rigid body movement is confined as shown in Figure 4.6.

- Load: initial strain of 1% is applied to shadow mesh element in both x and y directions.

- Material properties: demonstrated in table4.1

In this test, six cases are designed for different material properties to investigate their effects on expansion. The input is the applied initial strain in shadow mesh, and the output is the resulting final strain in both meshes. Because they share the same nodes so they will have the same final strain. For the intuitive reason, the word "final strain" is replaced by "expansion" in this thesis wrok. A layout of the cases is demonstrated in table 4.1

Table 4.1: Layout of single-element test

Material properties of structural mesh: Young's modulus: E_{st}=35GPa Poisson ratio: υ_{st}=0.15 Mean tensile strength: f_{ctm}=3.2MPa Tensile fracture energy: G_F=0.1N/mm Tensile curve: Hordijk shear retention factor: 0.01(if appliable) Compressive curve: Elastic Material properties of reinforcement: Young's modulus: 200GPa Nonlinear properties (if appliable): 		Young's modulus of shadow mesh, E_{sh}	Poisson ratio of shadow mesh, υ_{sh}	Reinforcement ratio, A_s	Hardening or No-Hardening	Cracking orientation	Material of shadow mesh
	Case1	E_{sh}=10%E_{st} E_{sh}=5%E_{st} E_{sh}=1%E_{st}	0.15	2%	No-hardening	Fixed	Isotropic
	Caes2	E_{sh}=10%E_{st}	0.15 0.35 0.5	2%	No-hardening	Fixed	Isotropic
	Case3	E_{sh}=10%E_{st}	0.15	0.50% 1% 2%	No-hardening	Fixed	Isotropic
	Case4	E_{sh}=5%E_{st}	0.15	2%	Hardening No-hardening	Fixed	Isotropic
	Case5	E_{sh}=1%E_{st}	0.15	2%	No-hardening	Fixed Rotating	Isotropic
	Case6	$E_{sh,x}$=$E_{sh,y}$=1%E_{st} $G_{sh,xy}$=0	0.15	2%	No-hardening	Fixed	Isotropic Orthotropic

29

4.3.1 The Non-linear Expansion Behaviour

Results obtained from case 1 with $E_{sh} = 10\%E_{st}$ is depicted in Figure 4.7 as an example to illustrate the non-linear expansion behaviour.

Figure 4.7 (a) shows the expansion development respect to initial strain. EXX represents the expansion in x direction (reinforced direction), and EYY represents the expansion in y direction (unreinforced direction). The **reference line** is simply a straight line with a slope of 45°. 45° is a special slope, whenever the slope of a line changes to 45°, it means that the increment of expansion will be exactly the same with the increment of initial strain, and this will only happen when $E_{st} = 0$.

Figure 4.7 (b) illustrates the development of expansion difference. Expansion difference is defined as the difference of expansion between unreinforced and reinforced direction. In this case, expansion difference equals to EYY minus EXX.
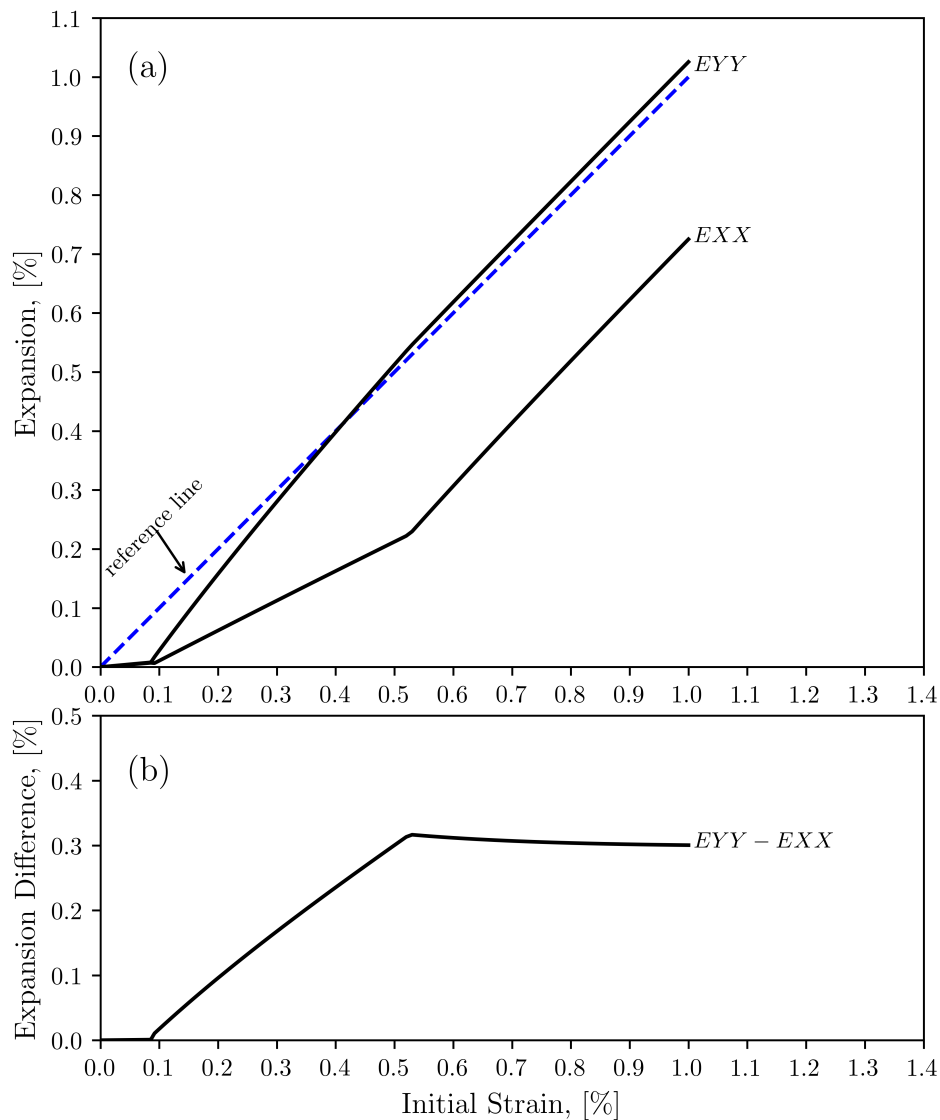
Figure 4.7: A typical expansion graph. (obtained from case 1 with $E_{sh} = 10\%E_{st}$.)

Expansion behaviour in y direction can be distinguished into two stages based on the two distinct slopes shown in line EYY. The first stage is a linear stage. Because E_{sh} is only 10 percent of E_{st}, there is almost no expansion within this stage. The start of cracking brings the expansion into the second stage. Cracks induced in structural mesh reduces E_{st}. Expansion can be effectively observed consequently. With the structural mesh continues to crack, E_{st} will be eventually reduced to zero, as can be seen in Figure 4.7 (a), EYY is almost paralleled to reference line at the end of the axis.

Expansion behaviour in x direction has an extra stage due to the existence of reinforcement. This extra stage starts from the beginning of cracking, and ends at the yielding of steel. In x direction, the reduction of E_{st} is compromised by the stiffness of steel, and this is the reason expansion in x direction is always smaller than y direction. However, the compensation disappears with the yielding of steel and eventually, the total stiffness in x direction will be reduced to zero as well. A sudden slope change can be observed along EXX when expansion equals to 0.225%, which coincide with the yielding strain of steel as can be calculated from table 4.1.

The development of expansion difference can be divided into three stages:

- Stage 1 starts from the beginning, and ends at the onset of cracking. The presence of reinforcement slight increase K_{st} in x direction. However, this slight increase can hardly be noticed because of the fact that K_{st} is overall relatively large comparing to K_{sh}, which is the reason that almost zero expansion can be observed at this stage

- Stage 2 starts from the onset of cracking and ends at the yielding of steel. K_{st} is reduced rapidly due to the presence of cracks. Thus, the existence of steel results in a huge difference of K_{st} in x and y direction. Expansion in y direction will be larger than x direction because of a smaller stiffness. A coroutines increase in expansion difference can be seen at this stage.

- Stage 3 starts from the yielding of steel. The contrition of steel disappears after yielding, resulting the same residual stiffness in x and y direction. As a consequence, the incremental expansion respect to initial strain is the same in both directions, leading to a constant expansion difference at this stage.

4.3.2 The Effects of Material Properties on Expansion

4.3.2.1 Young's modulus of Shadow Mesh

Case 1 studies the effects of E_{sh} on expansion, with E_{sh} equals to one percent, five percent and ten percent of E_{st} respectively. Result is depicted in Figure 4.8. The main effects of E_{sh} are:

- **A smaller E_{sh} postpones the initiation of cracks in structural mesh.** The reason is, a small E_{sh} needs a larger initial strain to reach the tensile strength of structural mesh. The smaller the E_{sh} is, the larger the needed initial strain.

- **A smaller E_{sh} enlargers the expansion difference.**

Figure 4.8: Effects of E_{sh} on expansion, results obtained from case 1.

4.3.2.2 Poisson Ratio of Shadow Mesh

Figure 4.9 shows the expansion behaviour of different ν_{sh}, obtained from case 2. Two main effects can be observed:

- **A higher ν_{sh} boosts the expansion in unreinforced direction.** Shadow mesh with high poisson raio works like "rubber", the confined part of the expansion in x direction is "squeezed" into y direction. The higher the ν_{sh}, the larger the expansion in unreinforced direction.

- **A higher ν_{sh} moves the initiation of cracks forward.**

- **A higher ν_{sh} enlarges expansion difference, but the effect is limited .** The enlargement is achieved by increasing expansion in the unreinforced direction.
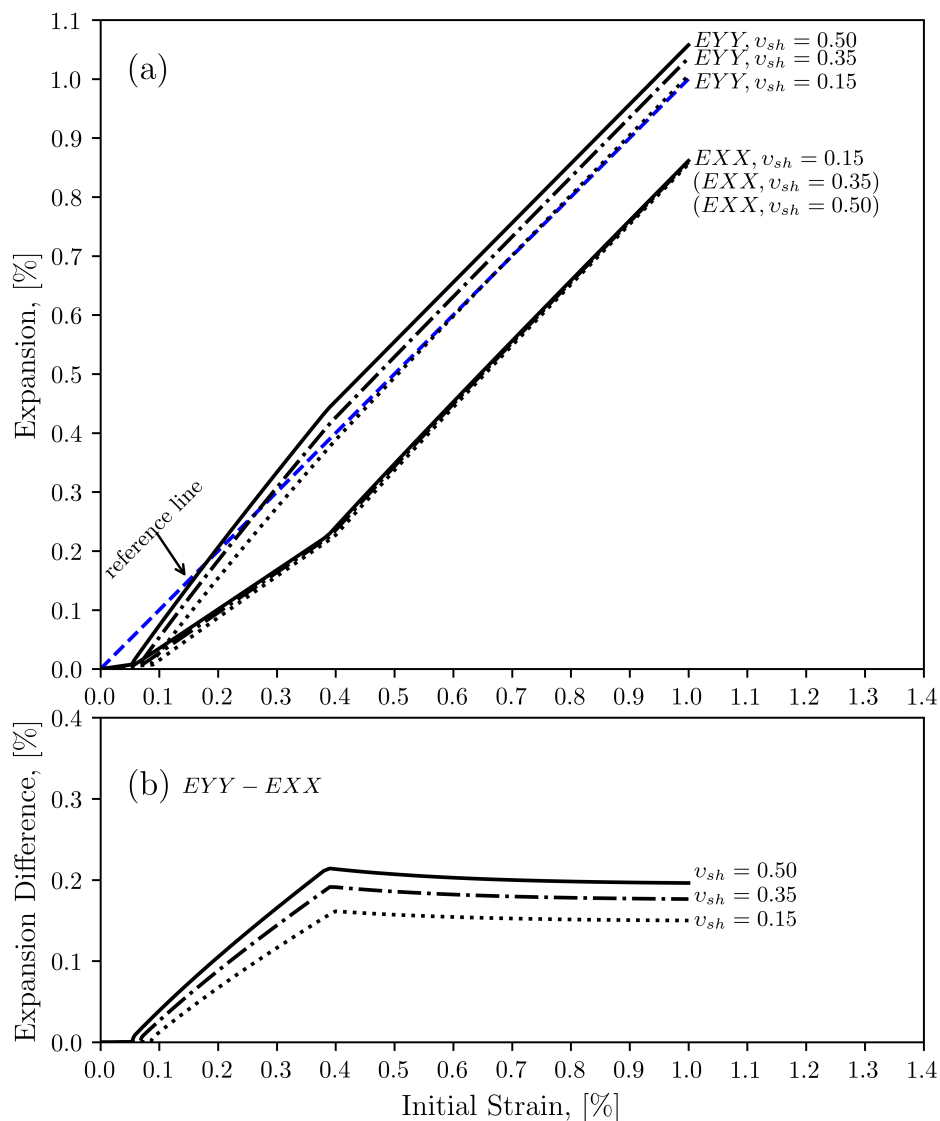
Figure 4.9: Effects of ν_{sh} on expansion, results obtained from case 2.

4.3.2.3 Reinforcement ratio

The effects of A_s is studied in case 3, and the result is demonstrated in Figure 4.10. The main effects of A_s on expansion are:

- **Reinforcement reduces the expansion along its own direction. The greater the amount of reinforcement, the greater the reduction.**

- **A higher A_s enlarges the expansion difference.** The enlargement is achieved by the reduction of expansion in reinforced direction.
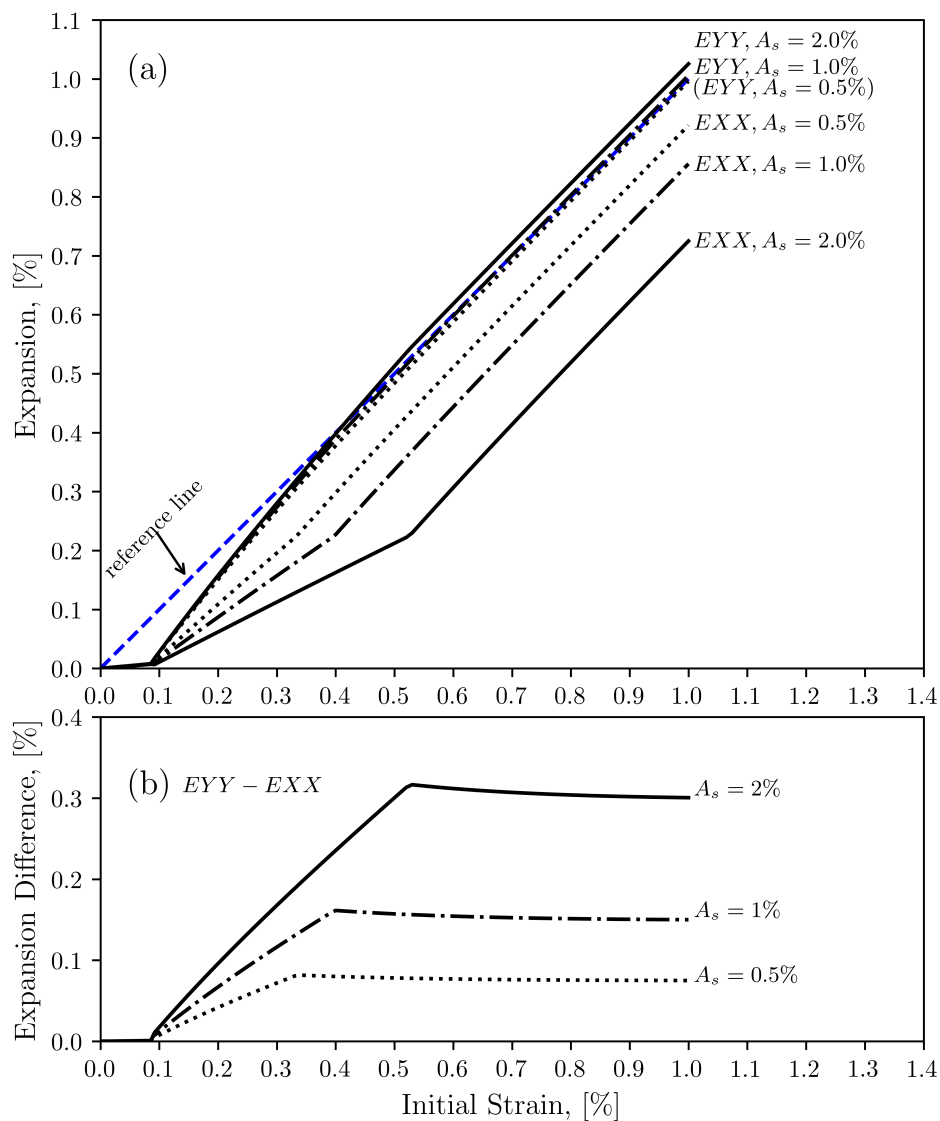
Figure 4.10: Effects of A_s on expansion, results obtained from case 3.

4.3.2.4 Hardening and No-hardening Steel

Hardening and No-hardening steel are studied in case 4 to investigate their influence on expansion. Material properties can be checked from table 4.1. As can be seen from Figure 4.11 that hardening and no-hardening steel show the same results. This is because despite the stiffness still exists in hardening steel after yielding, but the residual stiffness is very small compare to the elastic stage(only 1%). Thus, the influence is not notable.
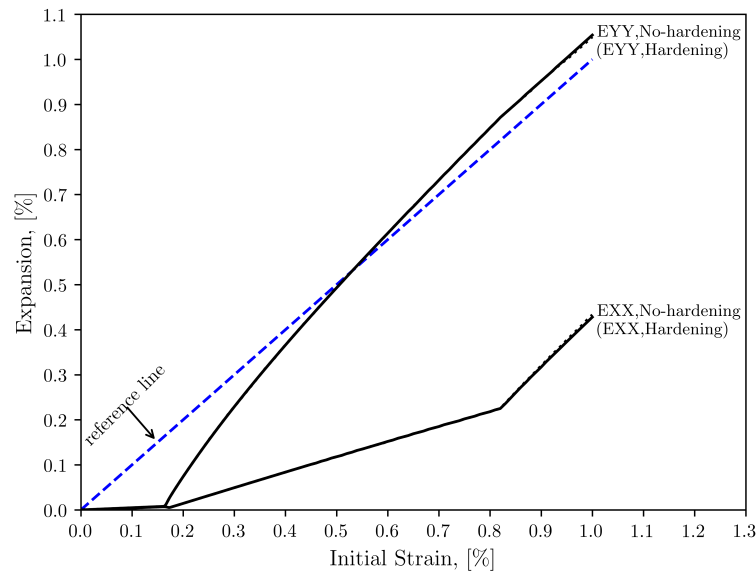
Figure 4.11: Effects of hardening and no-hardening steel, results obtained from case 4.

4.3.2.5 Fixed and Rotating Cracking Models in Structural Mesh

Structural mesh using fixed and rotating cracking models are studied in case 5. The result is depicted in Figure 4.12. Fixed and rotating cracking model show the same expansion behaviours. Considering the applied initial strains are axial strain and no shear component is involved, so the fixed and rotating cracking model are essentially the same.
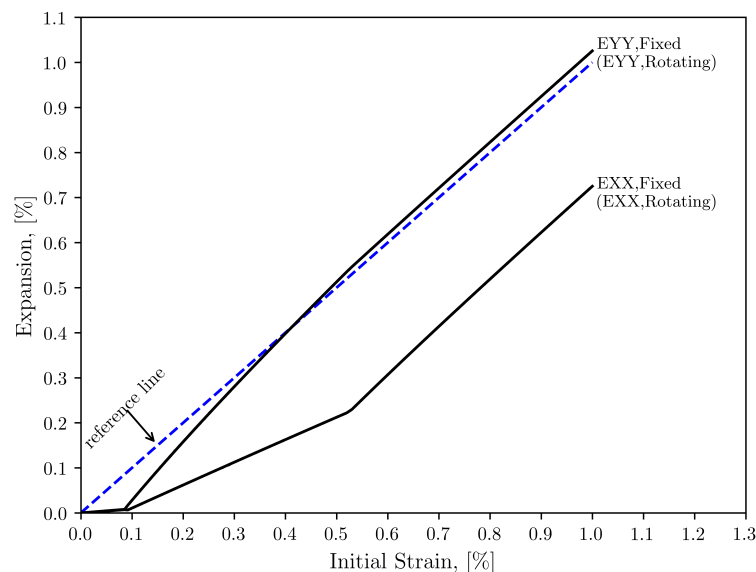
Figure 4.12: Effects of fixed and rotating cracking model, results obtained from case 5.

35

4.3.2.6 Isotropic and Orthotropic Shadow Mesh Materials

Shadow mesh with isotropic and orthotropic materials are applied in case 6 to study their effects on expansion. No difference is observed from Figure 4.13. Explanation is the same with case 5.
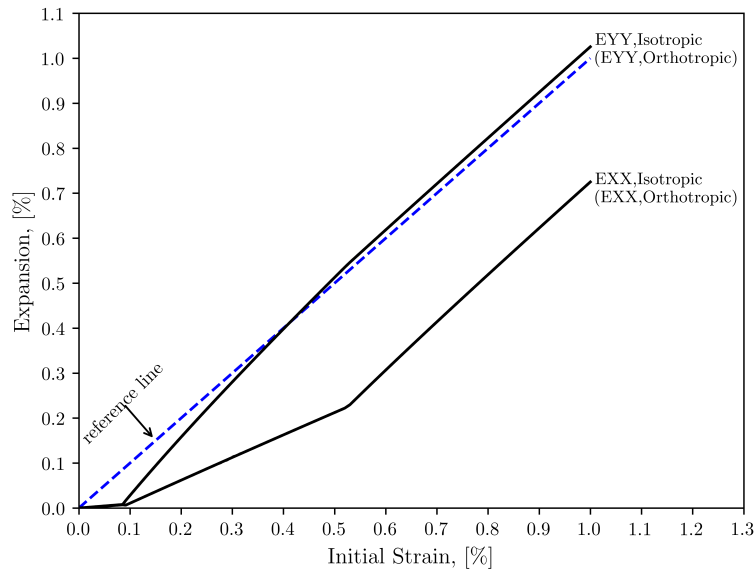
Figure 4.13: Effects of isotropic and orthotropic materials, results obtained from case 6.

4.4 Conclusions

The proposed double mesh model is investigated at single element level in this chapter. The applied initial strain on shadow mesh leads to expansion in structural mesh. The expansion is a result of the interaction between both meshes. The ability to achieve anisotropic expansion is regarded as the core reason that the double mesh model has the potential to simulate ASR expansion.

Expansion is analytically derived within the scope of elastic material properties. Two principal conclusions are derived from analytical solution. 1) The stiffness of the shadow mesh is the most important property that affects the expansion, the influence of poisson ratio is relatively small, yet not ignorable. 2)The anisotropic stiffness distribution due to the presence of steel is the radical reason for anisotropic expansion. For the normal material properties used in practice, every one percent of reinforcement ratio increases stiffness of five percent along the reinforced direction.

Single-element test is performed in finite element software to study the non-linear expansion behaviour as an extension of the linear expansion studied analytically. The presence of cracks reduce the stiffness of structural mesh dramatically, therefore the stiffness of shadow mesh is more dominating in the non-linear stage. It is found that, stiffness of shadow mesh, poisson raio of shadow mesh and reinforcement ratio are the most influential properties, and their influences are reflected from different aspects. Poisson ratio controls the expansion in unreinforced direction and reinforcement ratio restrains the expansion in reinforced direction, whereas the stiffness influences the expansion in both directions. Considering the reinforcement ratio is an inherent property which is already given for a specific case, the validation performed in next chapter mainly focus on the the properties of shadow mesh.

It should be noted that the effcts of changing from fixed to rotating cracking model and from isotropic to orthotropic structural mesh are not observed in expansion stage. The reason is that no shear component is involved. Whereas, this no longer holds in the mechanical loading stage when shear deformation has induced. Their influences on expansion in terms of strength will be investigated in the chapter 6.

Chapter 5

Model Validation: ASR induced Expansion

In the previous chapter, the double mesh model is examined analytically and numerically, but without any comparison. In this chapter, the proposed model is applied to simulate the expansion behaviour of concrete members based on benchmarks Wald et al. (2017), Koyanagi et al. (1992) and Mohammed et al. (2003). Shadow mesh properties are adjusted to find the most appropriate value for E_{sh} and ν_{sh} that results in the same expansion as the benchmarks.

Expansion behaviour is studied comparing with experimental results. The aim of this chapter is to answer the question: Is there a general shadow mesh property that can be used to simulate all ASR expansions? The answer will be concluded in the last section of this chapter

Layout of this chapter is shown in Figure 5.1. It should be noticed that this chapter focus on the validation of expansion, the resulting reduction in strength is validated in next chapter.
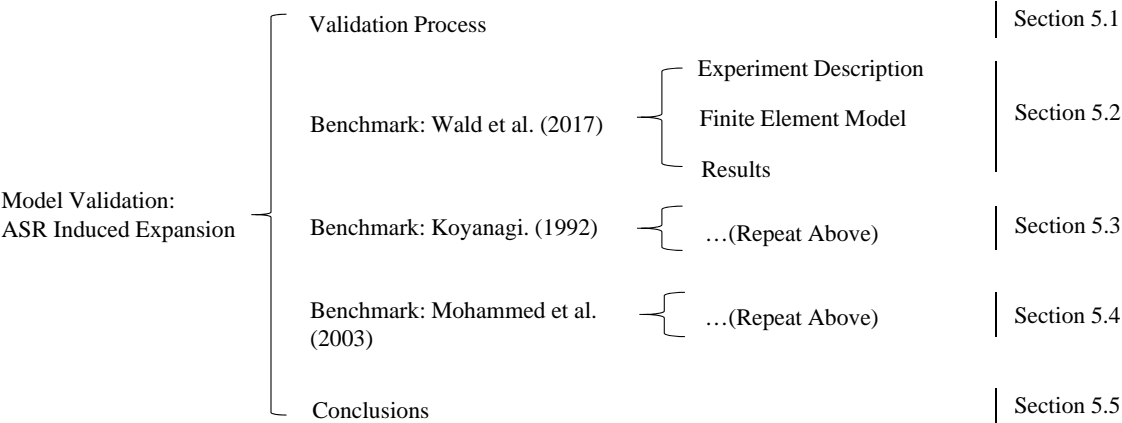
Figure 5.1: Layout of chapter 5

5.1 Validation Process

Validation process is performed in three steps as illustrated in Figure 5.2. Step 1 and step 2 are repeated for different shadow mesh properties: E_{sh} and ν_{sh}.

- Step 1: determining initial strain. In plain concrete model, a stepwise increased initial strain is applied on shadow mesh, resulting in a gradually increased free expansion in the model. The initial strain, which leads to the same free expansion as experiments is considered to be the input of the next step.

- Step 2: simulating restrained expansion. Initial strain obtained from the last step is applied in the reinforced concrete model. The output of this step is restrained expansion.

- Step 3: determining a appropriate value for E_{sh} and ν_{sh} respectively. Restrained expansions derived from different E_{sh} and ν_{sh} are compared against experimental results to search for the most appropriate shadow mesh properties.
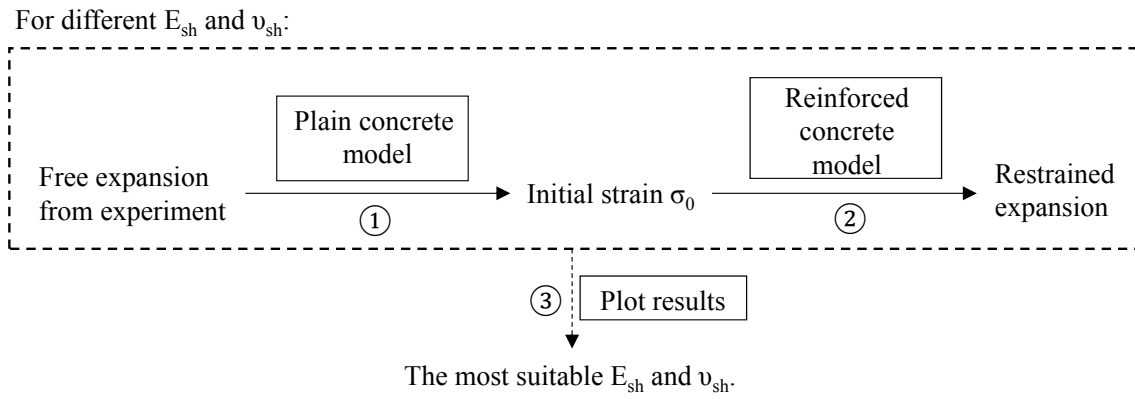
Figure 5.2: Demonstration of validation process

5.2 Benchmark: Wald et al. (2017)

A series of experiments were performed by Wald et al. (2017) to understand the multiaxial ASR expansion of reinforced concrete cubes. Cube A1-000b, A1-001a, A1-002 and A1-003 are selected from experiments and marked as case free expansion, $A_s = 0.5\%$, $A_s = 1.1\%$ and $A_s = 1.5\%$ in this thesis work.

5.2.1 Experiment Description

5.2.1.1 Experiment Layout

Four 480 mm concrete cubes are depicted in Figure 5.3. One concrete cude is not reinforced and other three concrete cubes are reinforced with #4, #6 and #7 rebars, achieving a reinforcement ratio of 0.5%, 1.1% and 1.5% respectively.

5.2.1.2 Material Properties

Material properties are illustrated in table 5.1. Compressive strength of concrete and yielding strength of steel are tested in the experiment, and other material properties are assumed based on Hendriks et al. (2017).
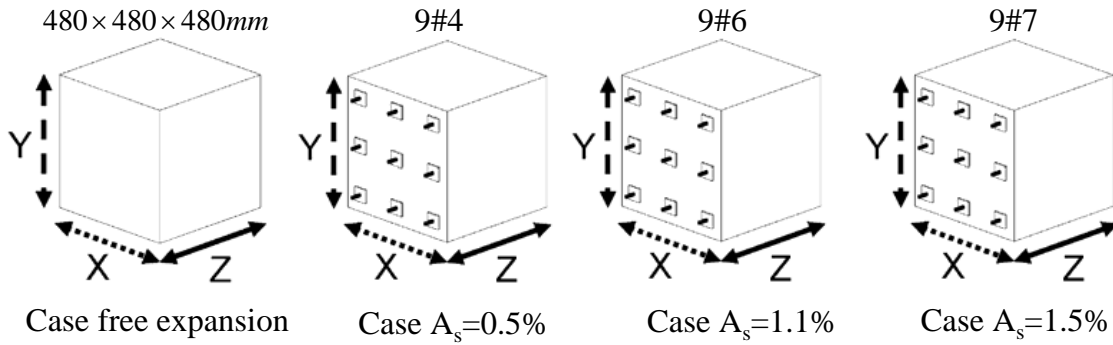
Figure 5.3: Experiment layout

Table 5.1: Material Properties

Concrete	Mean compressive strength	31 MPa (given)
	Mean tensile strength	2.43 MPa
	Tensile fracture energy	0.14 N/mm
	Compressive fracture energy	34 N/mm
	Young's modulus at 28 days	31.3 GPa
	Poisson ratio	0.15
Steel	Mean yielding strength	414 MPa (given)
	Young's modulus	200 GPa

5.2.1.3 Expansion Measurement

To ensure a meaningful comparison between the numerical and experimental expansions. Measurement location is of extreme importance considering the expansion is not uniform across the section. In this benchmark, the expansions of the cubes were monitored by taking measurements of the deformations between opposite specimen faces. Modified long-jaw calipers were used to periodically measure the distance between pairs of opposite target points, as shown in Figure 5.4
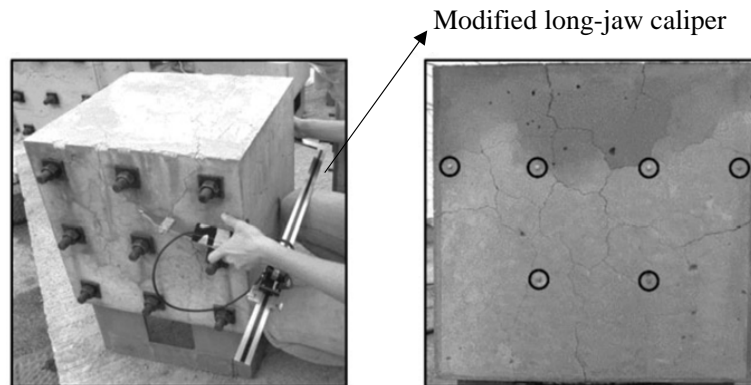
Figure 5.4: Expansion measurement, adopted from Wald et al. (2017)

5.2.1.4 Experimental Results

Results from experiment are shown in Figure 5.5. It should be noted that only the expansion at the final stage(as already noted in the figure) is of interest to simulate, instead of the entire expansion history.

Experiments monitored expansion in all the three directions, whereas the use of 2D model in this thesis work cannot validate the expansion along its thickness direction. During the validation process,

z direction (shown in Figure 5.5) is considered as the reinforced direction, and y is the unreinforced direction. Expansion in x direction is not considered.

Free expansion is considered to be uniform in this case. In the model, the adopted free expansion is the average of expansion in three directions.
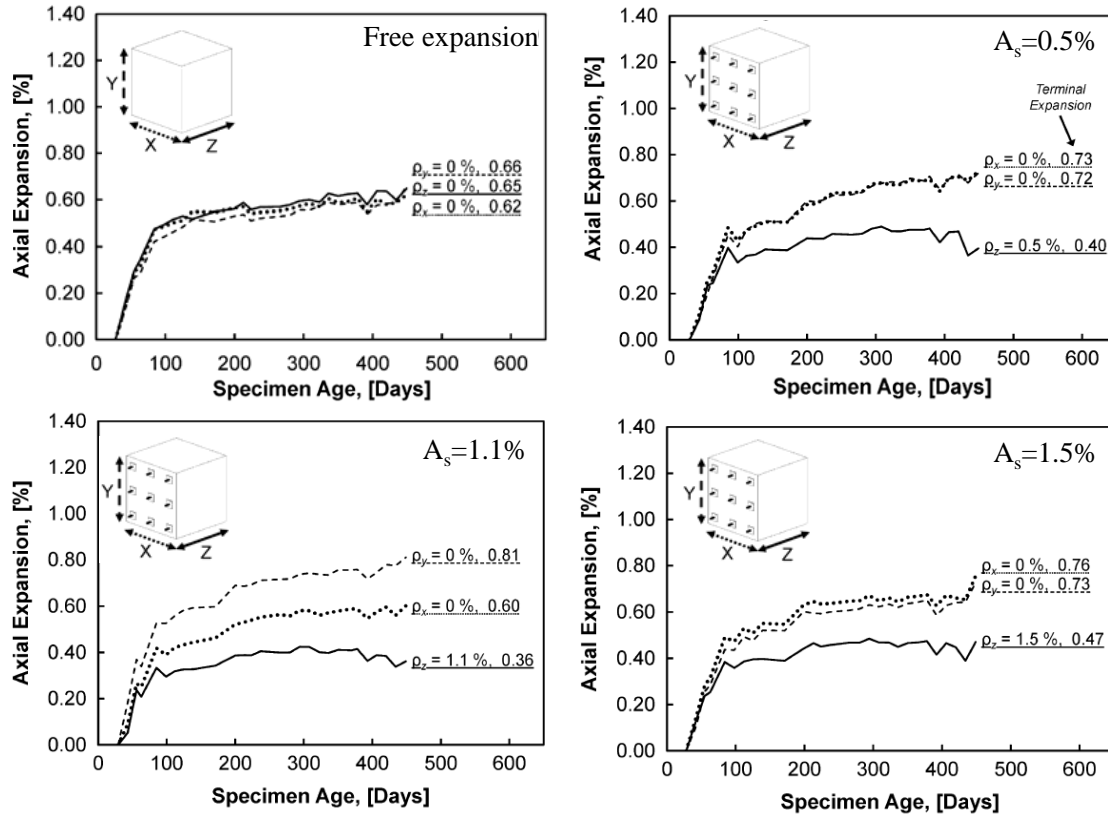
Figure 5.5: Experimental Results, adopted from Wald et al. (2017)

5.2.2 Finite Element Model

Plain concrete model and reinforced concrete model (shown in Figure 5.6) are created for simulating free expansion and restrained expansion. In reinforced concrete model, rebar is assumed to be fully bonded with its surrounding concrete. Rebar diameter is changed for different reinforcement ratio.
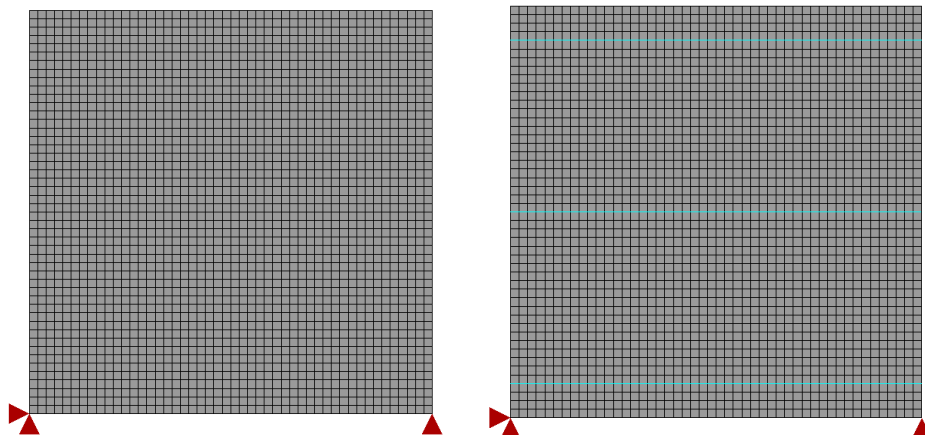
Figure 5.6: Plain concrete model (left) and reinforced concrete model (right), element size: 10 mm.

- **Structural mesh:** Total strain based crack model, material properties are listed in table 5.1

- **Shadow mesh:** Linear elastic isotropic material. Different values of E_{sh} and ν_{sh} are used. E_{sh} varies from 2% to 5% of E_{st}, ν_{sh} ranging from 0 to 0.5.

5.2.3 Results

Results of case $A_s = 0.5\%$, $A_s = 1.1\%$ and $A_s = 1.5\%$ are depicted in Figure 5.7, 5.8, and 5.10 respectively. Principal conclusion derived from figures are summarized as follows.

- Expansion in reinforced direction is always smaller than the unreinforced direction.

- A higher E_{sh} results in a larger expansion in reinforced direction.

- A higher ν_{sh} results in a larger expansion in unreinforced direction.

- The change of ν_{sh} has no affect on expansion in reinforced direction.

- The most appropriate shadow mesh properties for three cases are:
  $A_s = 0.5\%$: E_{sh}=2%E_{st}, $\nu_{sh} = 0.3$.
  $A_s = 1.1\%$: E_{sh}=2%E_{st}, $\nu_{sh} = 0.4$.
  $A_s = 1.5\%$: E_{sh}=5%E_{st}, $\nu_{sh} = 0.3$.

- Failed to find a certain value for E_{sh} and ν_{sh} that can simulate the expansion for different reinforcement ratio.
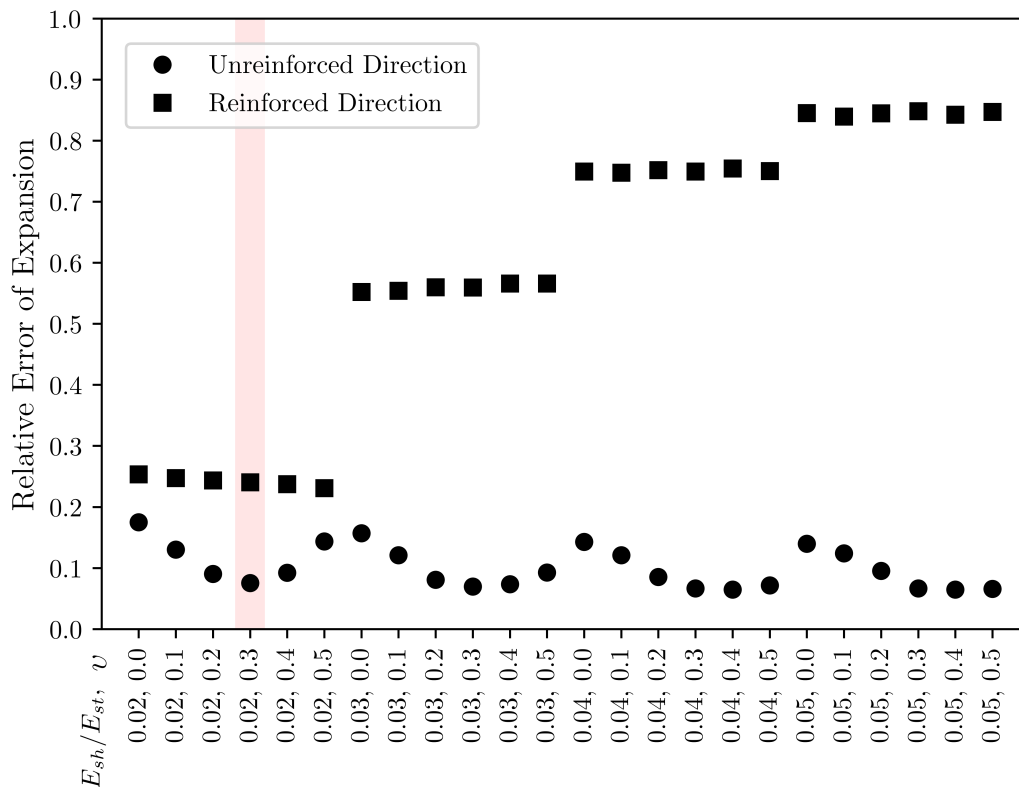
Figure 5.7: Numerical expansions derived from varied E_{sh} and ν_{sh} against experimental results, $A_s = 0.5\%$.
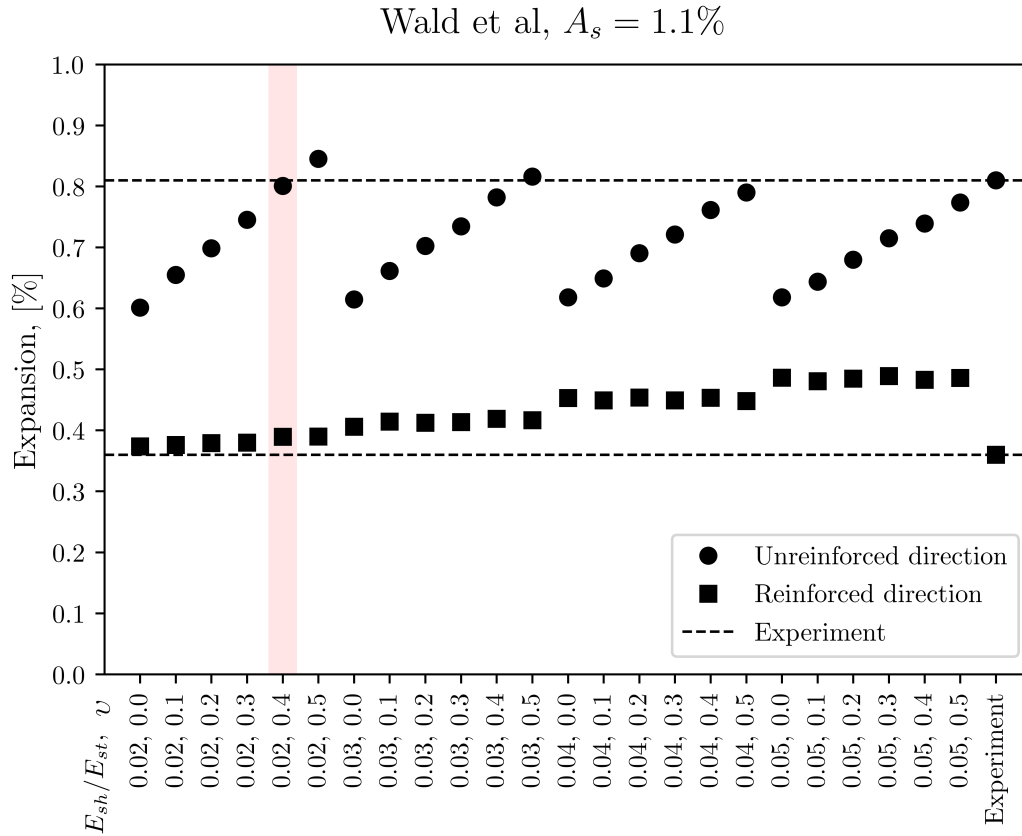
Figure 5.8: Numerical expansions derived from varied E_{sh} and ν_{sh} against experimental results, $A_s = 1.1\%$..
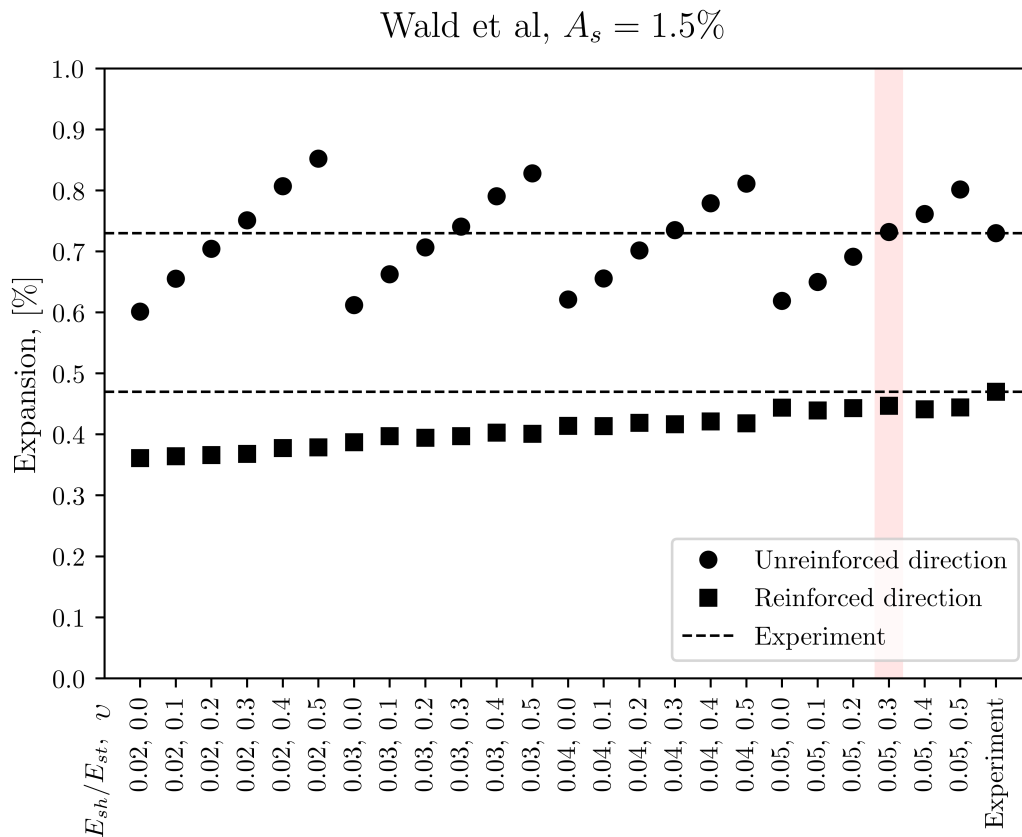
Figure 5.9: Numerical expansions derived from varied E_{sh} and ν_{sh} against experimental results, $A_s = 1.5\%$.

5.3 Benchmark: Koyanagi et al. (1992)

Koyanagi et al. (1992) studied the influence of reinforcement ratio on AAR expansion. One of the main conclusion from the paper is that expansion of concrete due to AAR is restrained by reinforcement and the restraining effect becomes higher with the increase of reinforcement ratio.

5.3.1 Experiment Description

5.3.1.1 Experiment Layout

Concrete prisms of dimension $100{\times}100$ mm in cross section and 1000 mm in length are cast with and without a single rebar in the middle. Rebar diameters of 3, 6, 10, 13 and 16 mm are used to achieve reinforcement ratios of 0.07%, 0.3%, 0.7%, 1.3% and 2%. Two prisms are cast for each configuration, 12 prisms in total.

$100{\times}100{\times}1000(mm)$

Case free expansion.

Case A_s=0.07%, 0.3%, 0.7%, 1.3%, 2%
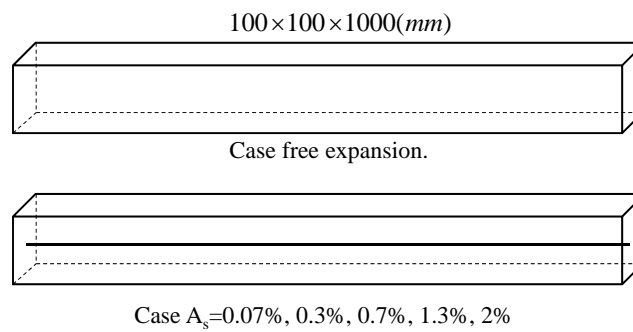
Figure 5.10: Experiment Layout

5.3.1.2 Material Properties

Young's modulus and compressive strength of concrete, and yielding strength of steel are tested for each case. Other material properties used in finite element model are assumed based on Hendriks et al. (2017). Table 5.2 shows the material properties.

Table 5.2: Material Properties

	Material properties	Free expansion	A_s=0.07%	A_s=0.3%	A_s=0.7%	A_s=1.3%	A_s=2%
Concrete	Mean compressive strength, MPa	33	33	31	35	38	42
	Mean tensile strength, MPa	2.57	2.56	2.44	2.73	2.88	3.14
	Tensile fracture energy, N/mm	0.14	0.14	0.14	0.14	0.14	0.14
	Compressive fracture energy, N/mm	34	34	34	35	35	36
	Young's modulus at 28 days, GPa	32	32	32	33	33	35
	Poisson ratio	0.15	0.15	0.15	0.15	0.15	0.15
Steel	Mean yielding strength, MPa	N.A.	333	421	382	372	362
	Young's modulus, GPa	N.A.	200	200	200	200	200

5.3.1.3 Expansion Measurement

The paper mentioned that length of the specimens was measured periodically, but did not specific the exact locations. Therefore, two positions are assumed, position 1 measured from the center of the cross section and position 2 measured the surface, as illustrated in Figure
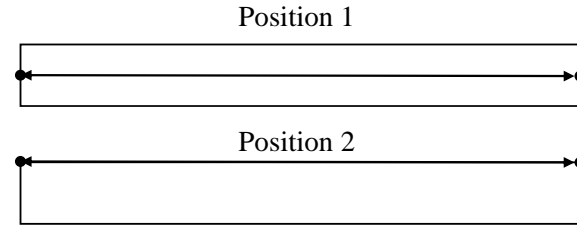
43

Figure 5.11: Two possible measurement positions

5.3.1.4 Experimental Results

Only expansion in the reinforced direction is measured from the experiments, results are illustrated in Figure 5.12. It can observed that the expansion is reduced with the increase of rebar diameter. Expansion is directly extracted from graph using a plot-digitizer. Free expansion is 0.27%, and the restrained expansion for rebar diameter of 3, 6, 10, 13, 16 mm are 0.23%, 0.15%, 0.12%, 0.095% and 0.074%.
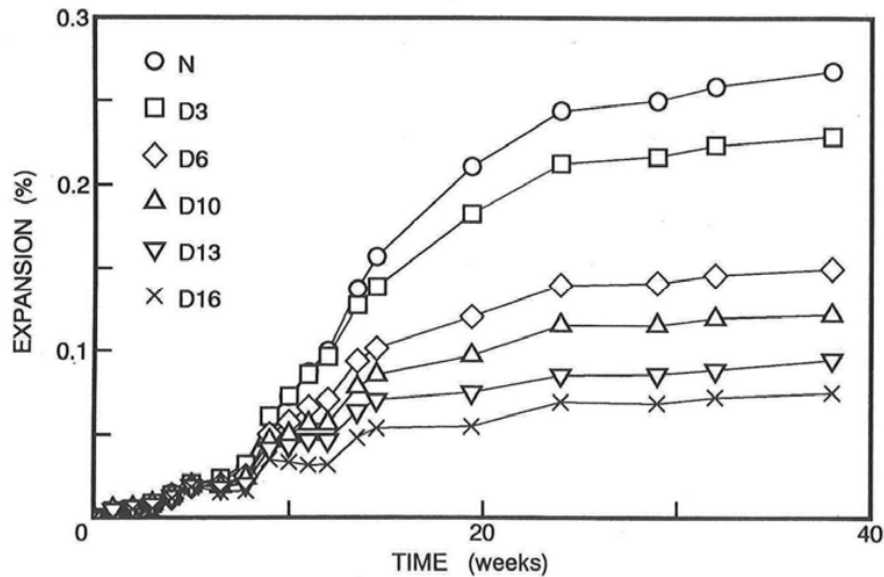

Figure 5.12: Experimental Results, adopted from Koyanagi et al. (1992)

5.3.2 Finite Element Model

Modelling procedure is the similar with the previous benchmark, as shown in Figure 5.13. Here, attention should be paid on the determination of shadow mesh properties. Only expansion along reinforced direction is measured in this benchmark, therefore v_{sh} cannot be validated. Considering that the value of v_{sh} does not affect the expansion in reinforced direction, in this benchmark, v_{sh} can be any random value between 0 to 0.5 since the only interest is in the reinforced direction.
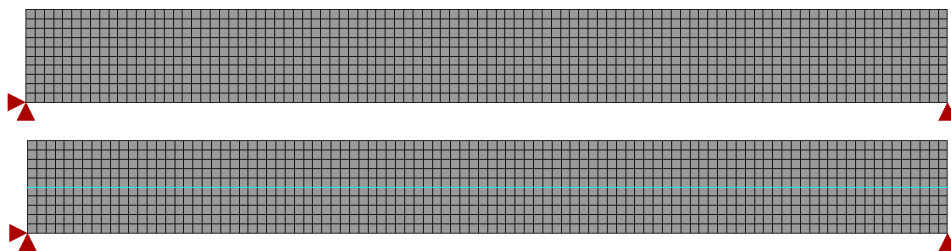
Figure 5.13: Plain concrete model (top) and reinforced concrete model (bottom), element size: 10 mm.

- **Structural mesh:** Material properties are described in table 5.2

- **Shadow mesh:** Different values of E_{sh} are used. E_{sh} varies from 1% to 5% of E_{st}, ν_{sh} is set to zero.

5.3.3 Results

Numerical expansions derived from measurement position 1 and 2 are depicted in Figure 5.14 and 5.15. Results are concluded as follow.

- Numerical expansions in position 2 is overall larger than expansion in position 1. This is because position 2 is less restrained.

- Expansion increases with the increase of E_{sh}, and it is faster when E_{sh} is relatively small, then tends to be gentle. This non-linear relation is caused by the non-linear interaction between structural mesh and shadow mesh as discussed before.

- It seems that the solid curve and dashed line intersect approximately at the same value of E_{sh} for different reinforcement ratio, which means there may exist a certain value of E_{sh} that can be used to simulate expansions for all the cases.

To validate the last conclusion, $E_{sh} = 1.8\%E_{st}$, and $E_{sh} = 1.6\%E_{st}$ are proposed to simulate the expansion of position 1 and position 2 for all the reinforcement ratio. As can be seen from Figure 5.16 and 5.17, the simulation is quite successful.
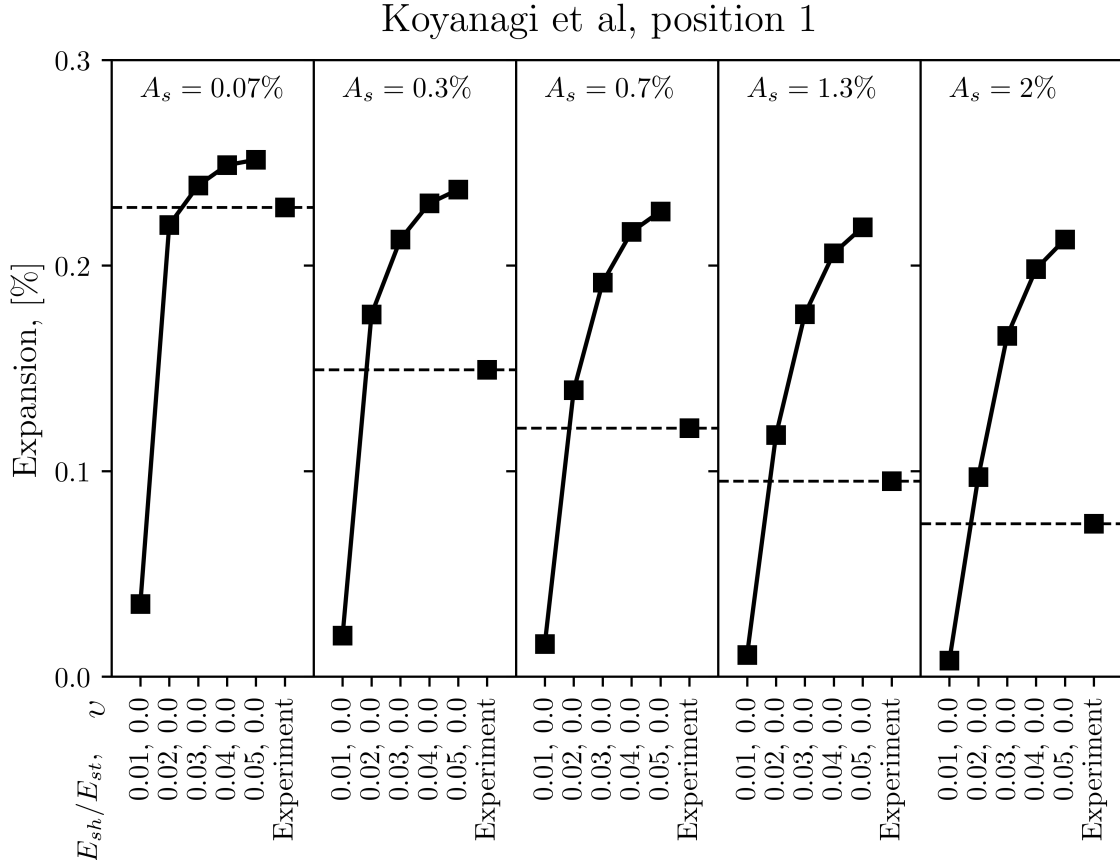
Figure 5.14: Numerical expansions derived from varied E_{sh} against experimental results, position 1.
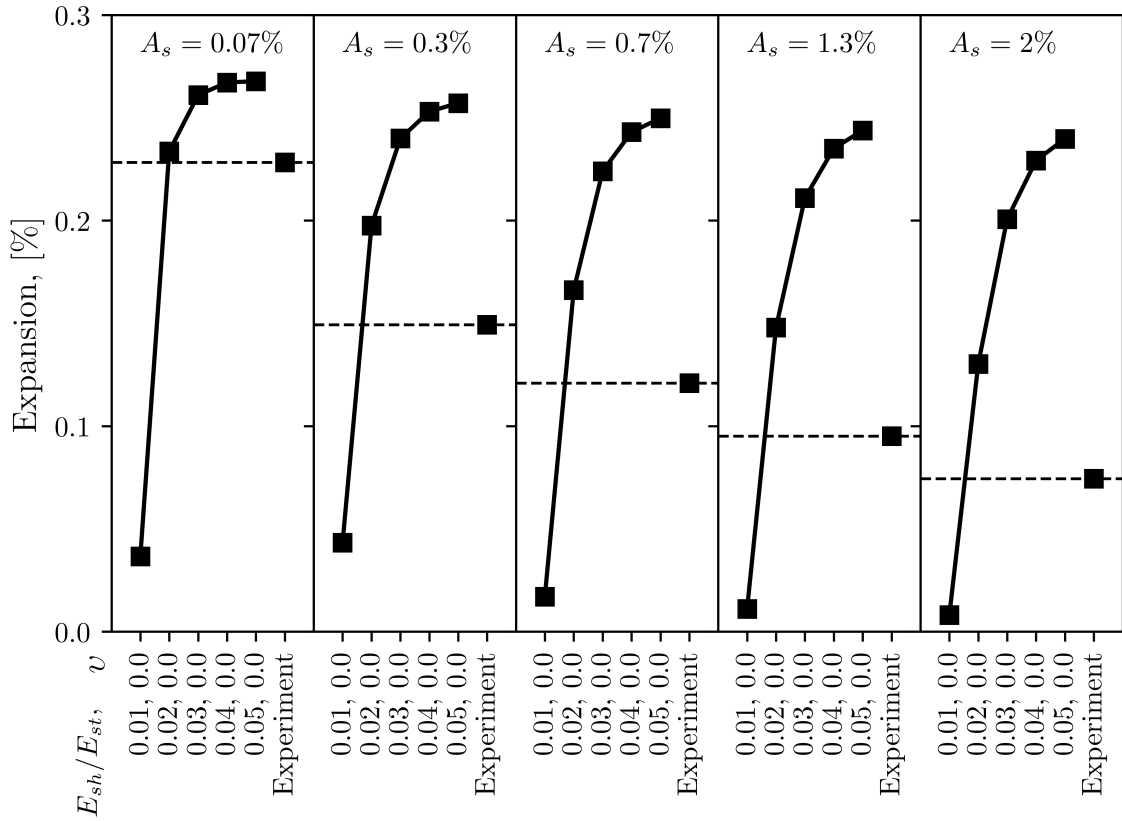
Figure 5.15: Numerical expansions derived from varied E_{sh} against experimental results, position 2.
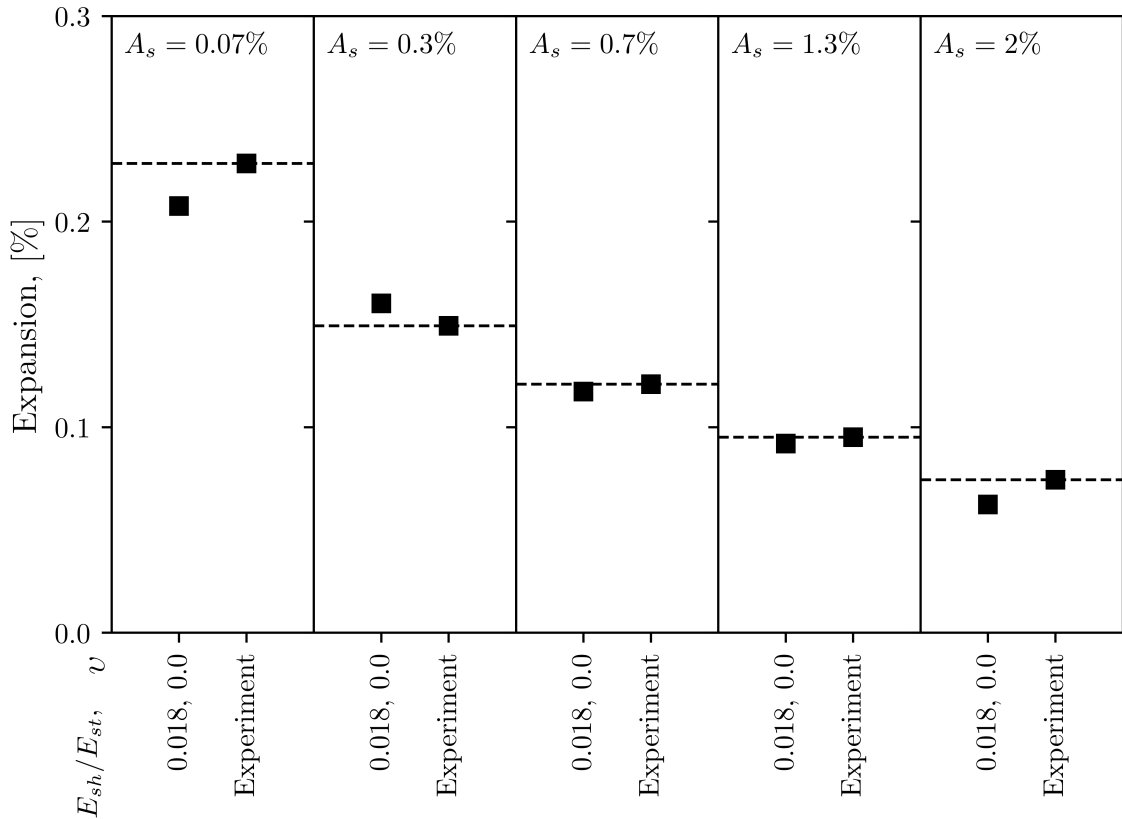
Figure 5.16: Numerical expansions derived from $E_{sh} = 1.8\% E_{st}$ against experimental results, position 1.
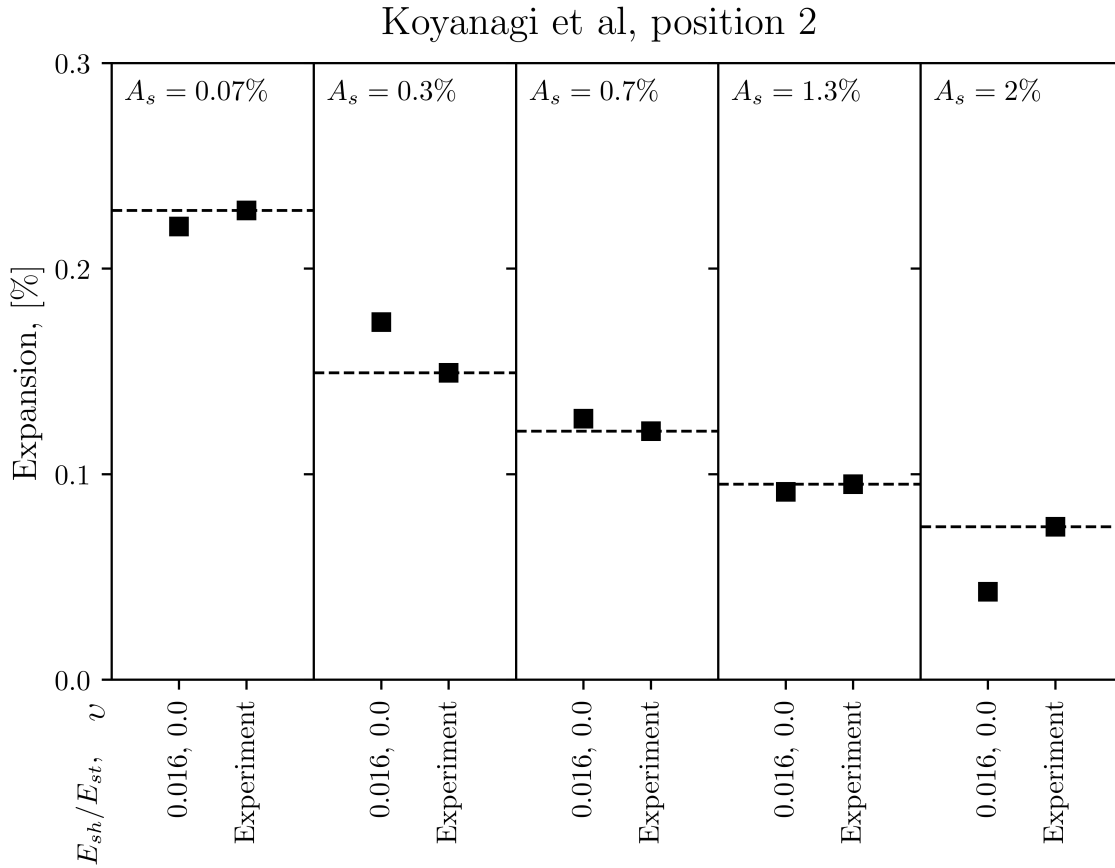
Figure 5.17: Numerical expansions derived from $E_{sh} = 1.6\%E_{st}$ against experimental results, position 2.

5.4 Benchmark: Mohammed et al. (2003)

Mohammed et al. (2003) studied the expansion behaviour of ASR-affected concrete prisms. Concrete prisms with different reinforcement ratios, rebar distributions and bonds are investigated. ASR-induced strains over concrete surface and steel bars are monitored in this benchmark, which makes the simulation of steel stains possible.

5.4.1 Experiment Description

5.4.1.1 Experiment Layout

Plain and reinforced concrete prisms of size $250 \times 250 \times 600$ mm are cast with different rebar configurations as illustrated in Figure 5.18. A combination of different cases implies different objective. A brief explanation is given as follow.

- Case 1 uses concrete prisms with non-reactively mixture regarded as a control case.

- Case 2 uses plain concrete prism with reactively mixture regarded as a free expansion case.

- Case 3, 4, 5 studies the effects of degree of bonds on ASR expansion.

- Case 3 ,6 studies the effects of reinforcement ratio on ASR expansion.

- Case 6 ,7 studies the effects of rebar distribution on ASR expansion.

- Case 7 ,8 studies the effects of stirrups on ASR expansion.
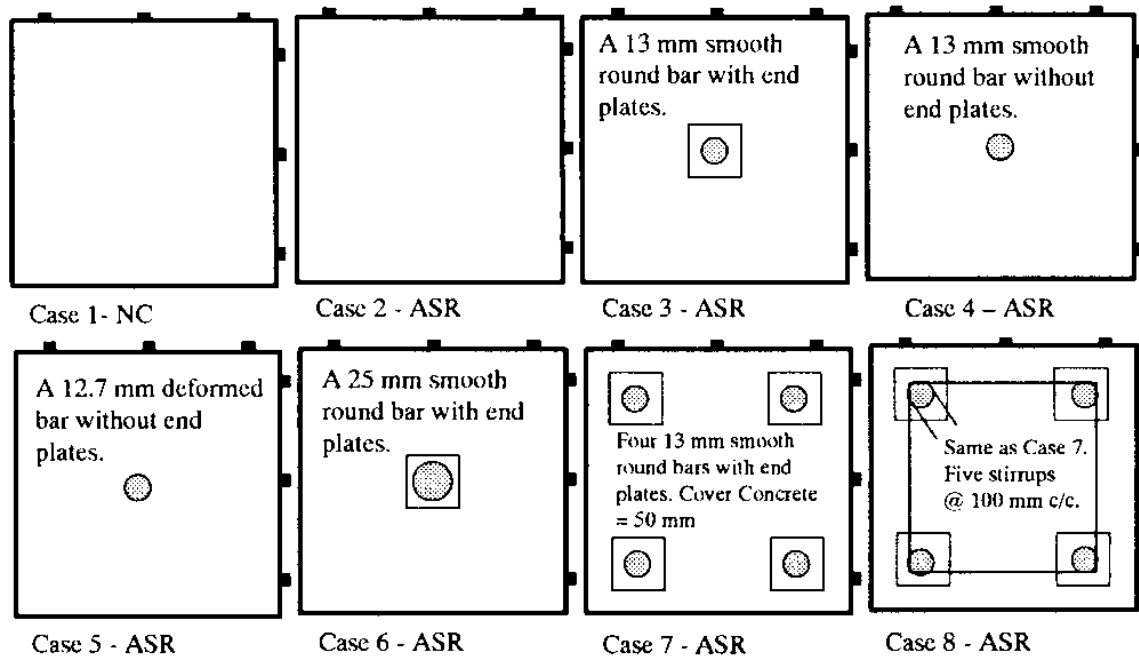
Figure 5.18: Experiment layout, adopted from Mohammed et al. (2003)

It should to noted that the finite element model assumed a fully bonding between steel and concrete, so the influence of bonds cannot be validated. Therefore, **only case 2, 3, 6, 7, 8 are simulated in this thesis work.**

5.4.1.2 Material Properties

Material properties are demonstrated in table 5.3. Mean compressive strength and young's modulus of concrete and all the steel peoperties are given in the paper. Other concrete properties are assumed based on Hendriks et al. (2017).

Table 5.3: Material Properties

		Round bar 13mm	Round bar 25mm	Round bar 6mm
Concrete	Mean compressive strength, MPa	33		
	Mean tensile strength, MPa	2.57		
	Tensile fracture energy, N/mm	0.14		
	Compressive fracture energy, N/mm	34		
	Young's modulus at 28 days, GPa	32		
	Poisson ratio	0.15		
Steel	Yielding stress, MPa	373	370	299
	Ultimate stress, MPa	547	561	489
	Young's modulus, GPa	203	211	196

5.4.1.3 Expansion Measurement

Strain in steel is the average of strains read from the gages attached on the rebar. Strains over concrete surface are measured from demec studs longitudinally (denoted as Lo) and laterally (denoted as La). It can be mathematically expressed as (i is the id of studs as denoted in Figure 5.19):

$$\varepsilon_{Lo} = \frac{\sum_{i=1}^{4} \varepsilon_{i,i+1} + \sum_{i=6}^{9} \varepsilon_{i,i+1} + \sum_{i=11}^{14} \varepsilon_{i,i+1}}{12}$$

48

$$\varepsilon_{La} = \frac{\sum\limits_{i=1}^{10} \varepsilon_{i,i+5}}{10}$$
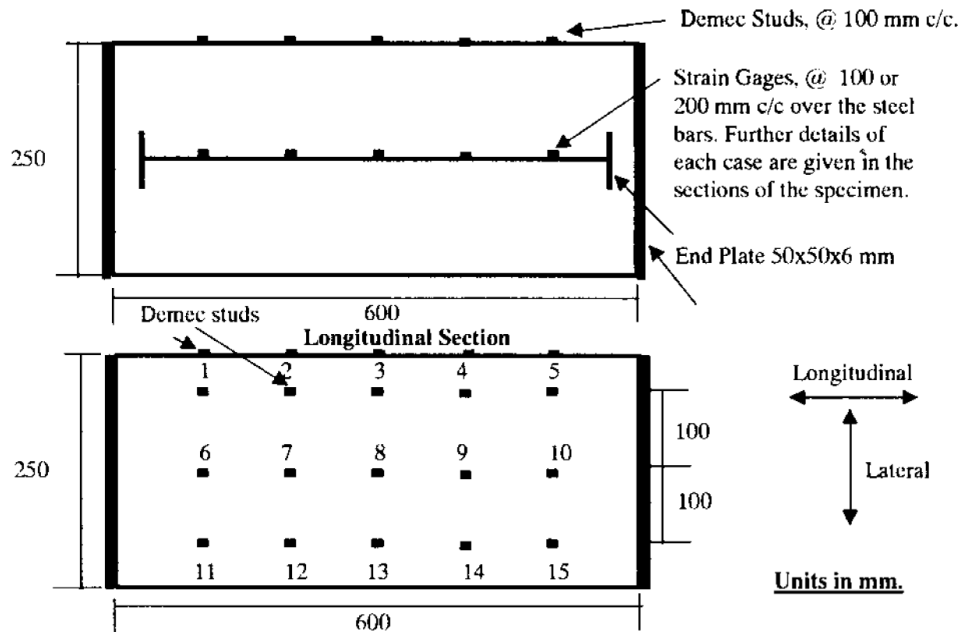

Figure 5.19: Expansion Measurement, adopted from Mohammed et al. (2003)

5.4.1.4   Experimental Results

Three prisms are cast for each case, and results of free expansion is plotted in Figure 5.20. The highly variable results depicted in Figure 5.20 makes the choice of free expansion difficult.
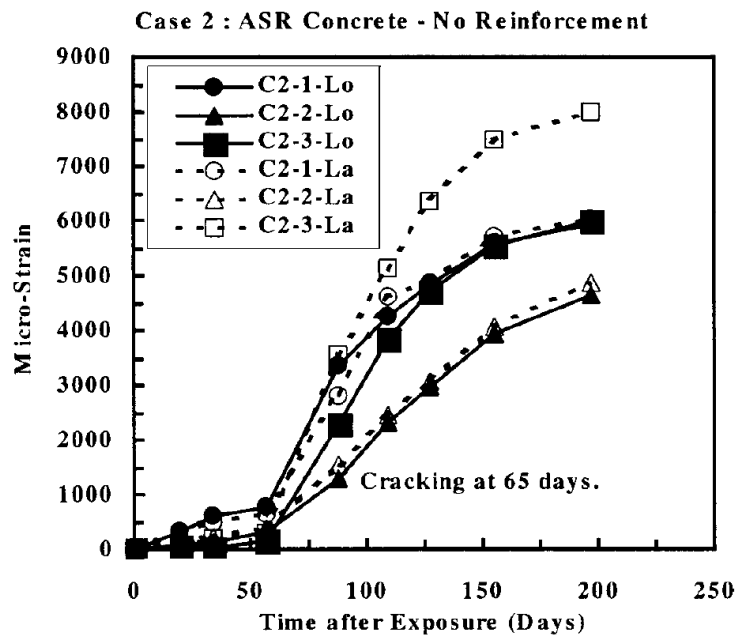

Figure 5.20: Free expansion, adopted from Koyanagi et al. (1992)

Instead of the just taking the mean value, three values, namely, the upper boundary value, mean value and lower boundary value of free expansions are used to simulate the expansion, so that the variability can be taken into account. As an consequence, the restrained expansion is illustrated as an range of upper and lower boundary in the "results" section.

5.4.2 Finite Element Model

Models used for different cases are demonstrated in Figure 5.21. Properties of structural mesh and shadow mesh are listed as below.

- **Structural mesh:** See table 5.3.

- **Shadow mesh:** E_{sh} varies from 1% to 5% of E_{st}, ν_{sh} ranges from 0 to 0.5.
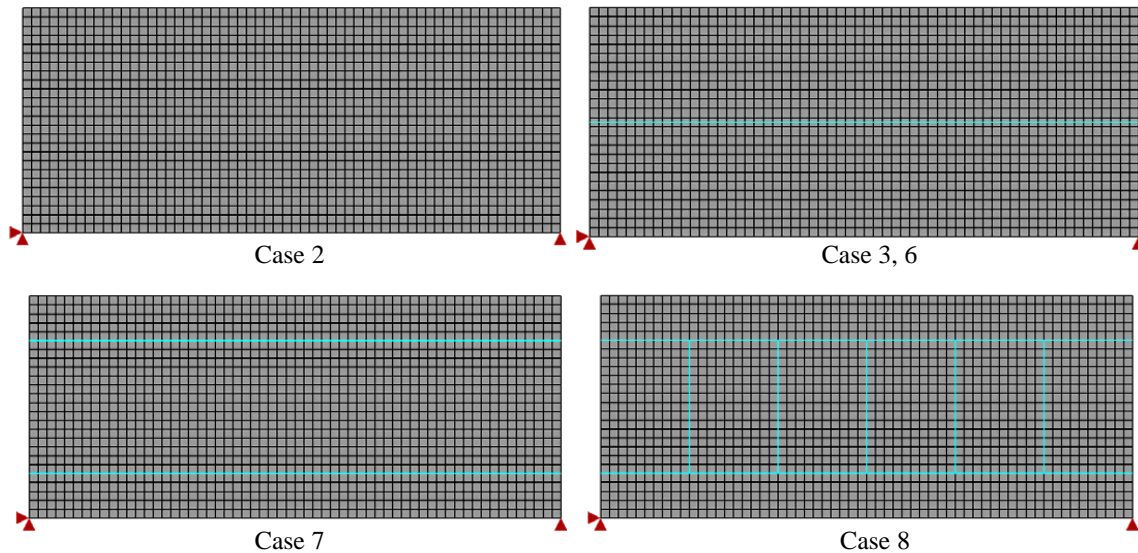
Figure 5.21: Finite element model for different cases, element size: 10 mm.

5.4.3 Results

The upper boundary value (0.79%), mean value (0.6%) and lower boundary (0.46%) value of free expansions are used to simulate the expansion to take into account the variability of free expansions. Main conclusions are given here. More detailed remarks of each case are given in next several pages accompanied with simulation results.

- Failed to find a certain shadow mesh property that can simulate all the cases.

- The use of mean free expansion usually gives a better simulation than using the upper or lower boundary value.

- For experiments with highly variable free expansions, there may exist multiple shadow mesh properties that can give proper simulations.

- Steel strains in numerical models are usually higher than experiments. This is because steel is assumed to be fully bonded with concrete in the model, whereas in reality hundred percent of fully bonding is difficult to achieve special when ASR happens.

- The effects of rebar distribution can be reflected from numerical model, but is less sensitive comparing to experiments. A decease of E_{sh} makes numerical model more sensitive to the effects of rebar distribution.

50

Remarks:

1. A larger free expansion results in a overall larger expansion in concrete and steel.

2. Expansion in lateral direction is always the largest and expansion in steel is always the smallest.

3. Expansion simulated by the chosen shadow mesh properties shows quite large differences comparing with experimental results. However, in the middle figure, a further decrease of E_{sh} seems will give a acceptable results.

● Expansion in concrete, lateral direction

■ Expansion in concrete, longitudinal direction

▲ Expansion in steel

Case 3 - ASR
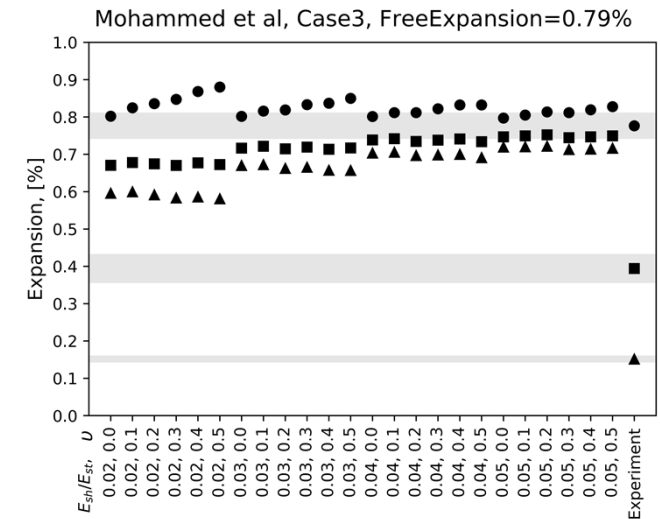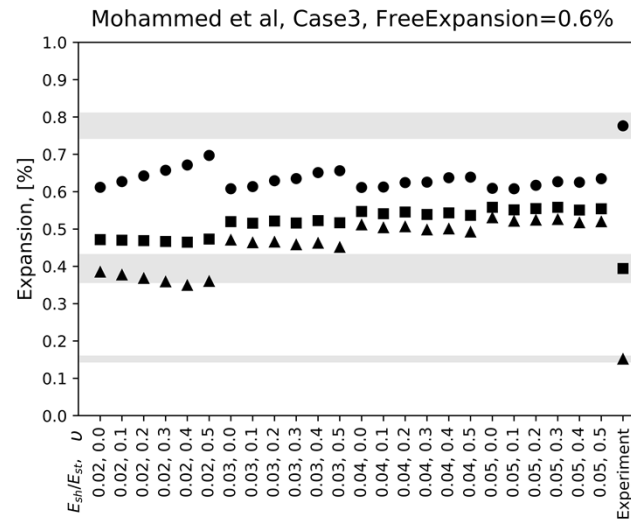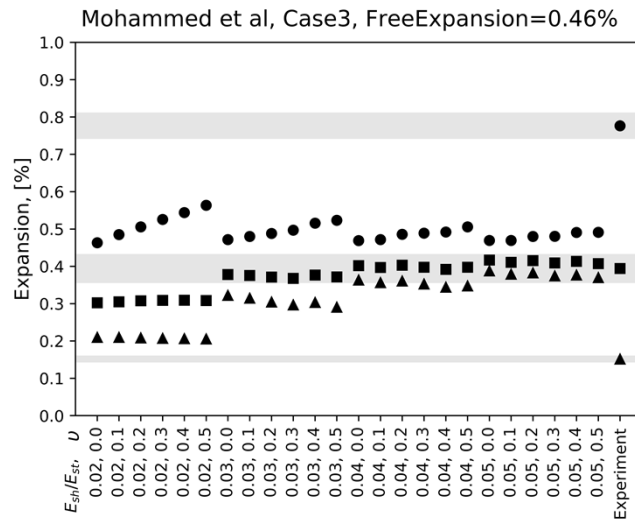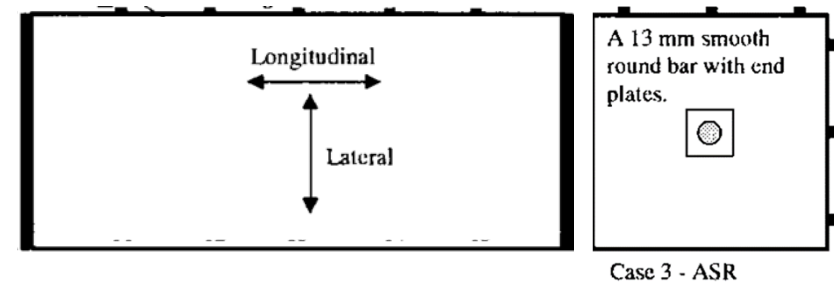
Remarks:

1. FreeExpansion=0.46% cannot give a proper result. FreeExpansion=0.6% and FreeExpansion=0.79% simulate concrete expansion correctly with shadow mesh properties E_{sh}=5%E_{st}, υ_{sh}=0.5 and E_{sh}=2%E_{st}, υ_{sh}=0 (denoted as red column). However, numerical expansion in steel is still higher than experimental results.

2. Both FreeExpansion=0.6% and FreeExpansion=0.79% give satisfying results in concrete expansion, but with different shadow mesh properties. This means for experiments with highly variable free expansions, there may exist multiple shadow mesh properties that can give proper simulations.

● Expansion in concrete, lateral direction

■ Expansion in concrete, longitudinal direction

▲ Expansion in steel

A 25 mm smooth round bar with end plates.
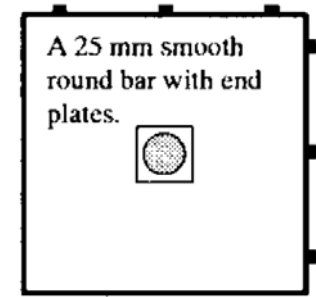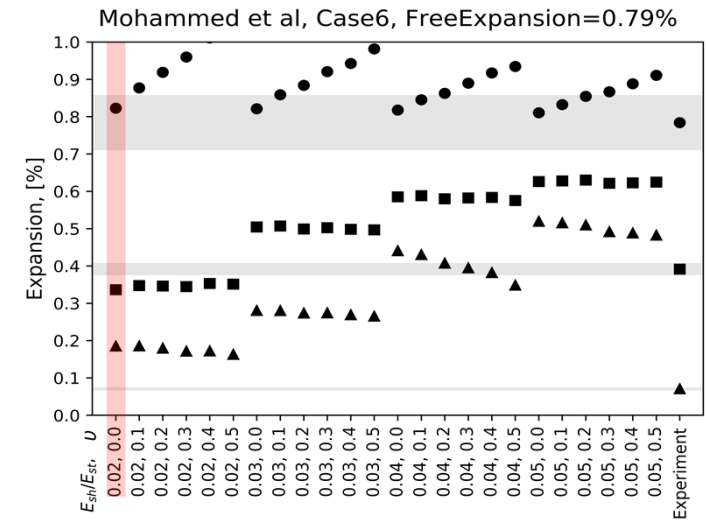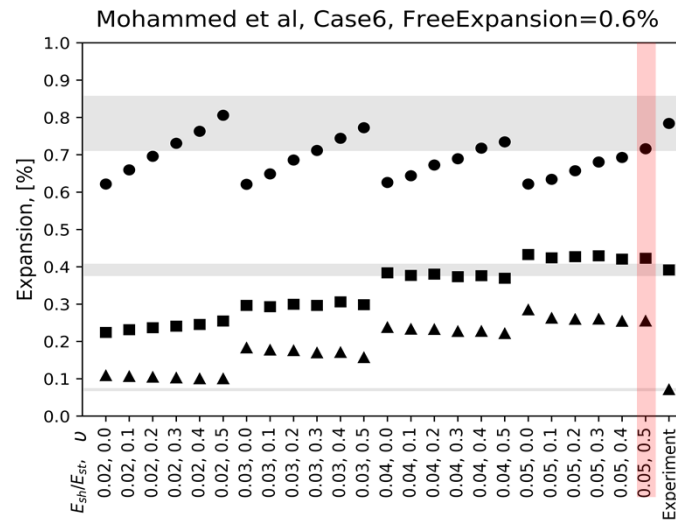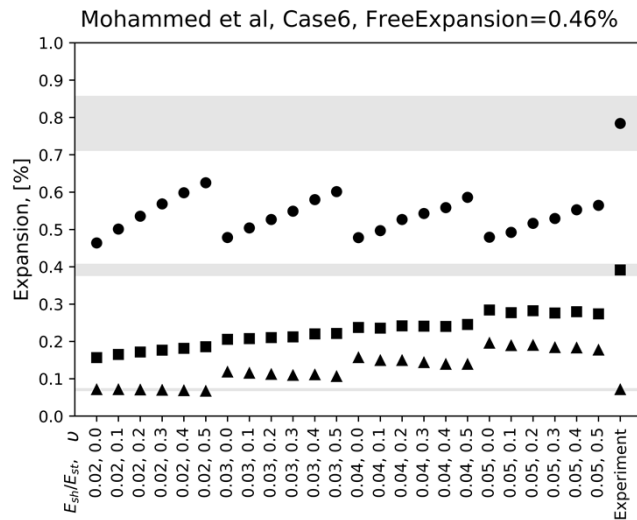
Case 6 - ASR

Remarks:

1. Case 6 and case 7 have a same reinforcement ratio but with different rebar distribution. Both numerical and experimental results indicate that "the four corner distribution" restrains expansion more effectively.
2. The influence of rebar distribution is more obvious when E_{sh} is relatively small. For instance, when $E_{sh}=5\%E_{st}$, longitudinal expansion is approximately the same between case 6 and 7, but when $E_{sh}=2\%E_{st}$, longitudinal expansion in case 7 is smaller than case 6. However, this reduction is even more dramatic from experimental point of view.
3. The best simulation (denoted as red column) is given when FreeExpansion=0.6% with $E_{sh}=2\%E_{st}$, $\upsilon_{sh}=0.2$.

Four 13 mm smooth round bars with end plates. Cover Concrete = 50 mm
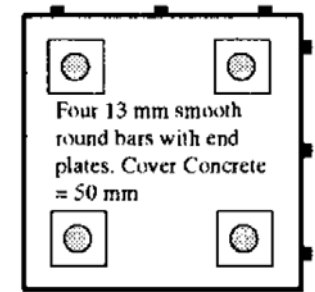
Case 7 - ASR

● Expansion in concrete, lateral direction

■ Expansion in concrete, longitudinal direction
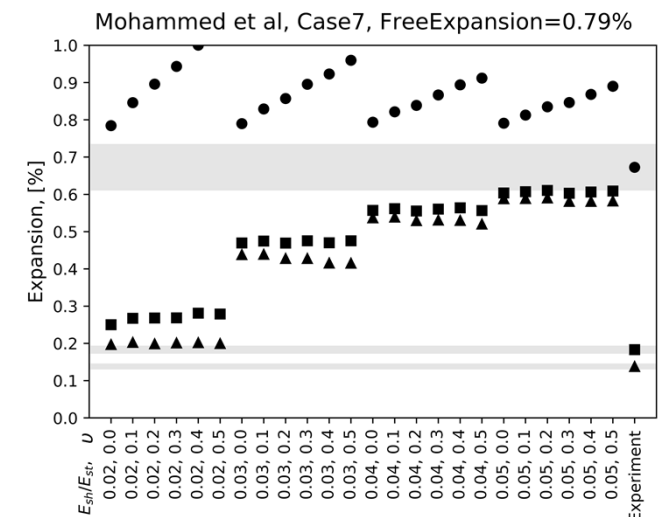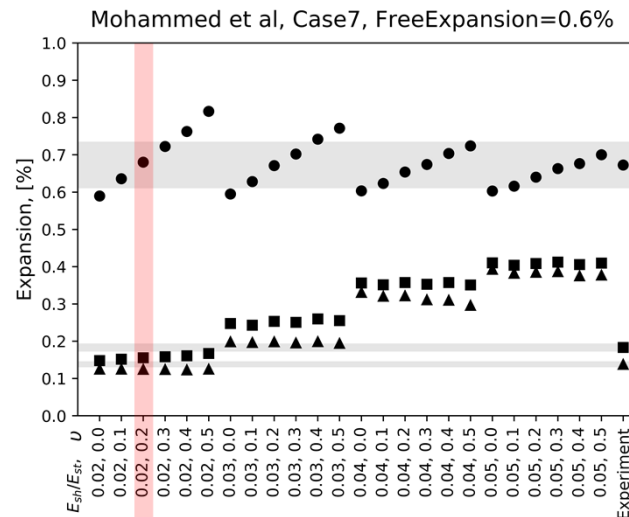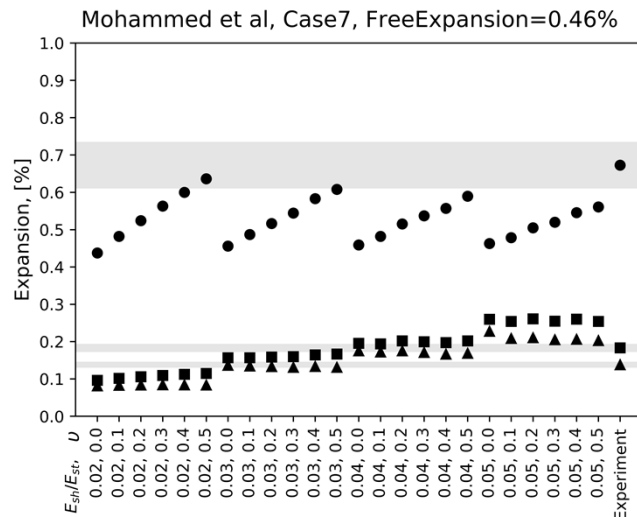
▲ Expansion in steel

Remarks:

1. When stirrup is added, numerical result shows a large reduction in lateral expansion, this reduction is not effectively observed from experimental result.
2. The presence of lateral reinforcement does not influence the longitudinal expansion and vice versa.
3. The best simulation (denoted as red column) is given when FreeExpansion=0.79% with $E_{sh}=2\%E_{st}$, $\upsilon_{sh}=0$.
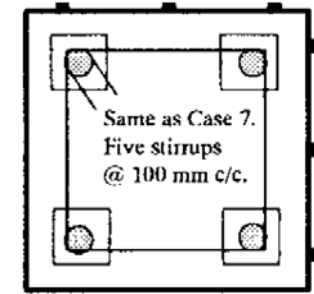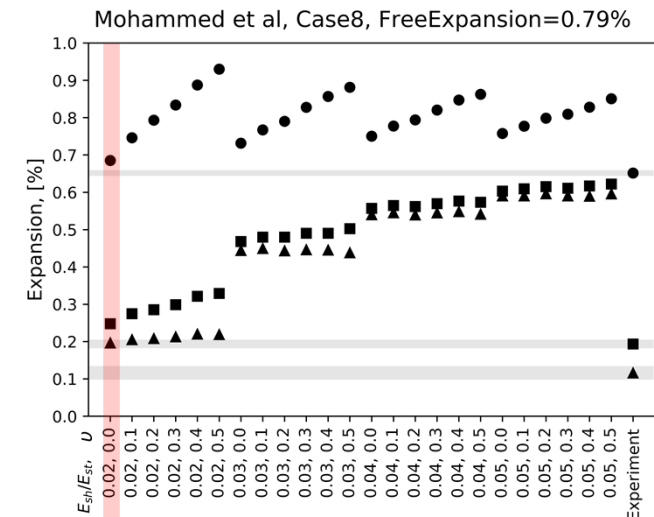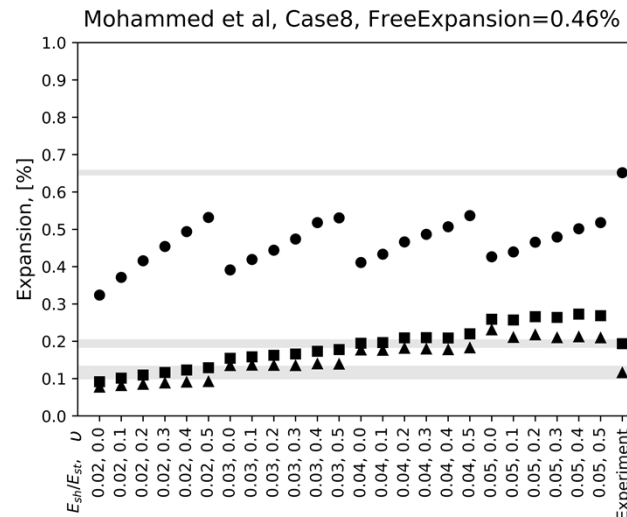

Case 8 - ASR

● Expansion in concrete, lateral direction

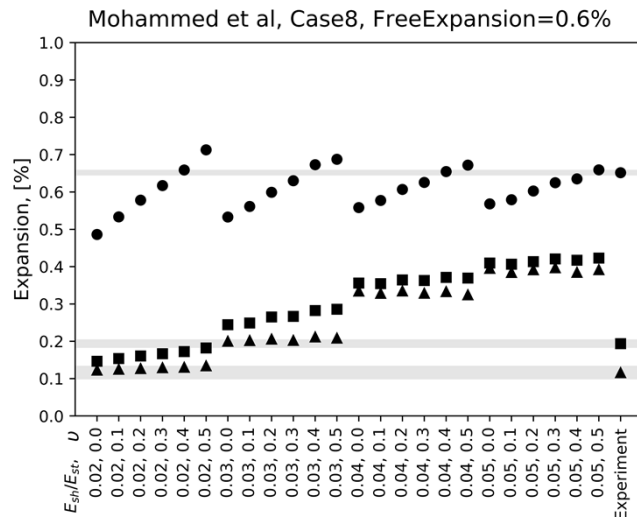■ Expansion in concrete, longitudinal direction

▲ Expansion in steel

Mohammed et al, Case8, FreeExpansion=0.6%

Mohammed et al, Case8, FreeExpansion=0.46%

Mohammed et al, Case8, FreeExpansion=0.79%

5.5 Conclusions

The most appropriate E_{sh} and ν_{sh} for all the cases are collected in Figure 5.22. Experiments from Koyanagi et al. (1992) only measured expansion in one direction, so no valid value for ν_{sh} can be derived from that benchmark. It can be seen that the distribution of ν_{sh} is quite arbitrary, ranging from 0 to 0.5, whereas most of the E_{sh} located close to $2\%E_{st}$ with only two exceptions.

Figure 5.23 shows the relative error between experimental results and numerical results for different value of E_{sh} and ν_{sh}. In the reinforced direction, the relative error decreases with the decrease of E_{sh}. $E_{sh} = 2\%E_{st}$ gives the lowest relative error. It should be noted that a further reduction of E_{sh} will increase the error again but it is not shown in this figure. In the unreinforced direction, $\nu_{sh} = 0.3$ gives the smallest relative error.

To answer the question: Is there a general shadow mesh property that can be used to simulate all ASR expansions? The answer given here is: to some extent, it is possible.

It is possible because by using $E_{sh} = 2\%E_{st}$ and $\nu_{sh} = 0.3$, the relative error of expansion in reinforced and unreinforced direction are 25% and 8%, which are totally acceptable.

However, it is not fully possible because suppose that a proper shadow mesh property is already used, to achieve a successful simulation, the following requirements are still need to be met:

I). A correct choice of free expansion value. Shadow mesh takes care of the physical effects. The chemical effects, such as the amount of reactants, temperature and humidity are taken in account by free expansion. Obtaining a correct free expansion is easy to achieve when the target is a spicemen in the laboratory, but difficult for a completed concrete structure.

II). A global presence of ASR. The numerical model based on the assumption that ASR will globally exist within a concrete member. However, in the reality ASR tends to present on the surface exposed to the environment.

III). Size effect. It is reported that the expansion behaviour between small and large specimens are different. The reason is unknown.
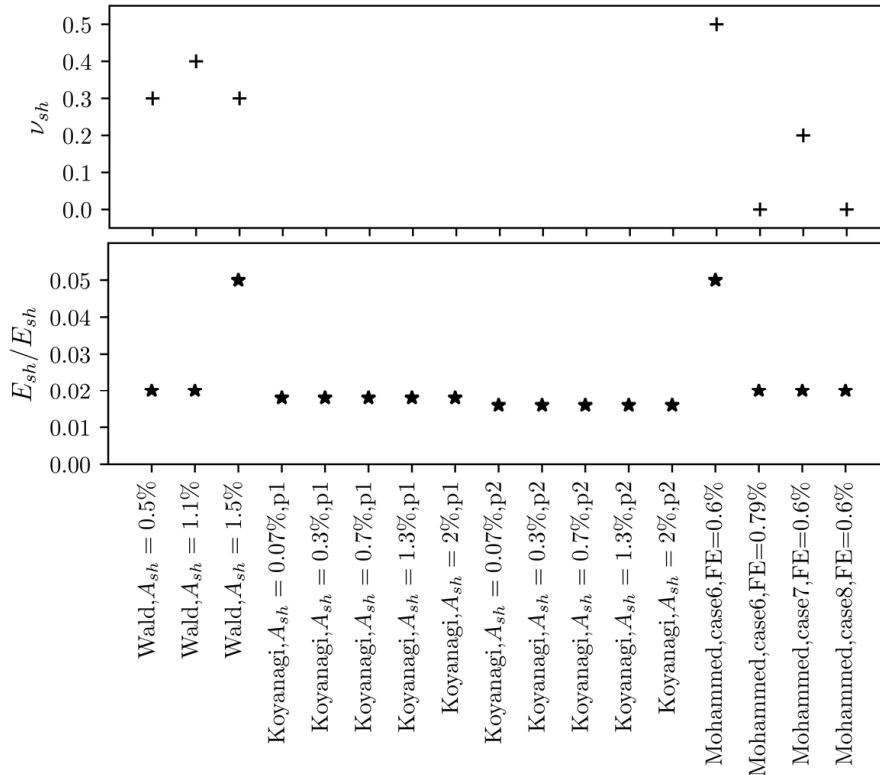

Figure 5.22: A collection of the best E_{sh} and ν_{sh} of all benchmarks.
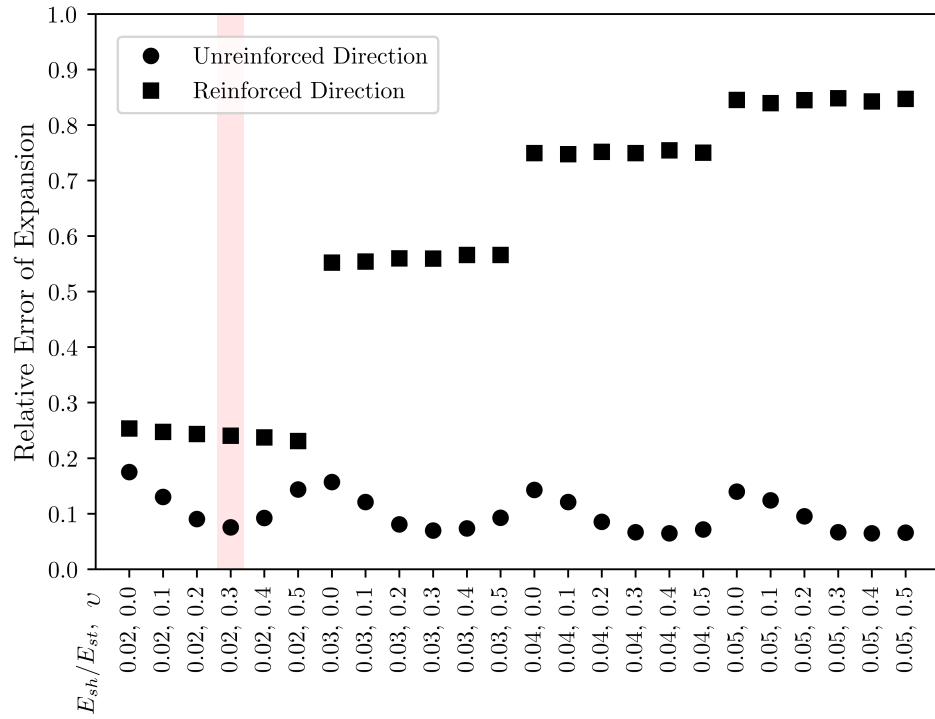
Figure 5.23: Relative error of expansion for different value of E_{sh} and v_{sh}.

.

6

Chapter

Model Validation: Shear Behaviour of ASR affected Concrete Beams

This chapter studies the shear behaviour of ASR-affected reinforced concrete beam. Considering the fact that ASR had a more detrimental effect on beam failed in shear than in bending according to literature review, most of the attention will be paid on the shear capacity of ASR affected beam. Two benchmarks, Ahmed et al. (1998) and Den Uijl and Kaptijn (2002) are selected. Beams from both benchmarks are failed in shear. The difference is that the beams from the Ahmed's benchmark were cast in laboratory, thus the ASR process is accelerated, and the beams from Den Uijl were taken from field and the ASR process was closer to reality.

Before applying shadow mesh to simulate the structural behaviour of ASR-affected beam, a more fundamental validation is performed at first, which is simulating the shear failure of normal (without ASR) reinforced concrete beam. A series of classic experiments performed by Vecchio and Shim (2004) is chosen as the benchmark of this part. Figure 6.1 illustrates the layout of this chapter.
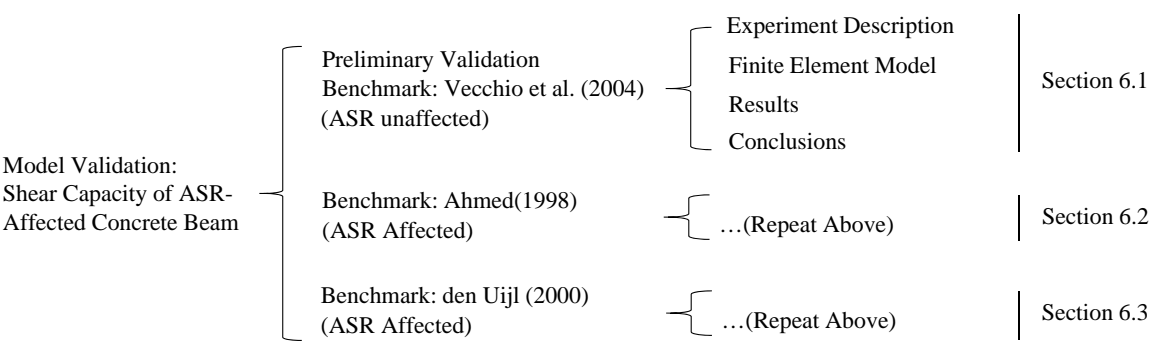
Figure 6.1: layout of this chapter

6.1 A Preliminary Validation: Shear Capacity of ASR Unaffected Concrete Beam. (Benchmark: Vecchio et al. (2004))

6.1.1 Experiment Description

The classic series of beam tests conducted by Bresler and Scordelis 40 years ago to investigate the behavior of reinforced concrete in shear, is commonly acknowledged as a benchmark against with finite element analysis models. Vecchio and Shim (2004) from the University of Toronto repeated the experiments and examined the structural behaviour in terms of load-deflection response, load capacity, and failure mode. It is found that most of the beams are quite well replicated.

For a more comprehensive analysis, one beam is selected from each failure mode to simulate. They are:

- Beam OA3, failed in flexural shear (diagonal tension according to the original paper).

- Beam A1, failed in shear compression.

- Beam C3, failed in flexure compression.

6.1.1.1 Layout

The cross section and elevation details of beam OA3, A1 and C3 are illustrated in Figure 6.2 and Table 6.1.
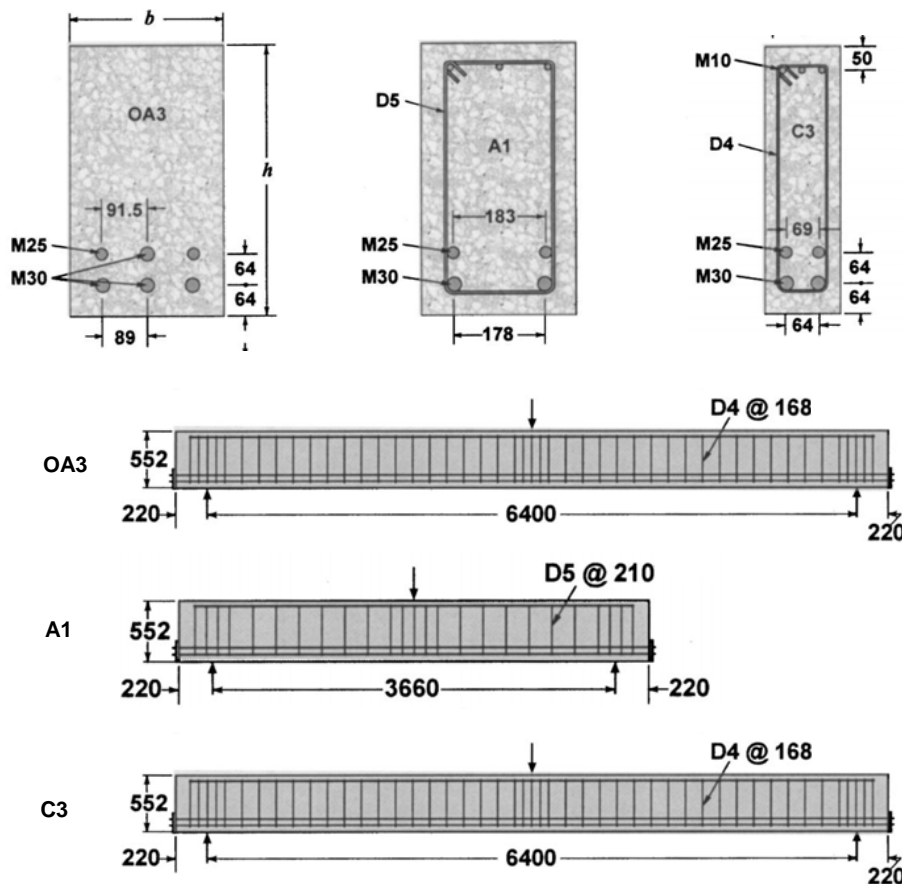

Figure 6.2: Cross section and elevation details

Table 6.1: Cross section and elevation details

Beam number	b (mm)	h (mm)	L (mm)	Span (mm)	bottom steel	top steel	stirrups
OA3	307	556	6840	6400	6 No.9	—	—
A1	307	561	4100	3660	4 No.9	2 No. 4	No. 2 at 210
C3	155	554	6840	6400	4 No.9	2 No. 4	No. 2 at 210

6.1.1.2 Failure Mode

Beam OA3 has failed in flexural shear. Flexural cracks are first initiated at the bottom part of the beam, and then the inclined cracks appear due to the increase of shear force and propagate from support to the concrete compression zone. Finally, the the opening of the critical inclined crack results in the collapse of the beam.

> **Note**
>
> It is worthy to note that in the original paper the failure mode of beam OA3 is defined as diagonal tension failure. According to Yang (2014), depending on whether the diagonal crack is generated from flexural crack or not, the traditional definition of diagonal tension failure can be further distinguished as diagonal tension failure and flexural shear failure. Considering that the diagonal cracks in beam OA3 is arisen from flexural crack, it is more appropriate to define OA3 is failed in flexural shear.

Beam A1 has failed in shear compression. The beginning of this failure mode is similar with flexural shear failure. The difference is that beam failed in shear compression loses its carry capacity because of the crush of concrete in compression zone, while beam failed in flexural shear is due to the opening of inclined cracks.

Beam C3 has failed in flexural compression. Flexural cracks are initiated at the bottom part of the beam, and the beam fails due to the crush of concrete.

6.1.1.3 Material Property

Material properties of reinforcement and concrete are collected in table 6.2. Compressive and tensile fracture energy are calculated based on Mode Code 2010, other properties are given by the paper.

Table 6.2: Mean material property of reinforcement and concrete

	Reinforcement				
Bar size	Diameter (mm)	Area (mm^2)	Yield stress (MPa)	ultimate strength (MPa)	Young's modulus (GPa)
M10	11.3	100	315	460	200
M25	25.2	500	440	615	210
M30	29.9	700	436	700	200
D4	3.7	25.7	600	651	200
D5	6.4	32.2	600	649	200
	Concrete				
Beam number	Cylinder compressive strength (MPa)	Compressive fracture energy (N/mm)	Splitting tensile strength (MPa)	Tensile fracture energy (N/mm)	Young's Modulus (GPa)
OA3	43.5	36*	3.13	0.144*	34.3
A1	22.6	32*	2.37	0.128*	36.5
C3	43.5	36*	3.13	0.144*	34.3

* Calculated based on Mode code 2010

6.1.2 Finite Element Model

Details of finite element model are demonstrated in Figure 6.3. It should be noted that all the three beams are simulated in the same way with the same material model, which is listed as below.

Finite Element Model
- Concrete
  - Element: Plane stress element
    - Nodes: eight-node
    - Size: 25mm
    - Integration scheme: 3 by 3 (high)
  - Material property: See the material property table
  - Material model: Total strain based crack model
    - Crack bandwidth: 25mm
    - Crack orientation: Fixed
    - Tensile behaviour: Exponential
    - Compressive behaviour: Parabolic
    - Shear behaviour: Al-Mahaidi, β=0
- Reinforcement
  - Type: fully embedded reinforcement(perfect bond)
  - Material property: See the material property table
  - Material model: Von Mises plasticity
    - Hardening hypothesis: Strain hardening
    - Hardening type: Isotropic hardening
- Interface(connect beam with supports and loading platforms)
  - Type: 2D line interface
  - Material model: Nonlinear elasticity
    - Normal stiffness modulus: the same as young's modulus of concrete
    - Shear stiffness modulus: young's modulus of concrete / 10^8
    - Normal and shear stiffness reduction in tension
      - Interface opening for reduction: 0.001
      - Reduction factor: 0
- Equilibrium iteration
  - Iterative method: Regular Newton-Raphson
  - Convergence norm(satisfy either of them)
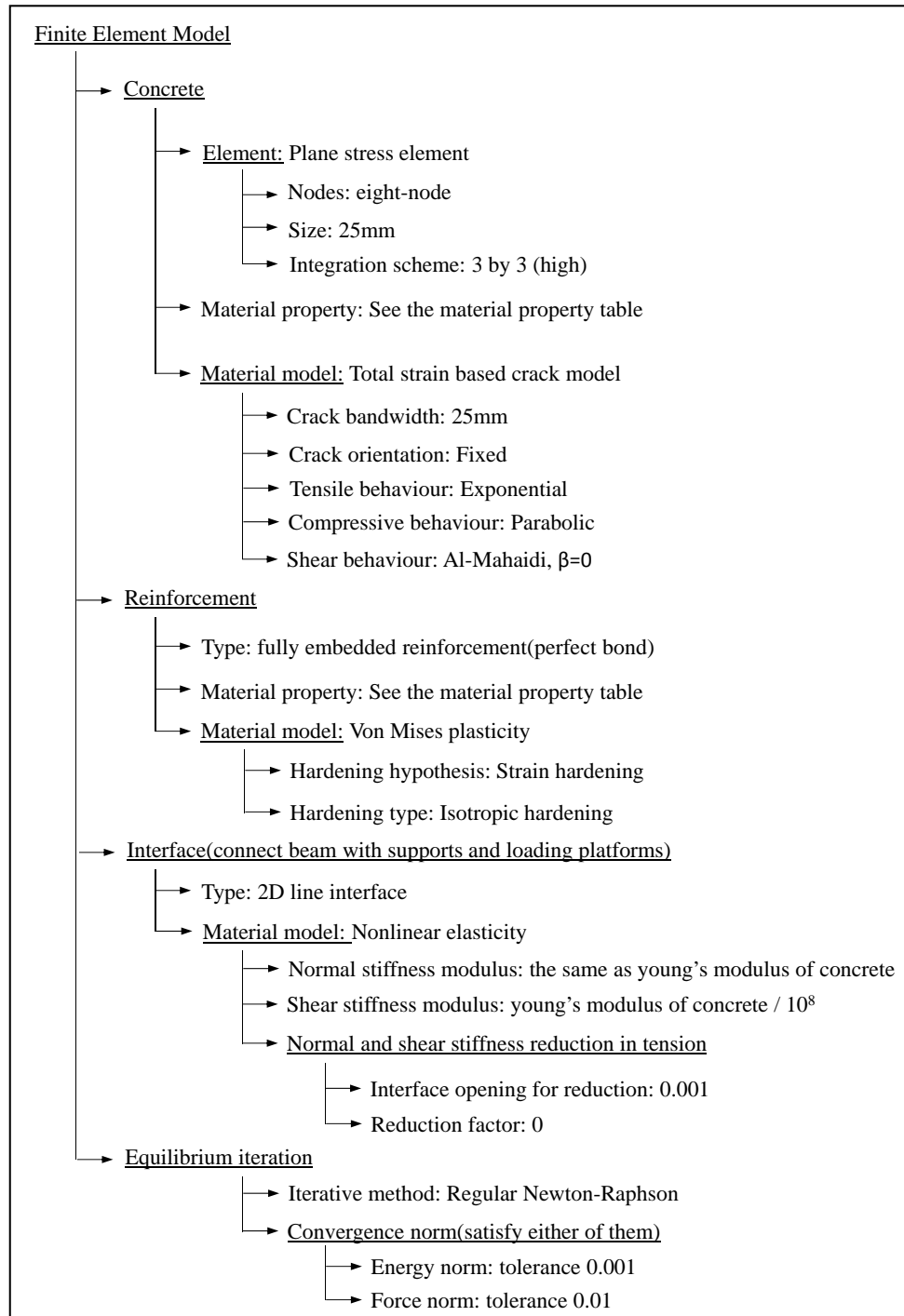   - Energy norm: tolerance 0.001
    - Force norm: tolerance 0.01

Figure 6.3: Details of finite element model

Displacement load is applied on the middle of the span. Basic rigid body movement is confined. Figure 6.3 shows the mesh (25mm) together with load and boundary condition.
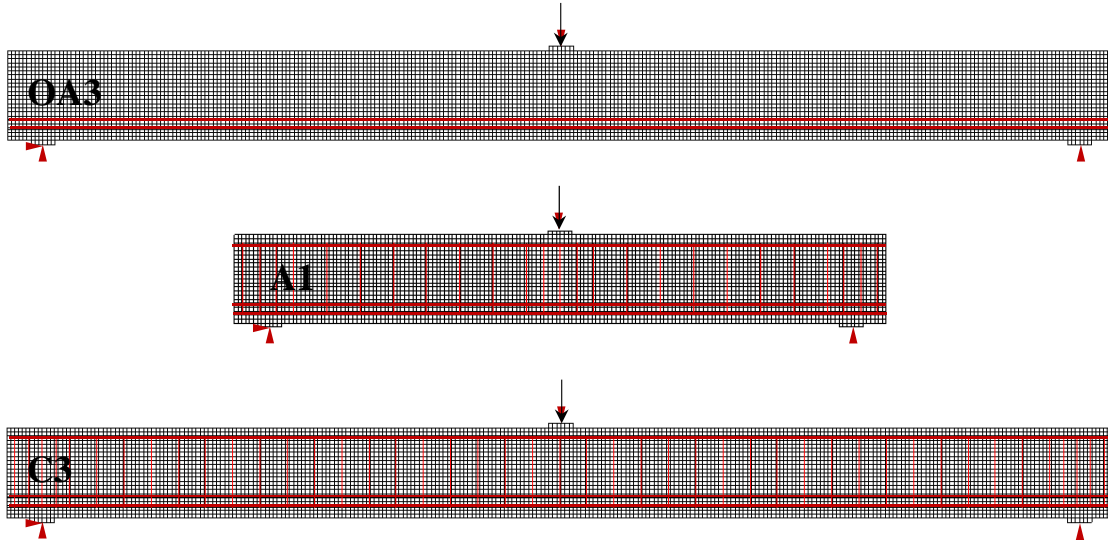
60

Figure 6.4: Mesh, load and boundary condition

6.1.3 Results

The result of beam OA3, A1 and C3 is presented individually. Aspects of behavior of the numerical and experimental beams are compared and discussed, including load-deflection response, load capacity, and failure mode.

6.1.3.1 Beam OA3

Beam OA3 has failed in flexural shear (diagonal tension as mentioned in the original paper) so that a brittle failure behaviour is observed from the load -deflection curve. A good agreement between numerical and experimental result is shown in Figure 6.5.
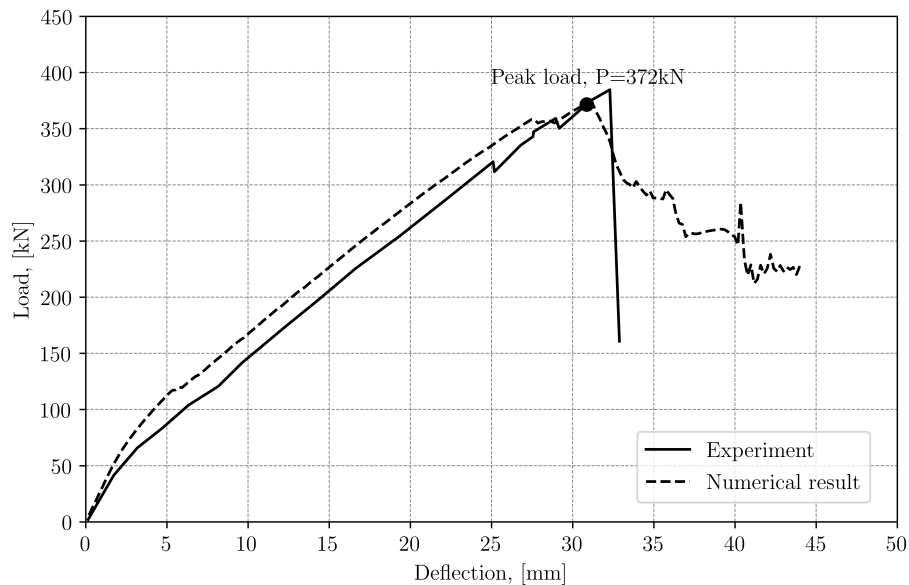
Figure 6.5: Beam OA3, load-deflection curve. [Keywords: fixed crack model, shear behaviour: Al-Mahaidi, $\beta = 0$, element size=25mm]

Parabolic curve is used for compressive behaviour, based on which, the corresponding principal strain at peak principal compressive stress is calculated as:

$$\varepsilon_0 = -\frac{5}{3}\frac{f_c}{E_c} = -\frac{5}{3} \times \frac{43.5}{34300} = -2.1 \times 10^{-3} \tag{6.1}$$

Concrete starts the crush softening when the minimum principal strain is smaller than ε_0. The part of the curve which represents crush is marked in red as shown in Figure 6.6 It should bear in mind that the red part curve is crack bandwidth dependent. The crack bandwidth of the presented curve is 25mm.

The crush area of beam OA3 at failure is very small, which verified that the loss of carry capacity is because of the opening of critical inclined crack instead of the crush of concrete in compressive zone.
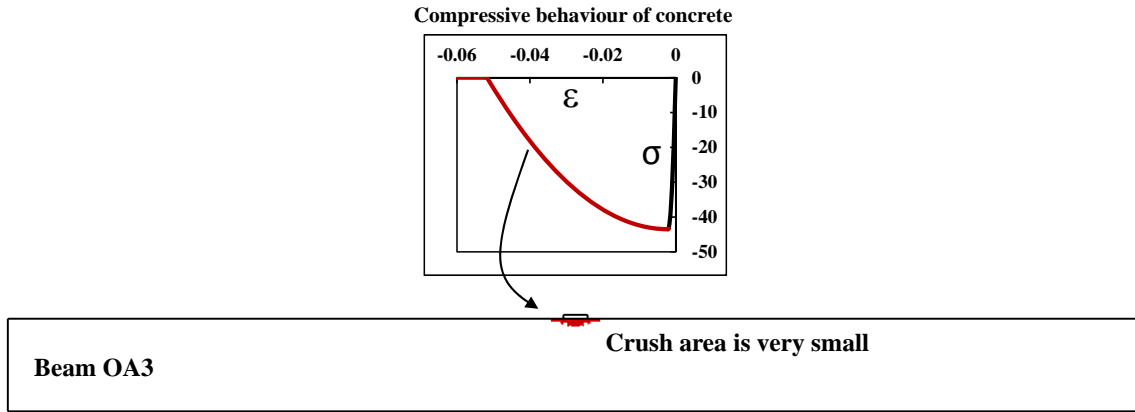

Figure 6.6: Beam OA3, minimum principal strain at peak load

Two longitudinal rebars are made from different steel. The upper rebar is made from M25 and the lower rebar is made from M30 (check table 6.2). The material properties of M25 and M30 are extremely close. For the convenient reason, the property of M25 is used for analysing both rebars. The yielding strain of M25:

$$\varepsilon_y = \frac{f_y}{E_s} = \frac{440}{210000} = 2.1 \times 10^{-3} \tag{6.2}$$

The ultimate strain is assumed to be 5% according to Mode Code 2010:

$$\varepsilon_u = 0.05 \tag{6.3}$$

Isotropic hardening is used for the steel material model. The hardening part is marked in red. As shown in Figure6.7 only the lower rebar is yielded at the peak load.
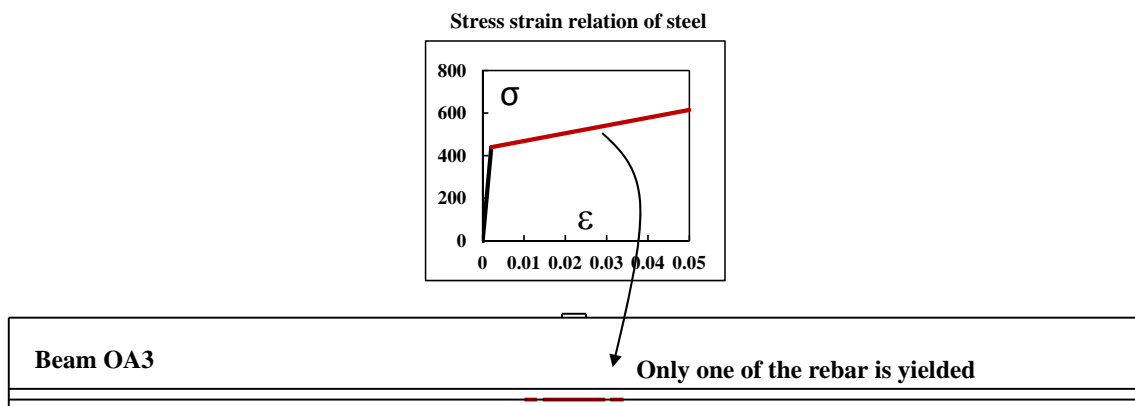

Figure 6.7: Beam OA3, yielding of bottom rebar at peak load

Figure 6.8 shows the crack pattern at the peak load against with the result of experiment. A good agreement can be observed on the small flexural cracks and the major inclined cracks. The horizontal crack that propagates towards the left support due to debond is not able to describe since the fully embedded reinforcement is applied in the model.

> **Note**
>
> In the total strain based crack model, the crack strain is calculated as follow:
>
> $$\varepsilon_{cr} = \varepsilon_i - \frac{\sigma_i}{E_0}$$
>
> Where,
> ε_{cr} is the crack strain
> ε_i is the total principal strain at current stage
> σ_i is the total principal stress at current stage
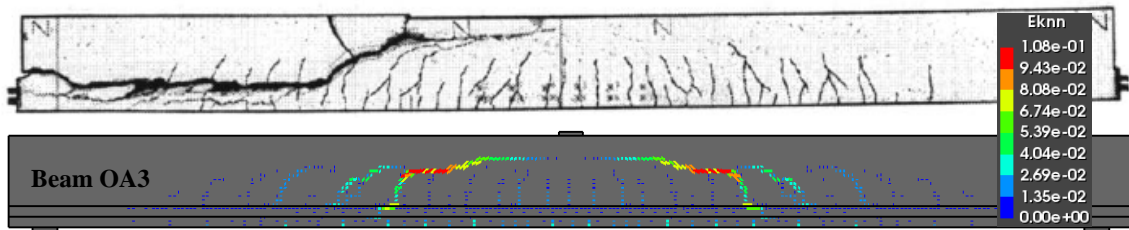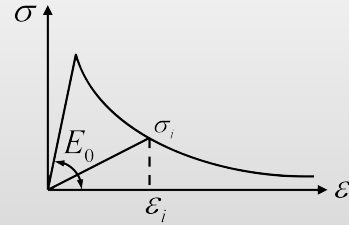> E_0 is the original Young's modulus

Figure 6.8: Beam OA3, crack strain at peak load comparing with experiment

> **Note**
>
> A plane stress element can have up to two cracks at the same time. Each crack has normal crack strain and shear crack strain. The "Eknn" shown in Figure 6.8 represents the normal crack strain of the larger crack among the two cracks.

6.1.3.2 Beam A1

Beam A1 has failed in shear compression. Beam failed in shear compression loses its load bearing capacity due to the crush of concrete in the compressive zone and usually shows a brittle failure behaviour. Figure 6.9 depicts the load-deflection curve of both the model and the experiment. An overestimation of initial stiffness can be observed from the numerical result. The beam failed at a larger deflection than the experiment but the peak load value is close.
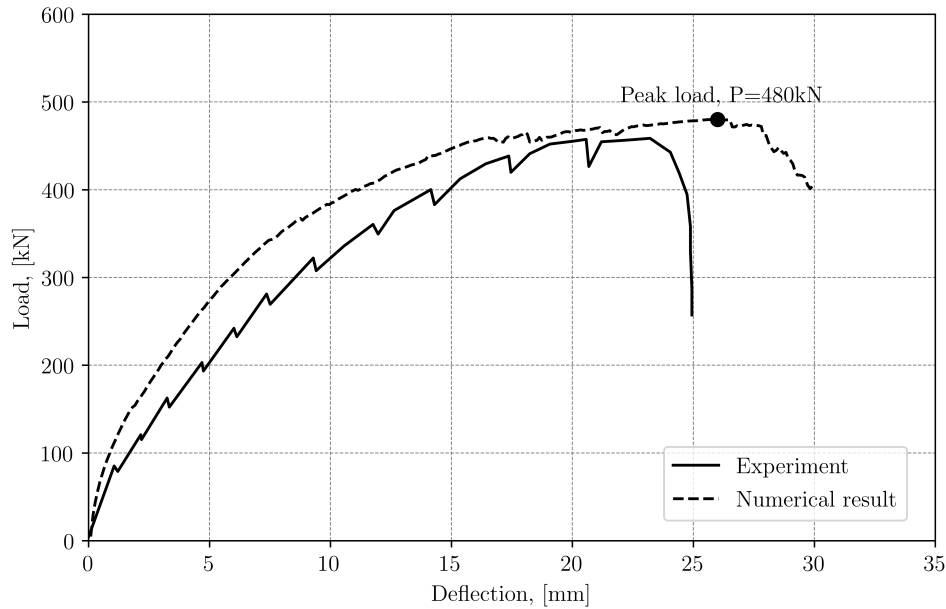

Figure 6.9: Beam A1, load-deflection curve. [Keywords: fixed crack model, shear behaviour: Al-Mahaidi, $\beta = 0$, element size=25mm]

The corresponding principal strain at peak principal compressive stress is calculated as:

$$\varepsilon_0 = -\frac{5}{3}\frac{f_c}{E_c} = -\frac{5}{3} \times \frac{22.6}{36500} = -1.03 \times 10^{-3} \tag{6.4}$$

Following the same procedure as performed for beam OA3. A larger crush area can be observed as shown in Figure 6.10, which verifies that beam A1 is failed in shear compression.
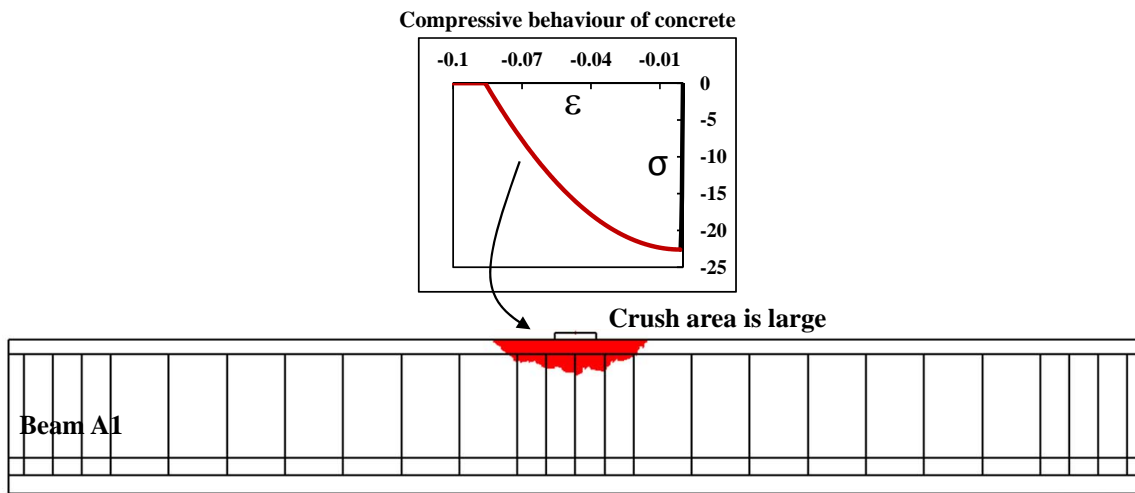

Figure 6.10: Beam A1, minimum principal strain at peak load

Both longitudinal rebars are yielded at the peak load. Shear capacity is increased due to the presence of stirrups. Therefore the longitudinal reinforcements can be utilized more effectively compared with beam OA3, where there is no stirrups so only the bottom rebar is yielded.
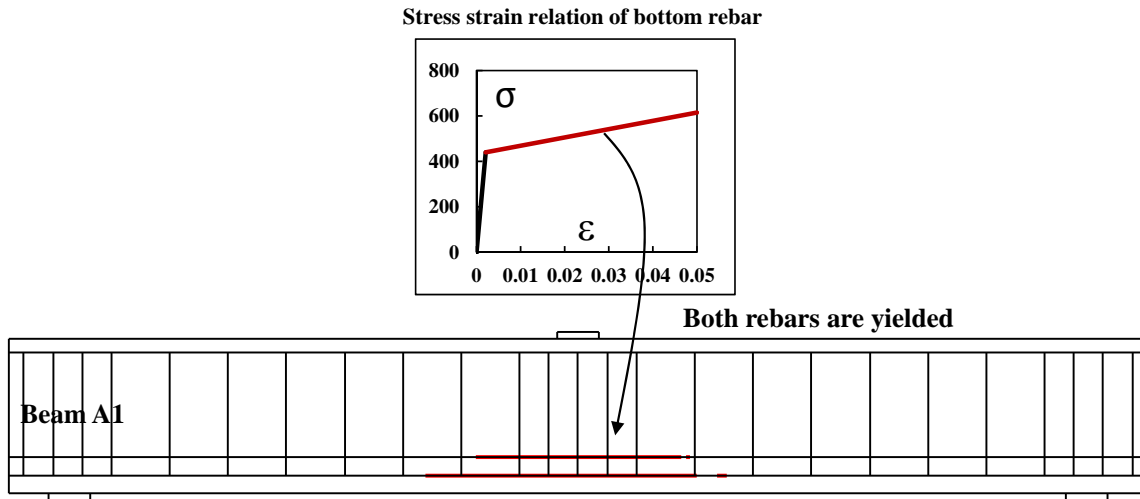
Figure 6.11: Beam A1, yielding of bottom rebars at peak load

The yielding stress of stirrups:

$$\varepsilon_y = \frac{f_y}{E_s} = \frac{600}{200000} = 3.0 \times 10^{-3} \tag{6.5}$$

The ultimate strain is assumed to be 5%:

$$\varepsilon_u = 0.05 \tag{6.6}$$

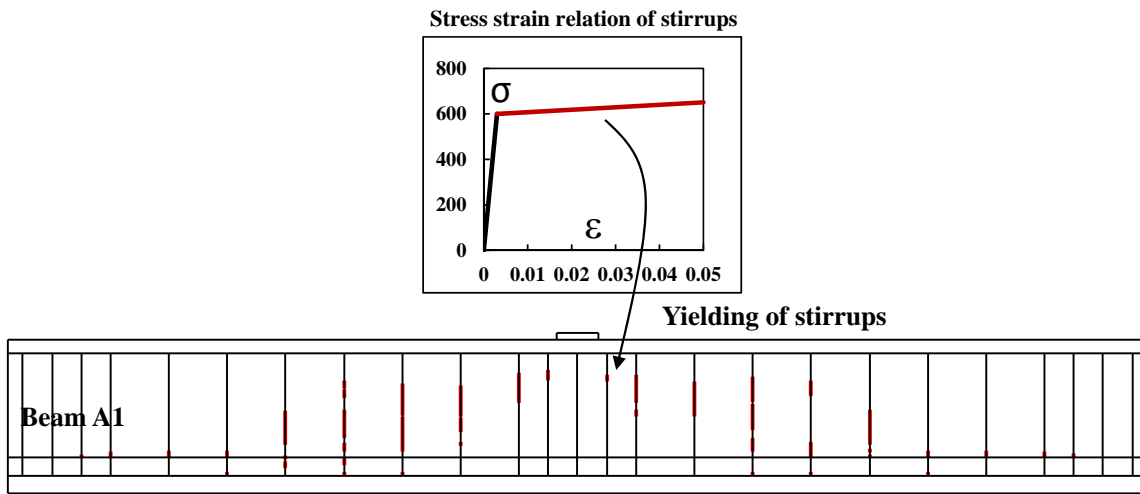Figure 6.12 demonstrates the yielding part of the stirrups.

Figure 6.12: Beam A1, yielding of stirrups at peak load

Figure 6.13 shows the crack pattern from numerical analysis compared with the experiment. A larger crush area at the concrete compressive zone can be observed from the experimental crack pattern, which verifies the crush area simulated in Figure 6.10. The crack pattern from numerical result shows a good agreement with the experimental result.
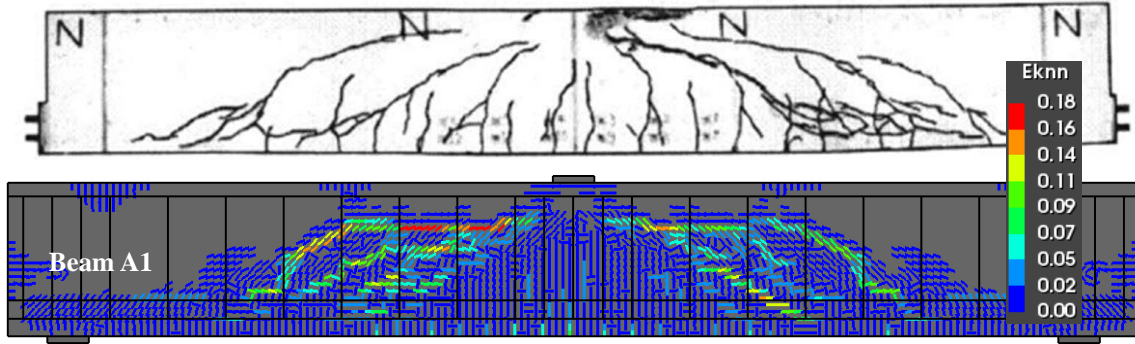
Figure 6.13: Beam A1, crack strain at peak load comparing with experiment

6.1.3.3 Beam C3

Figure 6.15 illustrates the load-deflection curve from experiment against with the numerical result, a good agreement in stiffness and peak load value is shown. The failure mode of beam C3 is flexural compression, which means the beam is failed in bending. Thus, a more ductile failure behaviour is observed. Eventually the beam loses its load bearing capacity due to crushing of concrete in compressive zone. The crush can be clearly seen in Figure 6.18.
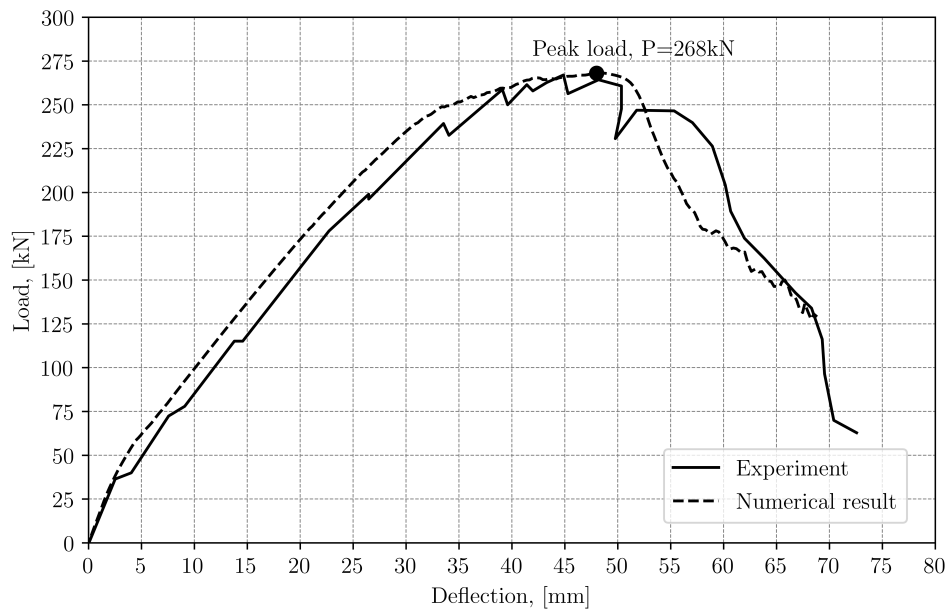

Figure 6.14: Beam C3, load-deflection curve. [Keywords: fixed crack model, shear behaviour: Al-Mahaidi, $\beta = 0$, element size=25mm]

Based on the parabolic compressive behaviour, the corresponding principal strain at peak principal compressive stress is calculated as:

$$\varepsilon_0 = -\frac{5}{3}\frac{f_c}{E_c} = -\frac{5}{3} \times \frac{43.5}{34300} = -2.1 \times 10^{-3} \tag{6.7}$$

Compressive strain where is vectorially larger than ε_0 is regarded as crushed and marked in red in Figure 6.15.
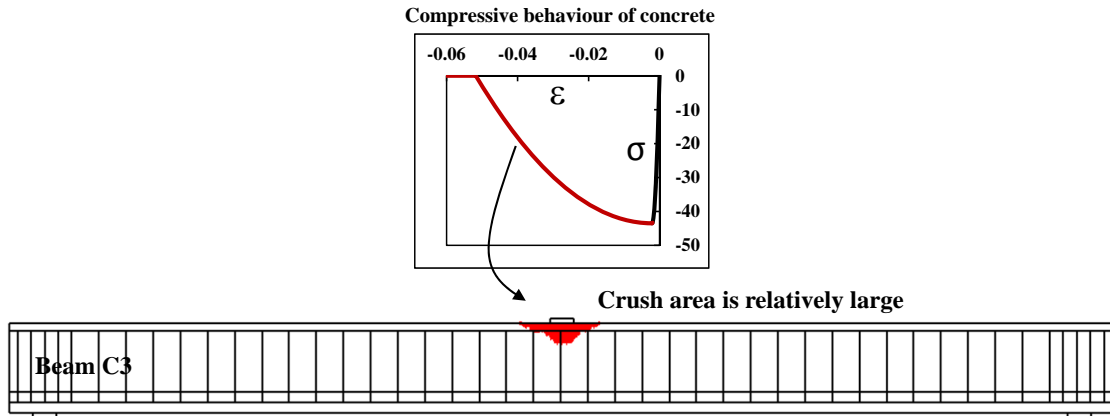
Figure 6.15: Beam C3, minimum principal strain at peak load

By using the same strategy for beam OA3, the yielding of bottom rebars of beam C3 is depicted in Figure 6.16.
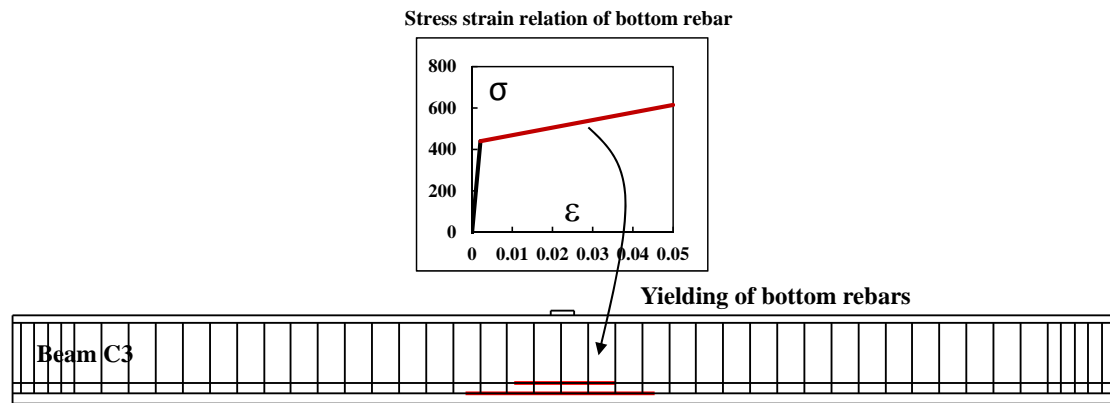
Figure 6.16: Beam C3, yielding of bottom rebars at peak load

Figure 6.17 shows the yielding of the stirrups at the peak load step.
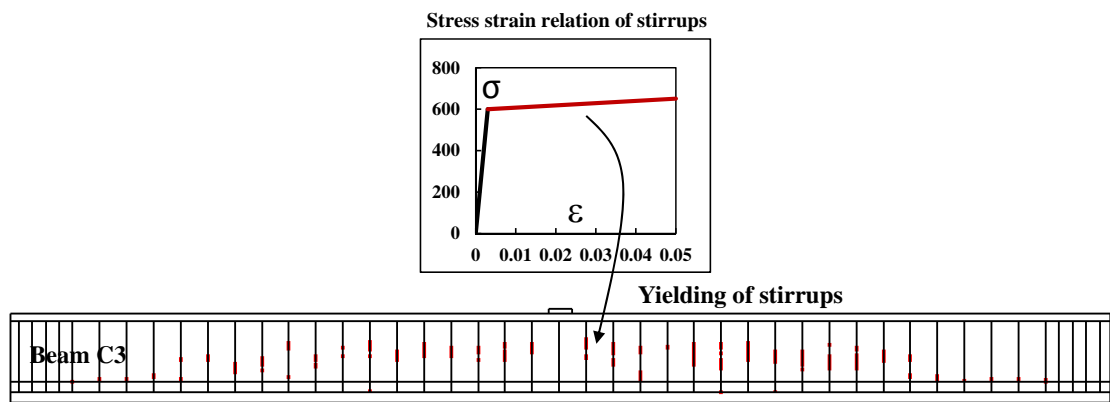
Figure 6.17: Beam C3, yielding of stirrups at peak load

Figure 6.18 shows the crack pattern of experiment at failure and numerical model at steps of peak load and 0.9 times peak load. The crack pattern at step of 0.9 times peak load is better coincided with experiment. With the further development of the compressive strut, horizontal cracks are arisen from flexural cracks, which are not observed from experiment.

Crack strain at 0.9 x peak load

Crack strain at peak load

Figure 6.18: Beam C3, crack strain at different load steps comparing with experiment

6.1.4 Sensitivity study

In the previous section, beam OA3, A1 and C3 are simulated by using the same material model, which is the fixed crack model of Al-Mahaidi shear behaviour with the minimum shear retention factor $\beta = 0$, and the element size is 25mm. The good aspect is 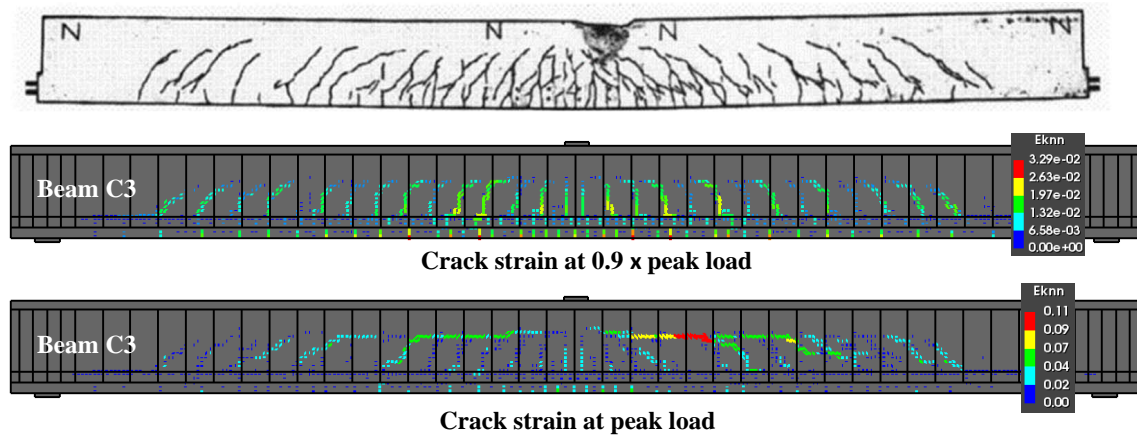that great agreements are obtained for all three beams by using the same material model, which ensures the consistency of the analysis. However, it is also found that the result is highly dependent on the choice of material model. Therefore, a sensitivity study is performed, aiming to point out the effects of different material models on the numerical result. The results demonstrated below are the results of sensitivity study of beam OA3, other two beams showed the same regularity.

Material model used in previous sections is noted as the reference case. Each time only one parameter is changed, and others are kept the same. Figure 6.19 shows the layout of sensitivity study.

The reference case :

Fixed crack model, Al-Mahaidi shear behaviour, minimum retention factor β=0, element size=25mm

Element size=75mm
others remain the same.

Change β to 0.01,
others remain the same.

Change to damaged based shear behaviour,
others remain the same.

Change to rotating crack model,
others remain the same.
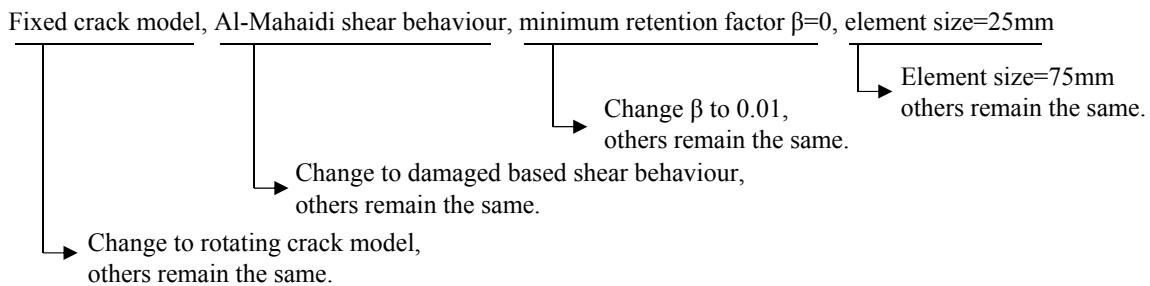
Figure 6.19: The layout of sensitivity study of beam OA3

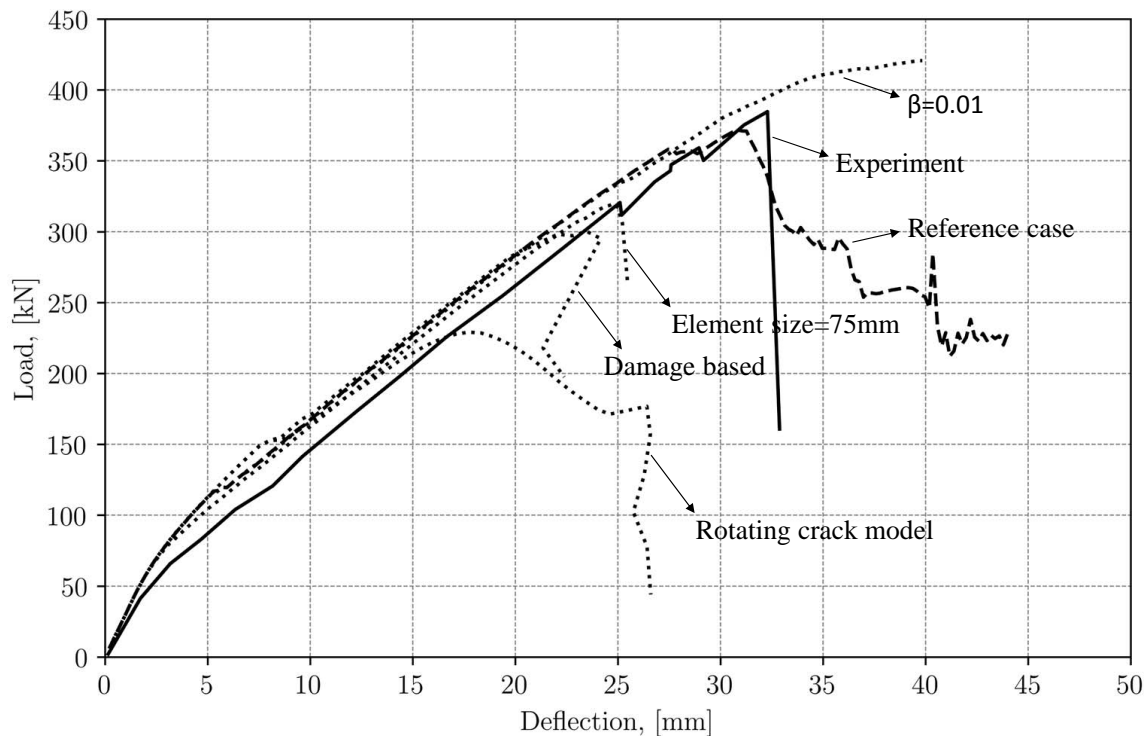Figure 6.20: The results of sensitivity study of beam OA3

As can be seen in Figure 6.20, the change of material property will not affect stiffness, but the peak load value is changed from case to case.

Rotating crack model gives the lowest peak load value, which is expected since in the rotating crack model the crack direction is always coaxial with the principal strain. Thus, with the increase

of principal strain, the decrease of stress (softening) is the fastest. Rotating crack model can be considered as a lower bond approximation.

Damage based shear behaviour gives lower peak load value than the Al-Mahaidi shear behaviour. In Al-Mahaidi, shear stiffness decreases as a function of normal total strain, and in the Damage Based model shear stiffness decreases with the decay of tensile stress. It seems that the shear stiffness in damage based model decreases in a more conservative manner than Al-Mahaidi model.

A larger minimum shear retention factor increases the peak load value.

The increase of element size decreases the peak load value. In smeared cracking model, the stress-strain relation is dependent on the the crack bandwidth, and usually the crack bandwidth is dependent on the element size. In a large element, the cracking stress at a certain strain stage is smaller than small element. This is the reason that in smeared crack model, a larger element size generally gives a lower resistance.

6.1.5 Conclusions

Beam OA3, A1 and C3 from benchmark Vecchio and Shim (2004) are simulated with fixed cracking model, accompanying with a sensitivity study. Results derived from three different beams indicated some general agreements. For the lower bond estimation, rotating crack model is recommended. For analysing the experimental result, fixed crack model with Al-Mahaidi shear behaviour function generally gives better simulations.

This section is regarded as a preliminary validation for simulating ASR affected beams and no aforementioned shadow mesh is involved. From the next section, we will start the simulation of ASR affected beams, with the application of the shadow mesh.

6.2   Benchmark: Ahmed(1998)

Ahmed et al. (1998) studied the shear behaviour of eight reinforced concrete beams affected by alkali silica reaction (ASR) under static and cyclic loading. The results of the ASR affected beams were compared to another eight identical reinforced concrete beams that were not affected by alkali-silica reaction. Results indicate that the ASR enhanced the shear capacity of reinforced concrete beams and ultimately lead to increases in their lifetimes.

6.2.1   Experiment Description

6.2.1.1   Layout of Specimens

Ahmed et al. (1998) studied the shear behaviour of ASR affected concrete beams under static and cyclic loads. In this thesis, only the static load is interested. Four beams are loaded statically:

- Beam S1: Beam without stirrups and poor anchorage of longitudinal reinforcement.

- Beam S2: Beam without stirrups and good anchorage of longitudinal reinforcement.

- Beam S3: Beam with stirrups and poor anchorage of longitudinal reinforcement.

- Beam S4: Beam with stirrups and good anchorage of longitudinal reinforcement.

Considering that the fully embedded reinforcement used in the numerical model representing a perfect anchorage, beam S2 is selected as the target beam to simulate. The details of beam S2 is depicted in Figure 6.21. Two concrete mixes were used for beam S2; one mix allowed the alkali-silica reaction to develop and is referred as Mix A. The second mix did not allow the ASR reaction to take place and is referred as the control or sound Mix C.
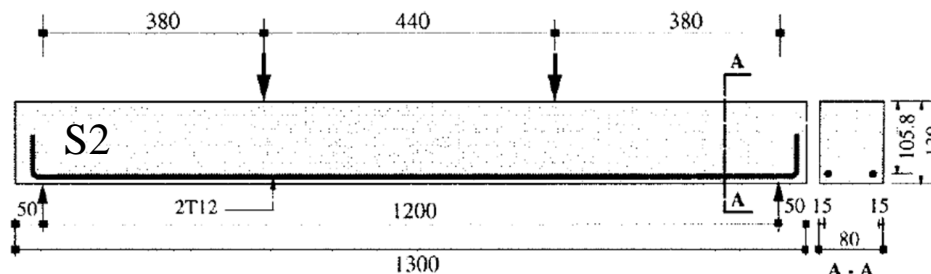

Figure 6.21: Details of beam S2

6.2.1.2   Material Properties

Three different levels of material properties are distinguished. The material property of level I is measured from ASR unaffected concrete, representing the material property of sound concrete. Level II is measured from ASR affected concrete, representing the real reduction in that specific case. In ASR affected concrete, the reduction of properties can be expressed as a function of expansion. Based on the relation between the lower bond residual mechanical properties and the expansion that given by ISE (1992), a more conservative property level can be defined, which is level III. Since at level III, material properties are predicted by using the lower bond residual properties, usually it gives the largest reduction and thus the most conservative results. Material properties at different levels are shown in Table 6.3.

Table 6.3: Material properties of reinforcement and concrete

Material properties	Steel					
	Diameter (mm)	Area (mm^2)	Number per beam	Yielding stress (N/mm^2)	Hardening	Modulus of elasticity (kN/mm^2)
bottom rebar	12	113.1	2	460	No hardening	200**
Material properties	Concrete					
	Compression strength cube (N/mm^2)	Compression strength cylinder (N/mm^2)	Compressive fracture energy (N/mm)	Indirect tensile strength (N/mm^2)	Tensile fracture energy (N/mm)	Modulus of elasticity (kN/mm^2)
Level I (Virgin)	61.6	50*	37**	4.11	0.148**	34
Level II	55 (11%↓)	44* (11%↓)	34(8%↓)	3.9 (5%↓)	0.14***(5%↓)	27 (20%↓)
Level III	37 (40%↓)	30* (40%↓)	23(38%↓)	1.64 (60%↓)	0.08***(46%↓)	22 (35%↓)

Level I: measured from ASR unaffected concrete.

Level II: measured from ASR affected concrete.

Level III: estimated based on the expansion according to the lower bond curve proposed by ISE (Details see section 3.1).

*Compressive strength of cylinder is estimted as 0.8 times compressive strength of cube

** Calculated based on Model Code 2010

***In the total strain based crack model, after the precrack, fracture energy will be reduced along the reloading stress-strain path, as illustrated below:
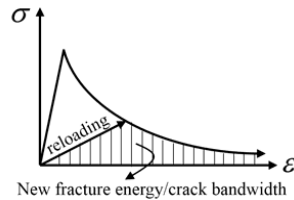
6.2.1.3 Expansion

For the ASR unaffected beam S2, no expansion is observed after 20 weeks. For ASR affected beam S2, because of the presence of the rebar, a non-uniformed expansion is observed over the beam. Expansion in the transverse direction is the largest since it is the least confined direction and the expansion is 0.48%. In the longitudinal direction, expansion at two places are measured, one is close to rebar and the other one is far from the rebar. It is found that concrete close to the rebar has less expansion (0.13%) than the place far from the rebar(0.2%). Expanion of ASR affected beam S2 is depicted in Figure 6.22. Besides the expansion, due to the presence of bottom rebars, a hogging of 7mm is also observed.
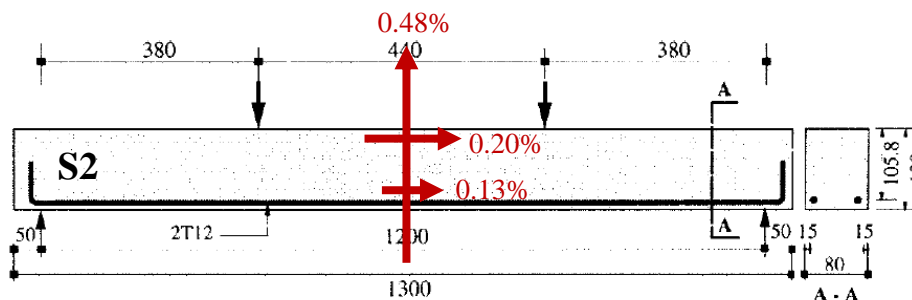

Figure 6.22: Expansion of ASR affected beam S2 after 20 weeks

6.2.1.4 Load-Deflection Relation

Figure 6.23 indicates the load-deflection curve of beam S2. ASR affected beam shows a higher load bearing capacity and a more ductile behaviour than the ASR unaffected beam.

The slopes of two curves are almost the same, which means that the reduction of elastic modulus did not result in the decrease of stiffness at structural level. To answer the question why a reduction of mechanical property will enhance the structural behaviour, the author attribute the reason to the chemical prestressing induced by ASR expansion.
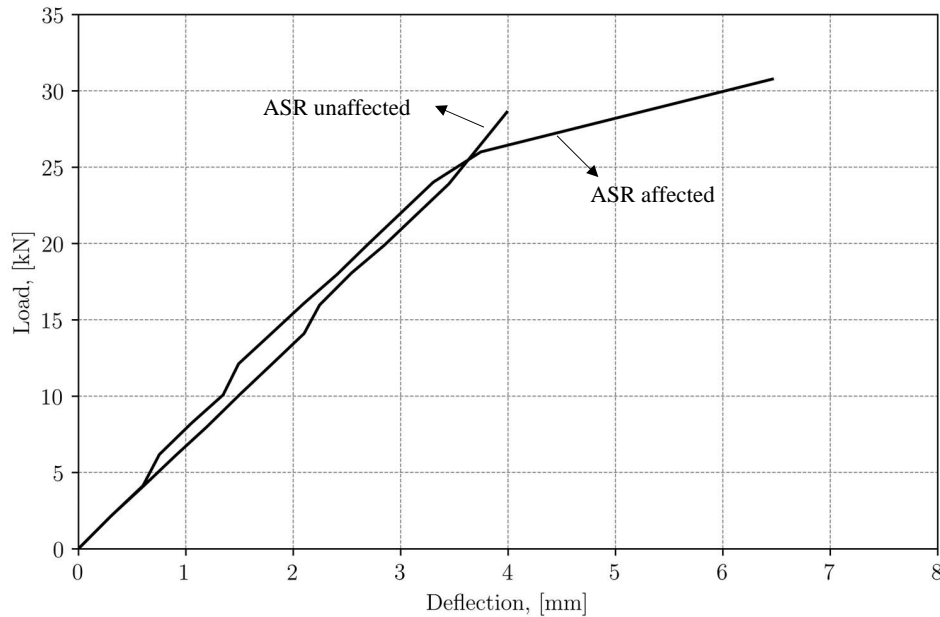

Figure 6.23: Load-deflection relation of beam S2 from experiment

6.2.2 Finite Element Analyses

To study the influences of ASR on shear failure behaviour of Beam S2, Two different mixes were used. Mix A consists of reactive aggregates which allows ASR to take place. Mix C is a non-reactive mix. To simulate the ASR unaffected beam S2, just need to apply the same procedure performed in the previous benchmark. To simulate the ASR affected beam S2, depending on the way to take into account the effects of ASR, two different paths are considered. The first path including the ASR effects by precracking. Using shadow mesh to pre-crack the model, material properties are reduced because of the precracks. In the second path, the effects of ASR is directly taken into account by using the reduced material properties as input.

The stiffness of shadow mesh used in the first path can be further distinguished as small stiffness and large stiffness. In this thesis, small stiffness means the stiffness of shadow mesh is 2% of the stiffness of structural mesh, and large stiffness means the stiffness is 100 times larger than structural mesh. The differences of using different stiffness for shadow mesh will be illustrated in the corresponding subsections.

As to the aforementioned three levels of material property (table 6.3), Figure 6.24 gives a clear demonstration of which level of the material property should be applied in different method.
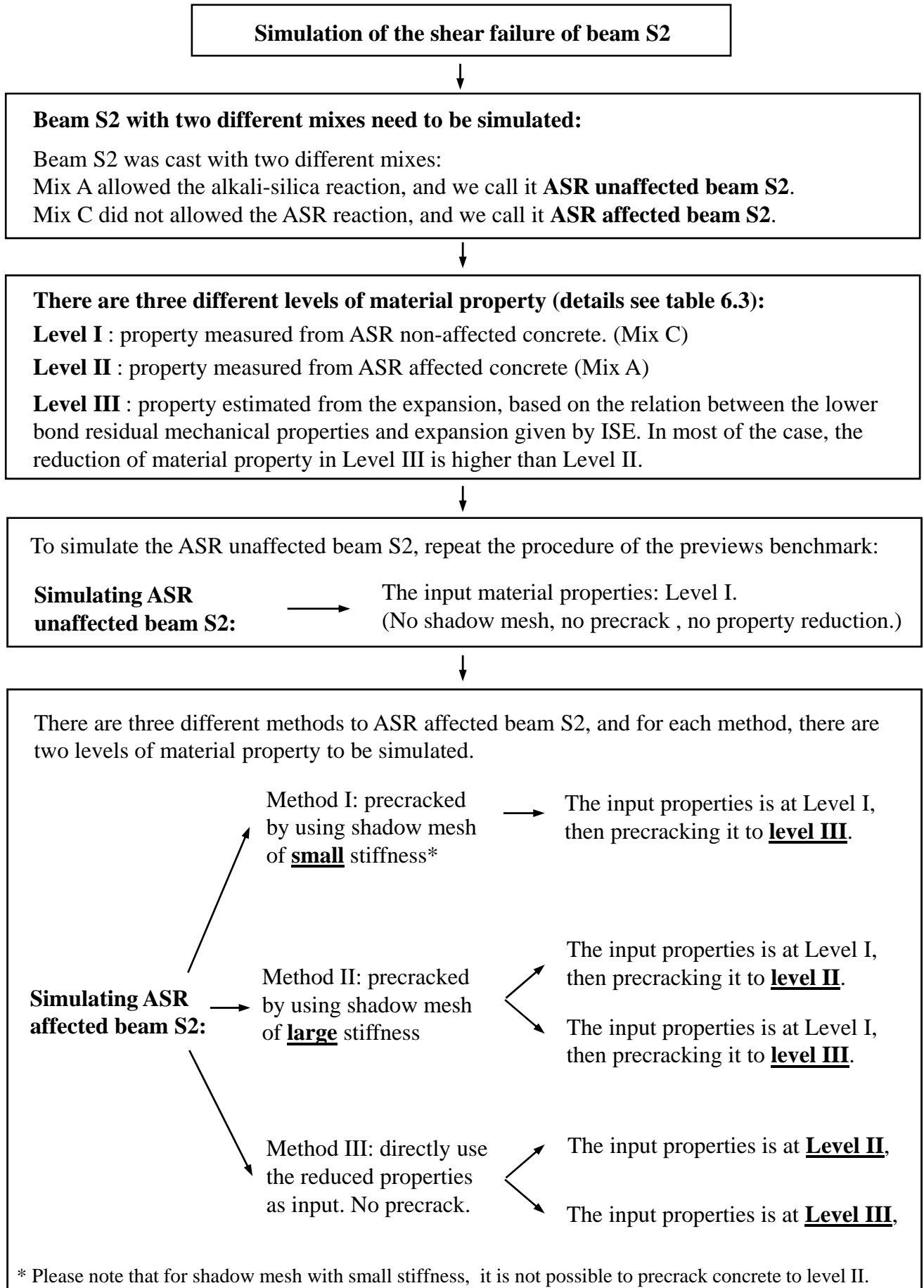
73

Simulation of the shear failure of beam S2

↓

Beam S2 with two different mixes need to be simulated:

Beam S2 was cast with two different mixes:
Mix A allowed the alkali-silica reaction, and we call it **ASR unaffected beam S2**.
Mix C did not allowed the ASR reaction, and we call it **ASR affected beam S2**.

↓

There are three different levels of material property (details see table 6.3):

Level I : property measured from ASR non-affected concrete. (Mix C)

Level II : property measured from ASR affected concrete (Mix A)

Level III : property estimated from the expansion, based on the relation between the lower bond residual mechanical properties and expansion given by ISE. In most of the case, the reduction of material property in Level III is higher than Level II.

↓

To simulate the ASR unaffected beam S2, repeat the procedure of the previews benchmark:

Simulating ASR unaffected beam S2: → The input material properties: Level I.
(No shadow mesh, no precrack , no property reduction.)

↓

There are three different methods to ASR affected beam S2, and for each method, there are two levels of material property to be simulated.

Method I: precracked by using shadow mesh of **small** stiffness* → The input properties is at Level I, then precracking it to **level III**.

Simulating ASR affected beam S2: → Method II: precracked by using shadow mesh of **large** stiffness

The input properties is at Level I, then precracking it to **level II**.

The input properties is at Level I, then precracking it to **level III**.

Method III: directly use the reduced properties as input. No precrack.

The input properties is at **Level II**,

The input properties is at **Level III**,

* Please note that for shadow mesh with small stiffness, it is not possible to precrack concrete to level II.

Figure 6.24: Layout of finite element analyses

6.2.2.1 ASR Unaffected Beam S2

To simulate ASR unaffected beam S2, similar procedures as performed in the previous benchmark is used here. Different shear functions are applied, and results showed that Al-Mahaidi still gives the best simulation. Therefore, only results obtained from Al-Mahaidi are shown in this subsection. It is also found that the result is element size dependent. Models with element size of 5mm, 10mm and 25mm are created to study the effects of element size on shear behaviour. The material model of concrete, steel, interface and the equilibrium iteration are the same with the previous benchmark, details are illustrated in Figure 6.3. The key information of 6.3 is list in the table below.

Table 6.4: Simulation of ASR unaffected beam S2

Material properties	Compression strength cylinder (N/mm^2)	Compressive fracture energy (N/mm)	Indirect tensile strength (N/mm^2)	Tensile fracture energy (N/mm)	Modulus of elasticity (kN/mm^2)
Level I (Virgin)	50	37	4.11	0.148	34

	Concrete		Steel	
Input material properties	Level I		Modulus of elasticity: 200GPa Yielying stress: 460MPa	
Material model	Total strain based crack model		Fully embedded reinforcement, Von Mises plasticity	
Crack direction	Fixed		—	
Tensile behaviour	Exponential		—	
Compressive behaviour	Parabolic		—	
Shear behaviour	Al-Mahaidi, β=0		—	
Element size	25, 10, 5mm		—	

Figure 6.25 shows the mesh of different element size, together with the loading and boundary condition. Rigid body movement is confined and the beam is loaded by displacement.
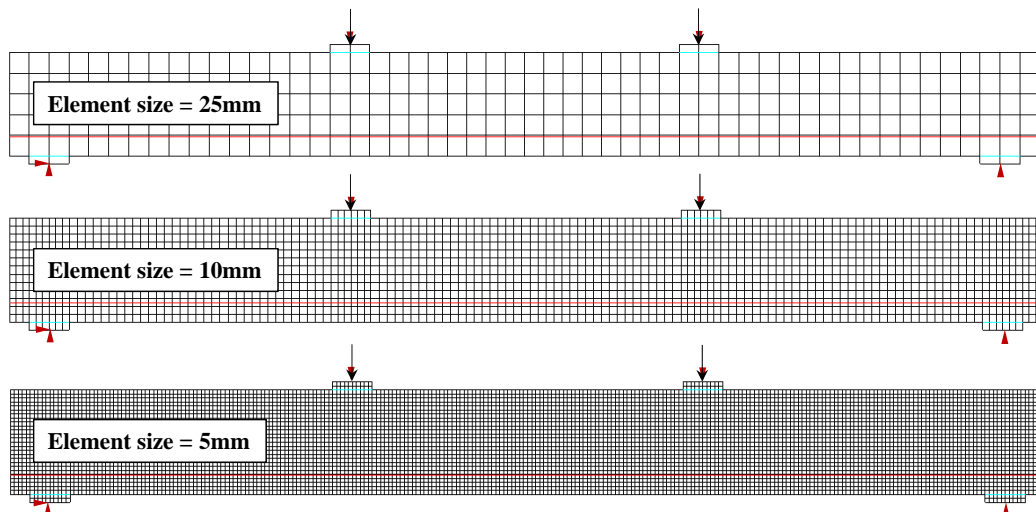

Figure 6.25: Mesh of ASR unaffected beam S2 with different element sizes.

The load-deflection curves are plotted in Figure 6.26 compared with experimental result. It is seen that for all three element size, an overestimation of initial structural stiffness is observed. After the generation of the first crack, stiffness starts to decrease and gradually close to the stiffness of experiment. The peak load value increases with the decrease of element size. This is because that in the total strain based crack model, the stress-strain relation of concrete is dependent to the crack

bandwidth, and usually the crack bandwidth is associated with element size. The decrease in element size will lead to a more ductile stress-strain behaviour, therefore, a higher peak load value.

Why a smaller element size leads to a higher peak load value?

Two elements are assumed. The crack bandwidth h_1 in the element I is two times large than h_2 in the element II. In the total strain based crack model, the area under the stress-strain curve is G_F/h (G_F is fracture energy), which means a larger crack bandwidth will result in a smaller area, as illustrated below. When the two elements reach the same strain ε_i, the stress in element 1 is already decreased to zero, and lost its resistance, but in element 2, still half of the stress is left. In most of the material model, crack bandwidth is associated with element size. The bandwidth decreases with the decrease of element size, and this is the reason that a smaller element size leads to a higher peak load value.
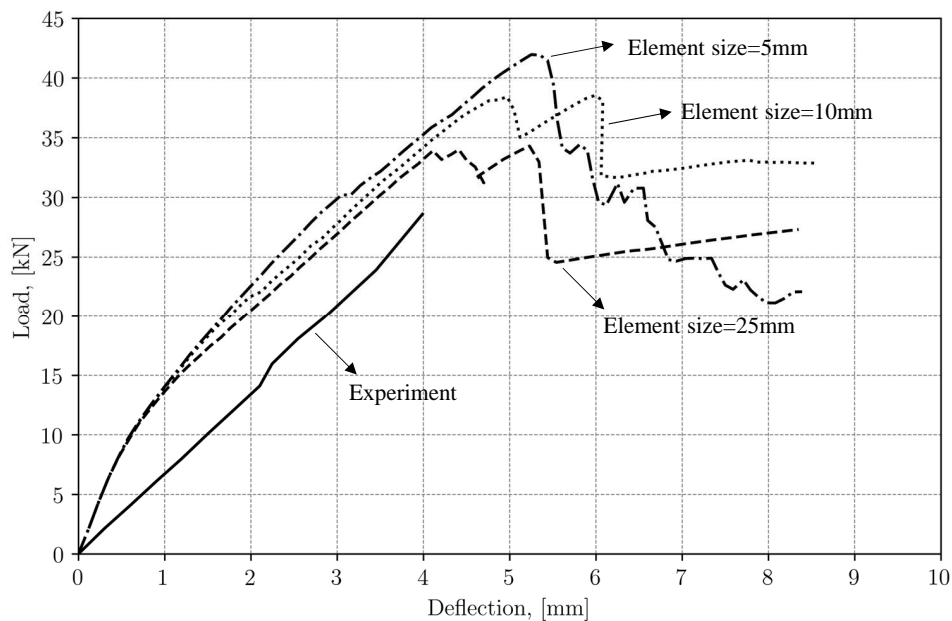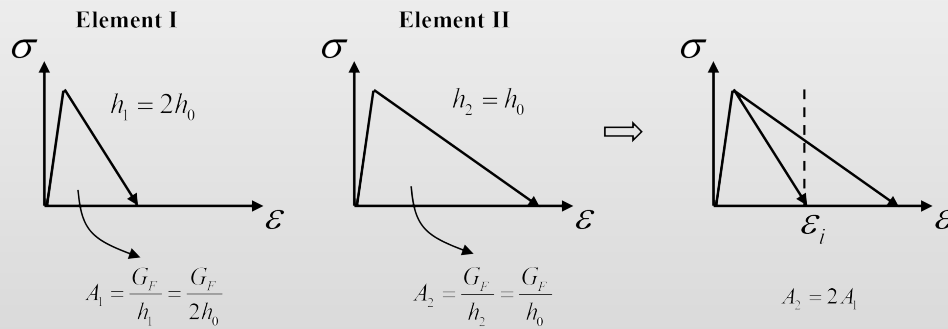
Figure 6.26: Load-deflection relation of ASR unaffected beam S2 with different element size.

Figure 6.27 demonstrates the crack strain obtained from different element size together with the crack pattern of experiment. The crack pattern is approximately the same in different element size, and all of them show a good agreement with the experiment.
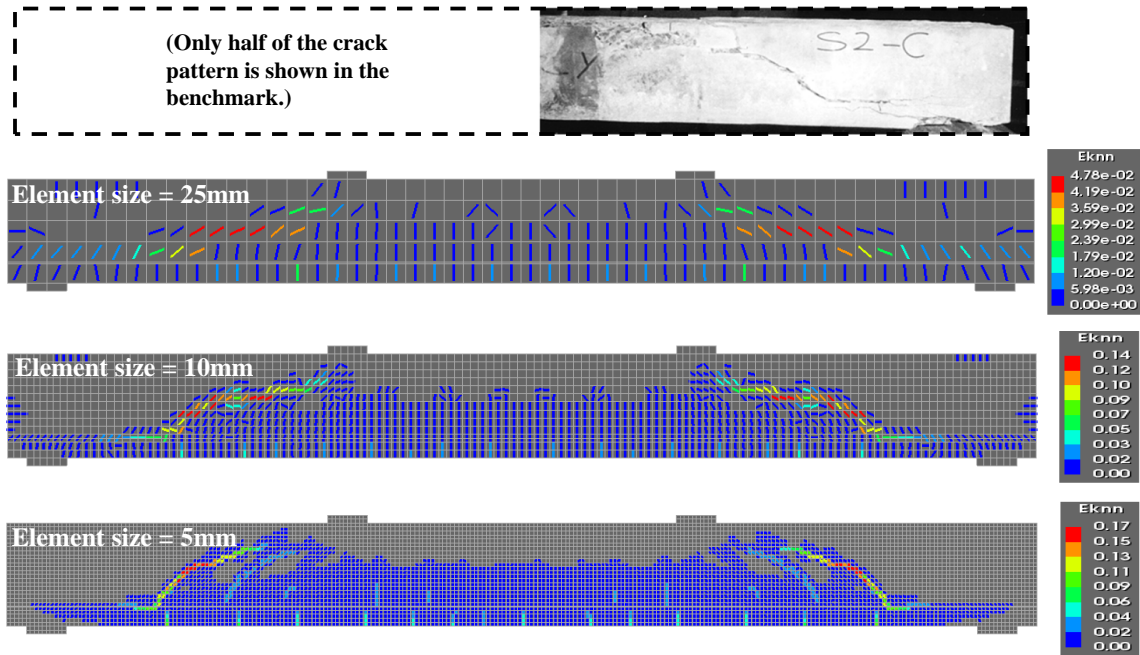
(Only half of the crack pattern is shown in the benchmark.)

Element size = 25mm

Element size = 10mm

Element size = 5mm

Figure 6.27: Crack strain at peak load value of different element size

6.2.2.2 ASR Affected Beam S2, precracked by Shadow Mesh of Small Stiffness

Validations performed in chapter 5 concluded that if the stiffness of shadow mesh is 2% of the stiffness of structural mesh, the ASR expansion can be simulated reasonably well. Because 2% of stiffness is very small, for the convenient reason, we call it small stiffness. In this subsection, shadow mesh with small stiffness is used to precrack the model, and then the model will be loaded in shear to exam the effects of ASR on shear failure.

The whole procedure is divided into two phases. Phase I is called the expansion phase. In this phase, shadow mesh is loaded by initial strain to expand the model and precrack the concrete (See chapter 4 for the theory). Phase II is the mechanical loading phase. The pre-cracked model in the previous phase will be loaded in shear to exam the effects of ASR on shear failure. Informations such as material properties, displacements, stresses, and cracks will be passed from phase I to Phase II, and by this way, the effects of ASR expansion are taken into account.

The boundary conditions in two phases are different. In phase I, only rigid body movement is confined thus the model can expand freely. 2D line Interface element with very small shear stiffness is applied between concrete beam and steel plate so that the steel plate will not restrain the expansion. In phase II, extra vertical confinements are needed since the beam is loaded by displacement, as shown in Figure 6.28.
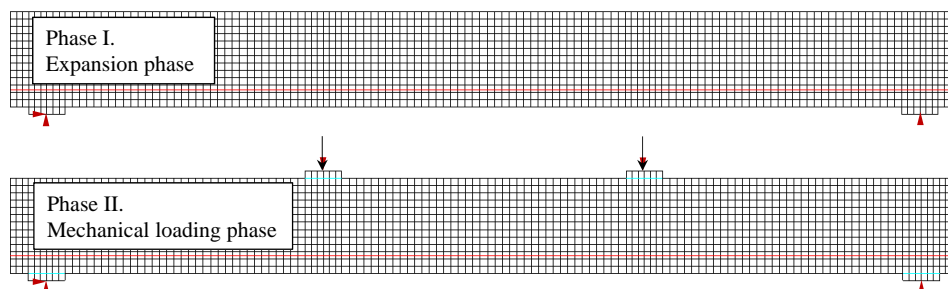

Figure 6.28: Different boundary conditions in phased analysis.

Phase I: Expansion Phase

Two goals need to be reached in phase I: to simulated the expansion and link the expansion to material property reduction. Figure 6.29 gives a brief demonstration of phase I.
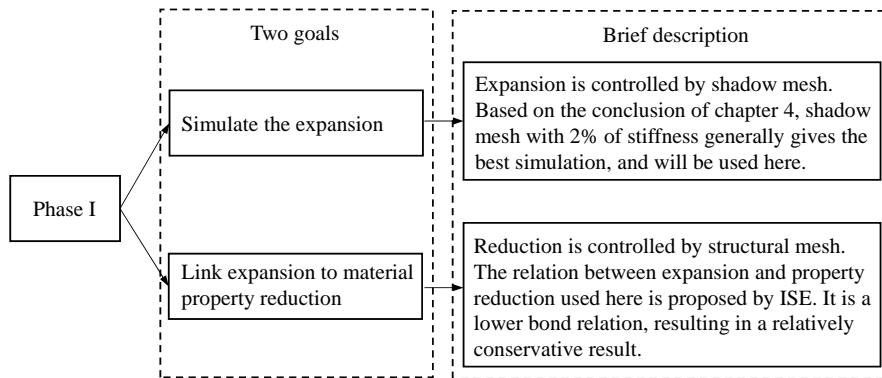

Figure 6.29: Strategies of phase I

Simulate the Expansion

Validations performed in chapter 4 concluded that using a stiffness of shadow mesh with 2% of the stiffness of structural mesh generally gives the best simulation for ASR expansion. The same procedure as performed in chapter 4 is applied here to simulate the expansion of beam S2. Key informations about the model are listed in table 6.5. Result is shown in Figure 6.30.

Table 6.5: The precracking method, precracked by shadow mesh with small stiffness

Material properties	Compression strength cylinder (N/mm^2)	Compressive fracture energy (N/mm)	Indirect tensile strength (N/mm^2)	Tensile fracture energy (N/mm)	Modulus of elasticity (kN/mm^2)
Level I (Virgin)	50	37	4.11	0.148	34
Level II	44 (11%↓)	34(8%↓)	3.9 (5%↓)	0.14(5%↓)	27 (20%↓)
Level III	30 (40%↓)	23(38%↓)	1.64 (60%↓)	0.08(46%↓)	22 (35%↓)

	Structural mesh (Concrete)		Steel	
Input material properties	Level I		Modulus of elasticity: 200GPa Yielying stress: 460MPa	
Properties after precracking	Tensile behaviour(anisotropic): In vertical direction: Level III In horizontal direction: not uniform, depends on the expansion. Compressive behaviour(anisotropic): In vertical direction: Level III In horizontal direction: not uniform, depends on the expansion. Young's modulus(anisotropic): In vertical direction: Level III In horizontal direction: not uniform, depends on the expansion.		—	
Material model	Total strain based crack model		Fully embedded reinforcement, Von Mises plasticity	
Crack direction	Fixed		—	
Tensile behaviour	Exponential		—	
Compressive behaviour	Parabolic		—	
Shear behaviour	Al-Mahaidi, β=0		—	
Element size	10mm		—	
	Shadow mesh			
Material model	isotropic elastic material			
Young's modulus (MPa)	680			
Poisson ratio	0.2			

The numerical result gives a good prediction of the expansion in the lateral direction where the expansion is 0.48% in experiment and 0.5% in FEM. In the longitudinal direction, area closes to the rebar gives a reasonable simulation as well, with 0.13% of expansion in experiment and 0.1% from FEM. Only the place away from the rebar, numerical result overestimated its expansion in longitudinal direction, with 0.2% of expansion in experiment, and the expansion doubled in numerical result. It is considered that numerical result shows a good agreement with the experiment.
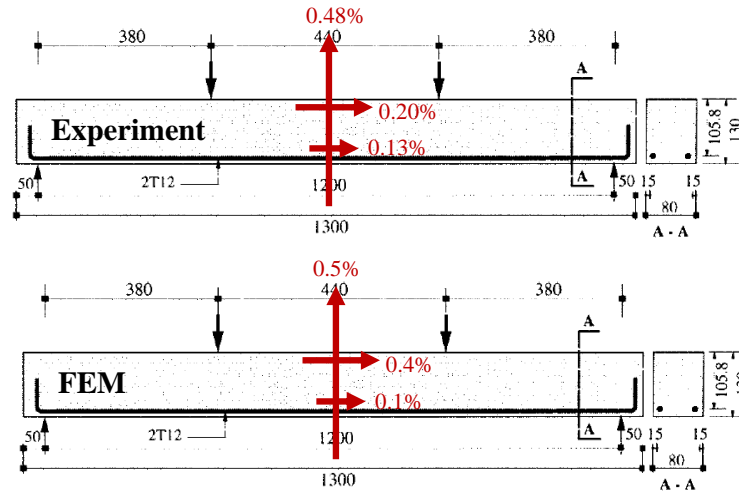
Figure 6.30: Numerical expansion compared with experiment.

Hogging is also observed from the numerical model, as shown in Figure 6.31. In experiment, the hogging is 7 mm. The numerical result shows a hogging of 10.6 mm. Considering that the self-weight is not taken into account, an overestimation of 3 mm is acceptable.
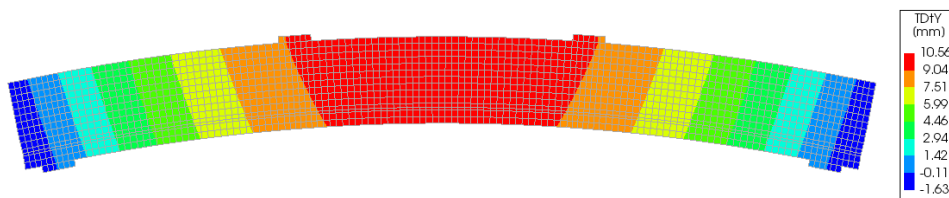
Figure 6.31: Deflection at the last expansion step.

Link Expansion to Properties Reduction

Studies showed that concrete mechanical properties decreases with the increase of ASR expansion. The more expansion, the greater the reduction. (Details see chapter 3). ISE (1992) collected the relation between the residual mechanical properties and ASR expansion. Figure 6.32 shows the lower bond residual mechanical properties as percentage of unaffected value.

Link the expansion to properties reduction meaning that when concrete experiences a certain amount of expansion, the mechanical properties should be reduced correspondingly based on the relations shown in Figure 6.32. The reduction of tensile strength, compressive strength and Young's modulus are explained below.
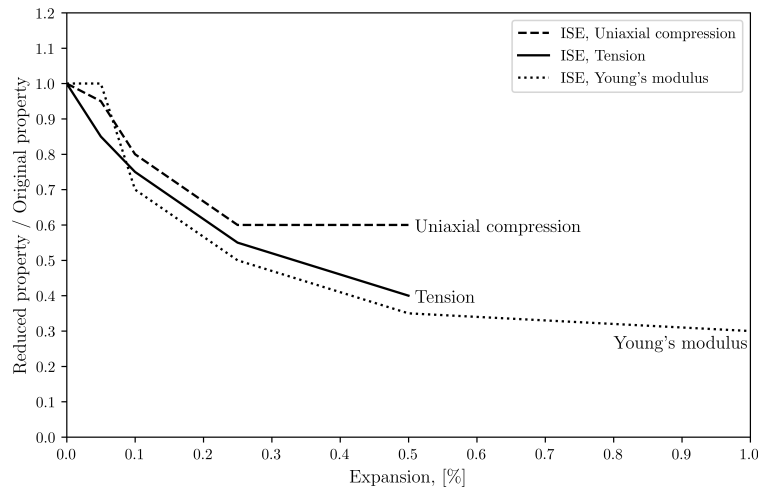
Figure 6.32: Lower bond residual mechanical properties as percentage of original value decreases with ASR expansion

The reduction of tensile strength

In ASR-affected concrete, the tensile strength is reduced because of the cracks initiated by the expansion. Note that the tensile strength decreases with expansion in an exponential-like manner, and in the model the exponential tensile softening is assumed. Taking the advantage of this, by changing the crack bandwidth, the stress-strain curve used in model is modified to fit the lower bond tensile strength curve. Since the crack bandwidth is defined as equal to the element size, the change of crack bandwidth is realized by the change of element size. It is found that the stress-strain curve fits the lower bond tensile strength curve when the element size is 10mm. Figure 6.33 demonstrates the reduction of tensile strength in FEM compared with in ISE.
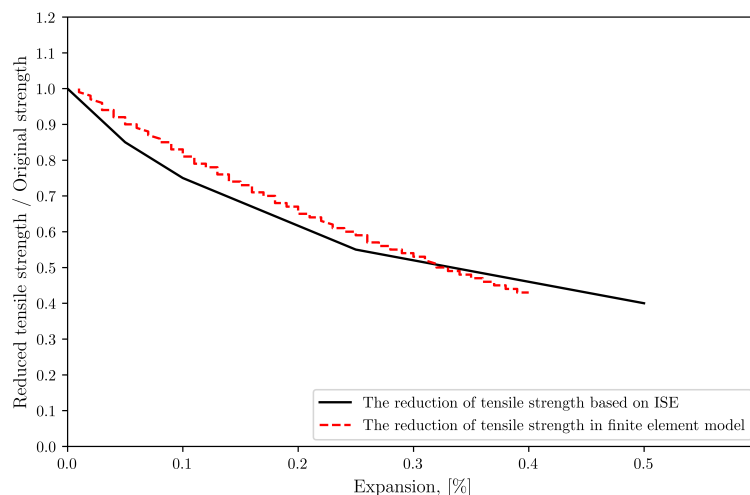

Figure 6.33: Reduction of tensile strength in FEM compared with in ISE

The reduction of compressive strength

Studies found that in ASR affected concrete the compressive strength is reduced as well. According to Vecchio and Collins (1993), concrete compressive strength decreases due to the presence of lateral crack. A multi-linear behaviour is defined based on exactly the relation given by ISE to take into account the reduction of compressive strength.
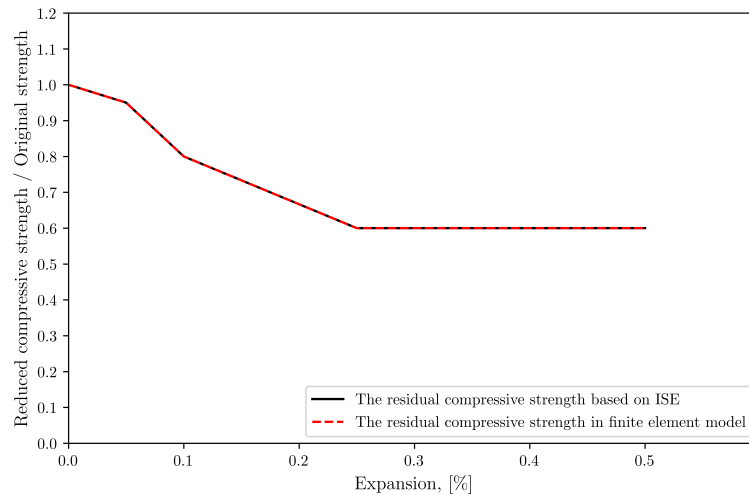

Figure 6.34: Reduction of compressive strength in FEM compared with in ISE

The reduction of Young's modulus

The reduced Young's modulus here is assumed to be the Young's modulus of the compressive part. In the material model, Young's modulus cannot be reduced directly. Therefore, the reduction of Young's modulus is actually a consequence of the reduction of compressive strength. For instance, Figure 6.35 shows the compressive behaviour of a concrete cylinder with an original compressive strength of 40MPa. Assuming that due to the lateral cracks, its compressive strength reduced 40%, to 24MPa. The slope between the peak compressive strength and zero point is defined as the compressive Young's modulus. The compressive Young's modulus decreased 40% as well.

In the material model, compressive Young's modulus decreases with the same rate as the decrease of compressive strength. Figure 6.36 depicts the reduction of Young's modulus in FEM compared with in ISE.
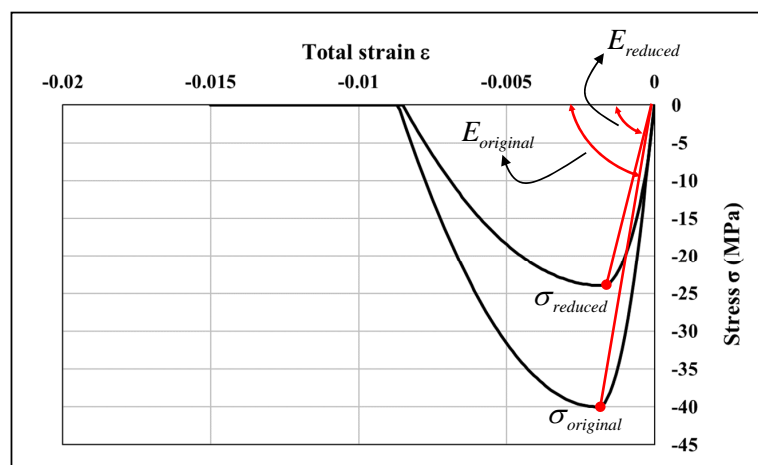

Figure 6.35: The reduction of Young's modulus is actually a consequence of the reduction of compressive strength
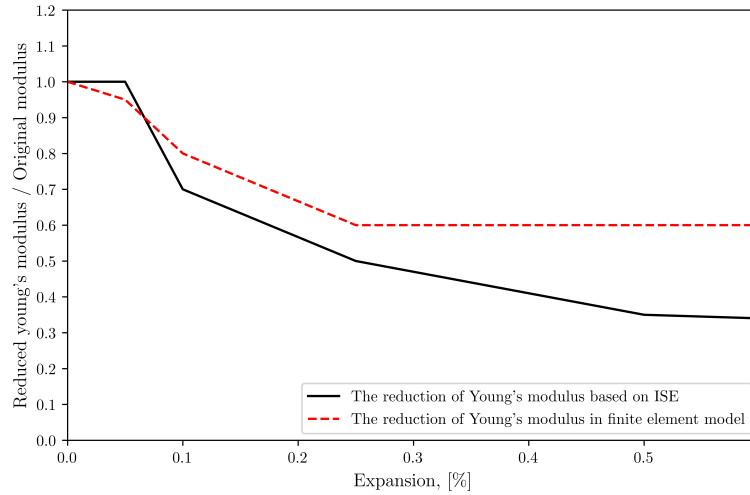
81

Figure 6.36: Reduction of Young's modulus in FEM compared with in ISE

Phase II: Mechanical Loading Phase

After the expansion, the next phase is to load the beam, but before applying the mechanical loads, there are two questions need to be answered:

Should the shadow mesh be deleted before applying the mechanical load?

In this subsection, small stiffness of shadow mesh is used, which is the reason that this question can be discussed here since if the large stiffness is used, it has to be deleted considering its influence on structural behaviour is not negligible. (Later the result will indicate that even by using a small stiffness the influence is huge.)

Initial strain is applied on shadow mesh to simulate the expansion of alkali-silica gel. The applied strain will be confined by structural mesh. As a consequence, shadow mesh will be loaded in compression, structural mesh and rebars wll be loaded in tension. If we consider the concrete beam is consisted by both the structural mesh and shadow mesh, then the concrete surrounded by rebars can be seen as loaded in compression as illustrated in Figure 6.37. According to the benchmark, concrete surrounded by the rebar is stressed in compression due to the chemical selft-prestressing. Therefore, it is physically more preferable to keep the shadow mesh since keeping shadow mesh has the potential to simulate the self-prestressing induced by ASR expansion. However, for a more comprehensive study, also to exam if shadow mesh with small stiffness is real negligible, both cases (keep and delete shadow mesh) are analysed.
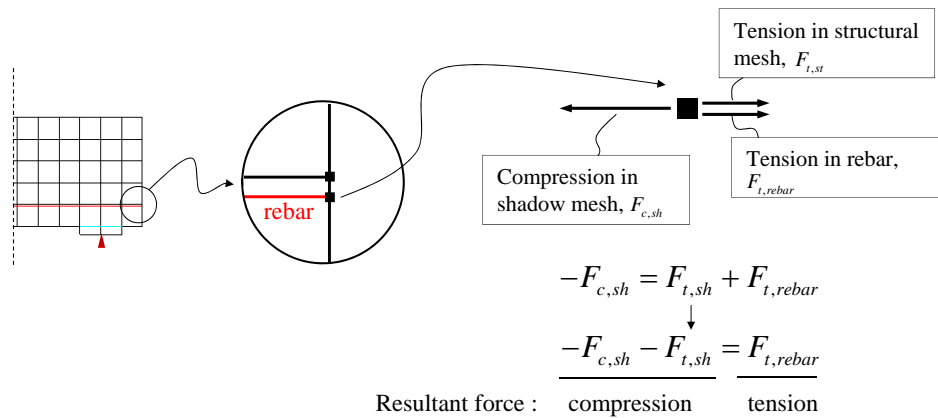

Figure 6.37: The equilibrium between structural mesh, shadow mesh and rebar.

Should the expansion be unloaded before applying the mechanical load?

It is physically more preferable not to unload the expansion since in the reality the expansion always exists. Unloading the expansion means that the compression in concrete and the tension in

rebar are unloaded as well. Cases of unloading and not unloading are analysed.

Figure 6.38 demonstrates the layout of the analysed cases. Since the case "keep expansion, delete SM" cannot meet the equilibrium, three cases are left.
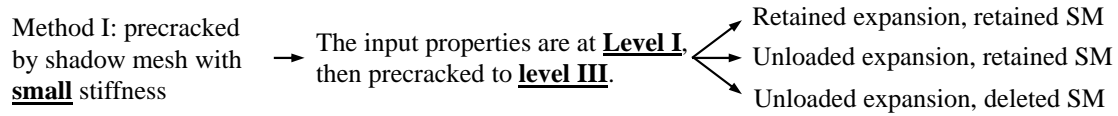

Figure 6.38: Layout of finite element analyses

Results

The load-deflection responses are shown in Figure 6.39. Remarks and conclusions derived from the results are discussed individually.
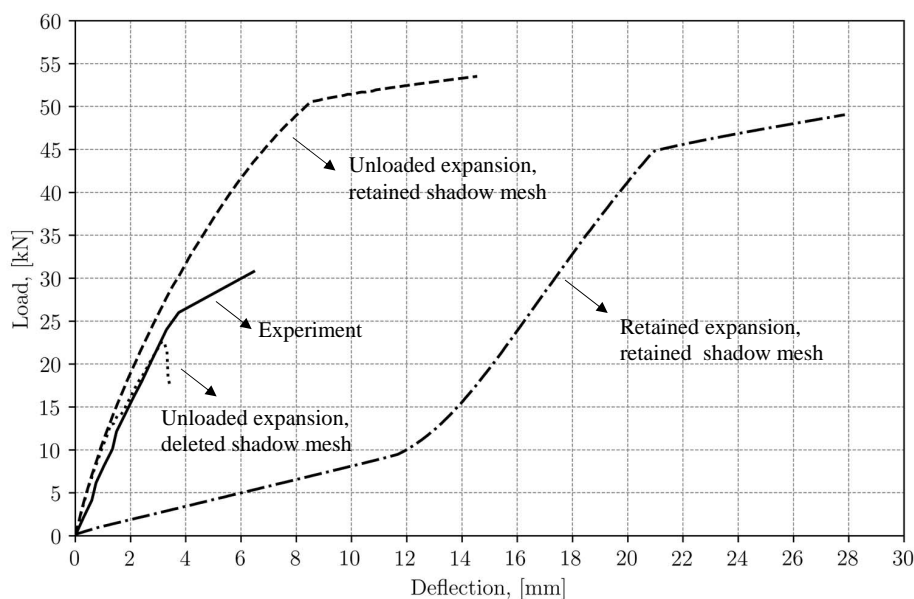

Figure 6.39: Simulation of ASR affected beam S2, precracked by shadow mesh of small stiffness, precracked to level III.
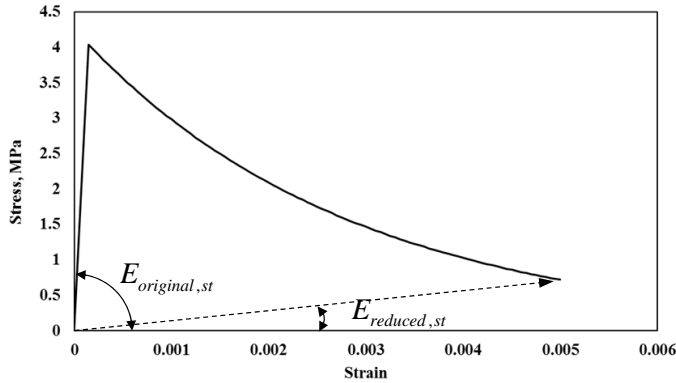
Remark 1: Retaining shadow mesh significantly overestimates the load bearing capacity.

Comparing the case "unloaded expansion, retained shadow mesh" and the case "unloaded expansion, deleted shadow mesh", all the input parameters are the same in two cases except that in the latter case shadow mesh was deleted before applying the mechanical load. However, the failure load in case "retained shadow mesh" is 2.5 times larger than case "deleted shadow mesh". Bear in mind that the numerical results shown in Figure 6.39 are precracked to level III, which means the residual material properties in case "retained shadow mesh" are much lower than the level II used in the experiment, but it still shows a much higher peak load value compared with the experiment. The only explanation is that the leave-in shadow mesh enhanced the shear capacity. The assumption that retaining small stiffness shadow mesh will not influence the structural behaviour is approved to be incorrect.

To answer why retaining a small stiffness shadow mesh will significantly enhance the load bearing capacity. A possible reason is given below:

It is true that the stiffness of shadow mesh is only 2% of the stiffness of structural mesh, but the stiffness in structural mesh is not constant. The (secant) stiffness in structural mesh decreases due to the tensile softening behaviour as illustrated in Figure 6.40 After the expansion, stiffness in structural reduces from 34000 MPa to 190 MPa. The stiffness of shadow mesh is 2% of the original stiffness of structural mesh, which is 680MPa, and the its stiffness is constant due to the elastic material model.

After the precrack, the stiffness of shadow mesh is much higher than the reduced stiffness of structural mesh, and it is not negligible any more.

In structural mesh:

Before precrack: $E_{original,st} = 34000 MPa$

After precrack: $E_{reduced,st} = 190 MPa$

In shadow mesh:

$E_{sh} = 34000 \times 2\% = 680 MPa$

Figure 6.40: The stiffness of structural mesh decreases due to the tensile softening.

Remark 2: Retaining expansion underestimates the initial structural stiffness.

Comparing the case "unloaded expansion, retained shadow mesh" and the case "retained expansion, retained shadow mesh", in the former case the expansion is unloaded before applying mechanical load, and in the latter case the expansion is retained. Attention is paid to the different structural stiffness at the beginning of the mechanical load. A smaller initial stiffness is observed when the expansion is retained in phase II. This smaller initial stiffness might be related the crack closure.

Figure 6.41 demonstrates the load-step relation together with the crack strain-step relation. X-axis represents the steps in non-linear analysis, and the left and right Y-axis represent the load (black line) and the crack strain (red line) respectively. The stiffness is smaller at the first 100 steps, and this is exactly the stage that the crack strain decreases. The upwards expansion decreases due to the applied downwards mechanical load, leading to the decrease of strain in vertical direction and the closure of horizontal cracks.
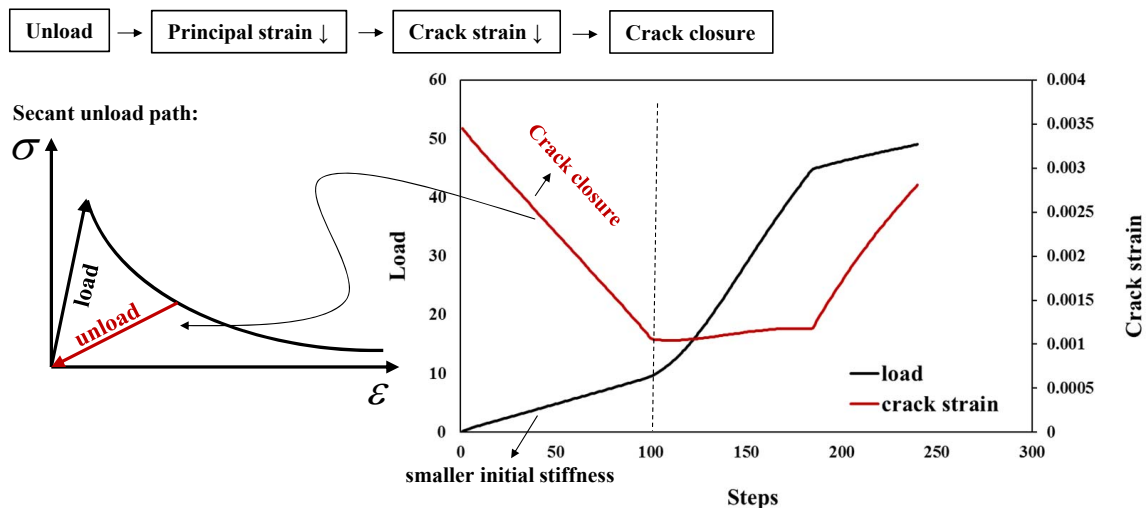

Figure 6.41: The smaller initial stiffness is caused by the closure of cracks.

Conclusions

It is physically more preferable to retain the expansion and shadow mesh. However, the numerical results indicate that retaining shadow mesh significantly overestimates the load bearing capacity, resulting an unsafe prediction. Retaining the expansion gives a smaller initial stiffness which was not observed in the experiment. If shadow mesh with small stiffness is used to precrack the model, it is recommended to unload the expansion and detele shadow mesh before applying the mechanical loads.

6.2.2.3 ASR Affected Beam S2, precracked by Shadow Mesh of Large Stiffness

In the previous subsection, shadow mesh with small stiffness is used to precrack the structural mesh. Nevertheless, it has a major problem: When the stiffness is shadow mesh is much smaller than the stiffness of structural mesh, the initial strain applied on shadow mesh has to be large enough so that the structural mesh can be cracked. If this initial strain is larger than the expansion of the corresponding properties reduction, there will be no cracks when the model reaches its expected expansion. This problem can be solved by changing small stiffness to large stiffness. When the stiffness of shadow mesh is much larger than the stiffness of structural mesh, the structural can be cracked by a very small initial strain applied in shadow mesh.

To link the expansion to the properties reduction, a small element size is required. However, this will result in an overestimation of the peak load value in the mechanical loading phase. Analyses performed in the previous subsection concluded it is better to unload the expansion before applying the mechanical load, which means there is no need to link the expansion to properties reduction any more. In this subsection, the structural mesh is precracked to different extents (level II or level III) without matching the expansion. Since the expansion is not linked to the properties reduction, the restriction of using small element size is not required as well. Therefore, element size of 25mm is applied in this subsection considering that it gives a better simulation in the ASR unaffected beam S2.

Phase analysis as performed in the previous subsection is also applied in the current analyses. In phase I, structural mesh is precracked due to the initial strain applied on shadow mesh. Then, the expansion is unloaded, and the shadow mesh is deleted. In phase II, the precraked structural mesh is loaded by the prescribed displacement. Figure 6.42 shows the layout of the current analysis. Figure 6.43 depicts the mesh of the finite element model. Table 6.6 demonstrates the related material properties.
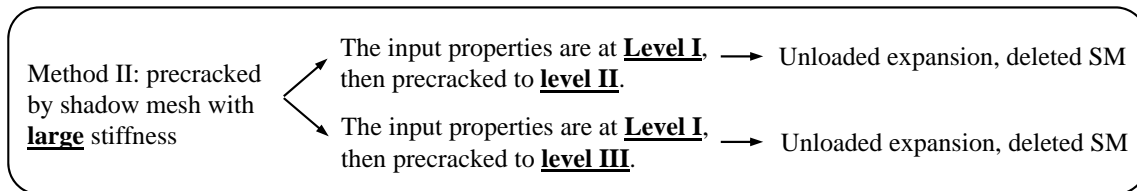

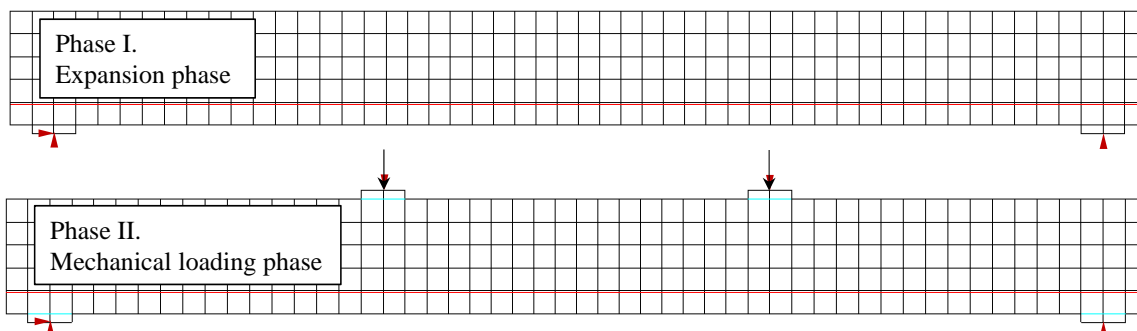Figure 6.42: Layout of current analysis

Figure 6.43: Mesh of current analysis

The reduction of tensile behaviour

The reduction of tensile behaviour includes the reduction of tensile strength and tensile fracture energy. The reduction is taken into account by precracking. The input tensile properties are at level

85

Table 6.6: The precracking method, precracked by shadow mesh with small stiffness

Material properties	Compression strength cylinder (N/mm^2)	Compressive fracture energy (N/mm)	Indirect tensile strength (N/mm^2)	Tensile fracture energy (N/mm)	Modulus of elasticity (kN/mm^2)
Level I (Virgin)	50	37	4.11	0.148	34
Level II	44 (11%↓)	34(8%↓)	3.9 (5%↓)	0.14(5%↓)	27 (20%↓)
Level III	30 (40%↓)	23(38%↓)	1.64 (60%↓)	0.08(46%↓)	22 (35%↓)

	Structural mesh (Concrete)	Steel
Input material properties	Level I	Modulus of elasticity: 200GPa Yielying stress: 460MPa

Properties after precracking	Tensile behaviour(anisotropic):
	    In vertical direction: Level II (for case level II)
	                   Level III (for case level III).
	    In horizontal direction: level I.
	Compressive behaviour(isotropic):
	    Level II (for case level II)
	    Level III (for case level III)
	Young's modulus(isotropic):
	    Level II (for case level II)
	    Level III (for case level III)
		–

Material model	Total strain based crack model	Fully embedded reinforcement, Von Mises plasticity
Crack direction	Fixed	–
Tensile behaviour	Exponential	–
Compressive behaviour	Parabolic	–
Shear behaviour	Al-Mahaidi, β=0	–
Element size	25mm	–

	Shadow mesh
Material model	isotropic elastic material
Young's modulus (MPa)	3400000
Poisson ratio	0.2

I, after the expansion, they are precracked to level II or level III. Figure 6.44 illustrates the tensile behaviour at different precrack levels. It should be noted that only horizontal precracks are initiated, which means only the properties along vertical direction are reduced. The tensile behaviour in horizontal direction is still at level I. After the precracking, elements have orthotropic tensile behaviour.
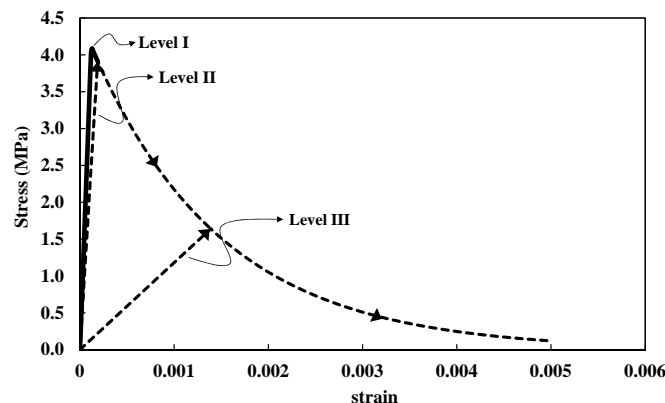

Figure 6.44: Tensile behaviour at different precrack levels.(Element size=25mm)

The reduction of compressive behaviour

The reduction of compressive behaviour is taken into account by directly changing the input compressive properties. Therefore, the compressive behaviour is isotropic.

The reduction of Young's modulus

The reduction of Young's modulus is taken into account by directly changing the input Young's modulus. (For the specific value please check table 6.3)
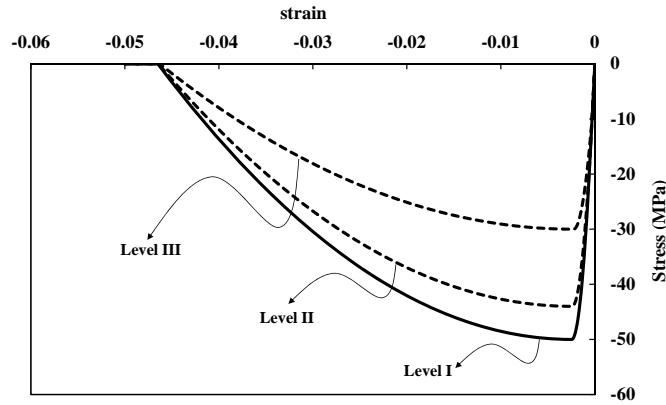
Figure 6.45: Compressive behaviour at different levels.(Element size=25mm)

Results

Figure 6.46 shows the load-deflection relations obtained from numerical results compared with the experiment. In the experiment, the material properties of ASR affected concrete is at level II. However, a significant overestimation is observed when concrete is precracked to level II. Even when concrete is precracked to level III, at which level the residual properties are much lower than residual properties of the experiment, an overestimation is still indicated. There must be something enhanced the load bearing capacity. In the current analysis, shadow mesh is deleted after the precrack, so it cannot be shadow mesh. The suspect falls on the cracking direction. Since the expansion is applied vertically and horizontally, the cracks are initiated vertically and horizontally as well. Fixed cracking model is used, cracks cannot change its direction after the initiation, which means they can only propagate vertically and horizontally. When the beam is loaded in shear in Phase II, the direction of principal strain is not in vertical and horizontal direction any more. This leads to a situation that the coordinate axis of crack strain is not coaxial with the coordinate axis of principal total strain. The consequence is that the shear resistance is enhanced due to this uncoaxiality. In case of level II, beam failed in bending instead of shear due to the enhancement in the shear zone. A more detailed explanation about this phenomenon is described in appendix A.
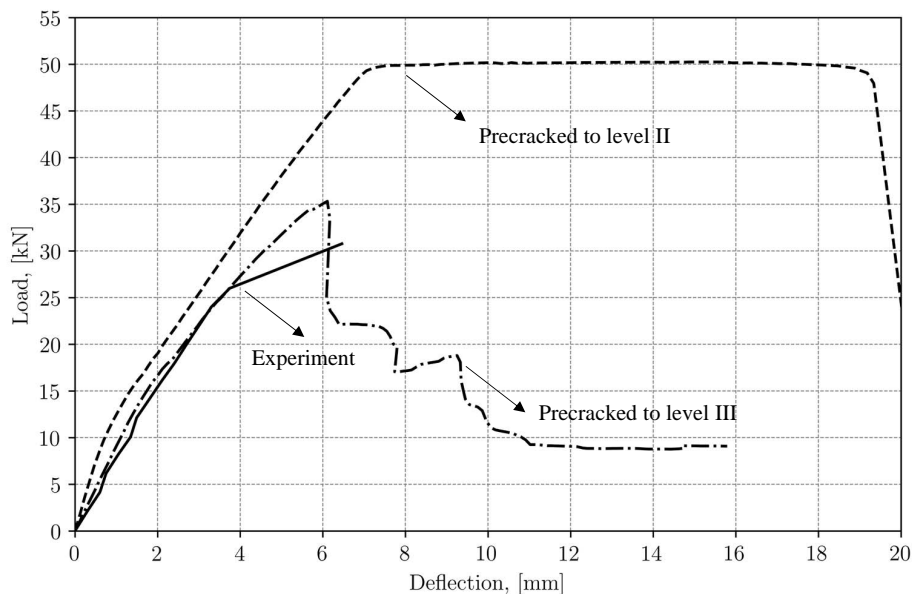

Figure 6.46: Simulation of ASR affected beam S2, precracked by shadow mesh of large stiffness
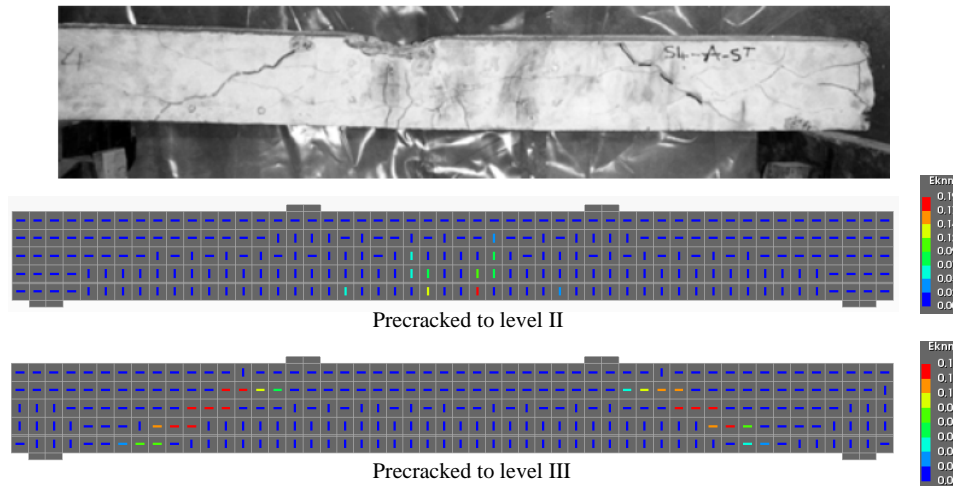
87

Figure 6.47: Crack strain at the peak load step

6.2.2.4 ASR Affected Beam S2, Directly Reduce the Input Material Properties

In the previous two subsections, the input material properties are at level I. Property reductions are taken into account by the precracks initiated in Phase I. In this subsection, the reduced material properties are directly used as the input material properties. Therefore, no shadow mesh is involved, and no expansion is applied.

The layout of current analysis is demonstrated in Figure 6.48. The residual properties at level II and level III are directly used as the input properties. The only difference between the current analysis and the analysis of ASR unaffected beam is that the current analysis uses the reduced material properties. Key informations about the finite element models are shown in Table 6.7.
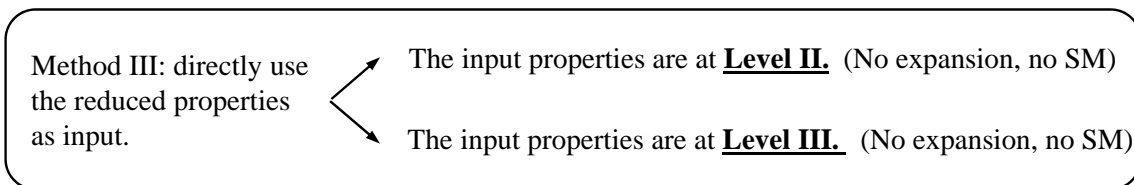

Figure 6.48: Layout of current analysis

No phase analysis is applied in the analysis. The beam is directly loaded by prescribed displacement. Mesh, load and boundary conditions are shown in Figure 6.49.
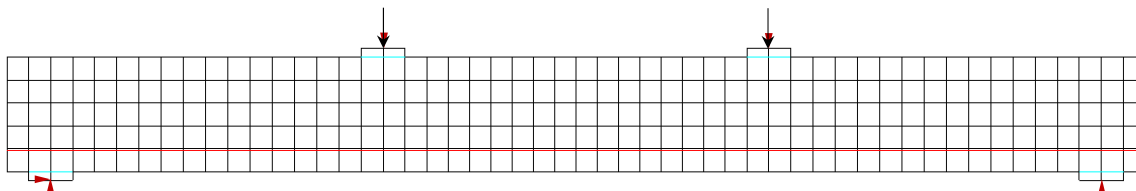

Figure 6.49: Mesh of current analysis

Results

Figure 6.50 illustrates the load-deflection relations obtained from numerical results compared with the experiment. It should be noted that in experiment the residual properties are at level II. The numerical result at level II shows a good agreement with the experiment. A lower load bearing capacity is observed in numerical result at level III since the residual properties at level III are much lower than level II.

Table 6.7: The traditional method, directly reduce the input properties.

Material properties	Compression strength cylinder (N/mm^2)	Compressive fracture energy (N/mm)	Indirect tensile strength (N/mm^2)	Tensile fracture energy (N/mm)	Modulus of elasticity (kN/mm^2)
Level I (Virgin)	50	37	4.11	0.148	34
Level II	44 (11%↓)	34(8%↓)	3.9 (5%↓)	0.14(5%↓)	27 (20%↓)
Level III	30 (40%↓)	23(38%↓)	1.64 (60%↓)	0.08(46%↓)	22 (35%↓)

	Structural mesh (Concrete)	Steel
Input material properties	Tensile behaviour(isotropic): Level II (for case level II) Level III (for case level III) Compressive behaviour(isotropic): Level II (for case level II) Level III (for case level III) Young's modulus(isotropic): Level II (for case level II) Level III (for case level III)	–
Material model	Total strain based crack model	Fully embedded reinforcement, Von Mises plasticity
Crack direction	Fixed	–
Tensile behaviour	Exponential	–
Compressive behaviour	Parabolic	–
Shear behaviour	Al-Mahaidi, β=0	–
Element size	25mm	–

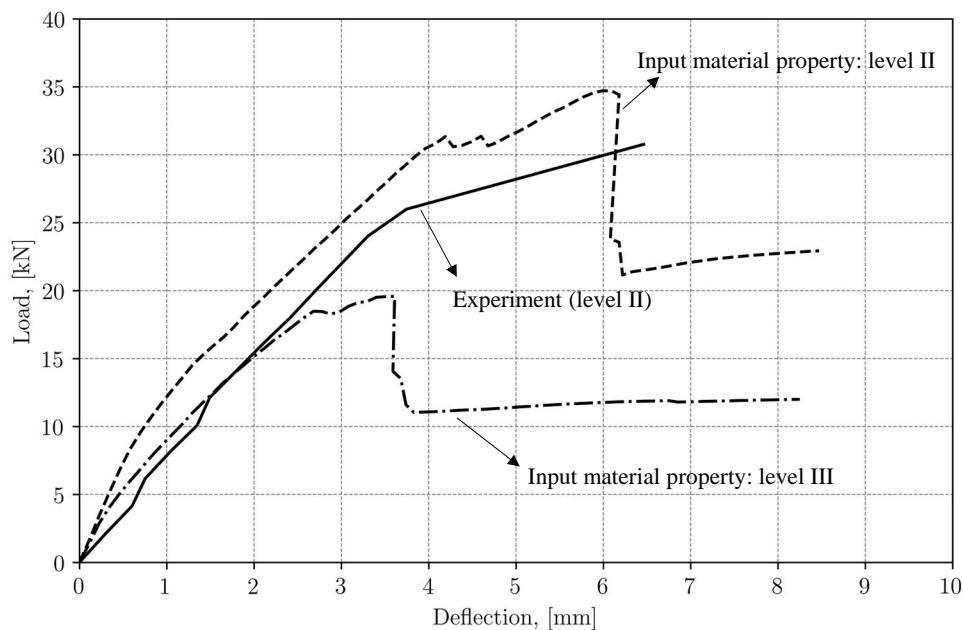|	Shadow mesh
Material model	
Young's modulus (MPa)	No shadow mesh
Poisson ratio	

Figure 6.50: Simulation of ASR affected beam S2. Direct reduction of material properties

Figure 6.51 shows the crack strain at peak load value. Eknn represents the normal crack strain of the larger crack among the two cracks that can present in plane stress element. Crack strain in case level III is smaller than level II, which means beam in case level III lost its load bearing capacity earlier than case level II. The crack pattern obtained from level II shows a good agreement with the experiment.
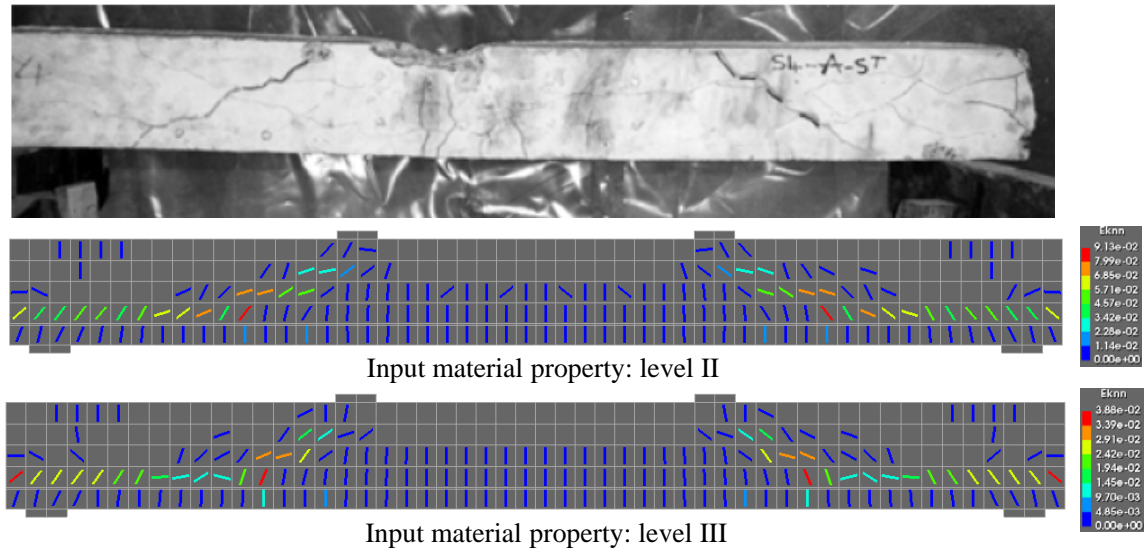

Input material property: level II

Input material property: level III

Figure 6.51: Crack strain at peak load value

6.2.3 Conclusions

The shaer capacity of reinforced concrete beam S2 from paper (Ahmed et al., 1998) is simulated. Beam S2 is cast with two different mixes. One is ASR affected and the other one is ASR non-affected.

The analysis starts with the simulation of ASR unaffected beam S2. In the previews section, it is concluded that Al-Mahaidi shear retention function gives the best simulation, and this conclusion still holds in this benchmark. The peak load value is element size dependent. The small the element size, the larger the peak load vlaue. Numerical result obtained from element size of 25 mm shows a good agreement with the experiment.

Depending on the way to take into account the reduced material properties due to ASR, three different methods are used to simulate the ASR affected beam S2. Method I and II take into account the property reductions by precracking. The difference is stiffness of the shadow mesh. In method I small stiffness is used, and in method II large stiffness is used. In method III, the property reductions are taken into account by directly change the input material properties. Therefore, no shadow mesh is involved.

In method I, the structural mesh is precracked by shadow mesh with small stiffness. The stiffness of shadow mesh is 2% of the stiffness of structural mesh (concrete). It is concluded in chapter 5 that 2% is the most suitable stiffness for simulating the expansion. To link the expansion to properties reduction, a small element size is needed, which arises the first problem: a small element overestimates the load bearing capacity. Then, discussion about should the expansion be unloaded and shadow mesh be deleted before applying the mechanical load is illustrated. It is physical more preferable to retain the expansion and shadow mesh since in the experiment the expansion is always there and retaining shadow mesh has the potential to simulate the chemical self-prestressing observed in experiment. Nevertheless, the numerical result shows that retaining shadow mesh will significantly overestimate the load bearing capacity. Retaining the expansion will lead to an softening of initial structural stiffness which is not observed in the experiment. Therefore, it is concluded that the expansion should be unloaded and the shadow mesh should be deleted before applying the mechanical load in Phase II.

In method II, the structural mesh is precracked by shadow mesh with large stiffness. The stiffness of shadow mesh is 100 times larger than the stiffness of structural mesh. Precracking by using shadow mesh with large stiffness is more stable and more controllable. Since large stiffness cannot be used to predict the expansion, the expansion has to be known before hand. Considering the conclusions obtained from small stiffness, the expansion is unloaded and the shadow mesh is deleted before applying the mechanical load. The numerical results obtained in this method still give overestimated load bearing capacity. In method I and II, cracks can only propagate vertically and horizontally due to the precracking. However, the principal strain in Phase II is not in these two directions anymore. This uncoaxiality between the principal strain coordinate axis and the cracking coordinate axis leads to a slower reduction in tensile strength, which is the reason of the overestimated numerical results.

In method III, the reduced properties due to ASR are taken into account by directly changing the input material properties, and no shadow mesh is involved. The numerical results showed a good agreement with the experiment.

Among the three methods, method III shows the closest numerical result comparing with the experiment. Numerical results obtained at level III always gives a lower load bearing capacity than the experiment, which means that, in practice when the residual properties are unknown, the residual properties calcalated based on the lower bond curve given by ISE (1992) can always give a conservative but safe prediction.

6.3 Benchmark: den Uijl (2000)

Viaduct Heemraadsingel (HS) located in Netherlands has been traced that suffered by ASR. To exam whether the residual shear strength would still satisfy the requirements. Six beams, sawn from Heemraadsingel viaduct, was subjected to shear tests in the Stevin Laboratory at Delft University of Technology. Details of the experiments are decribed in report Den Uijl and Kaptijn (2002). Beam HS1 is selected as the benchmark considering its loading and boundary conditions are relatively simple.

6.3.1 Experiment Description

6.3.1.1 Layout the Specimen

Figure 6.52 shows the details of beam HS1. The total dimension is $7500 \times 670 \times 480$ mm. Beam is supported by steel plate with a distance of 6000 mm. Load is applied in the middle of the beam. External strips are attached at the bottom of the beam to force it failed in shear.
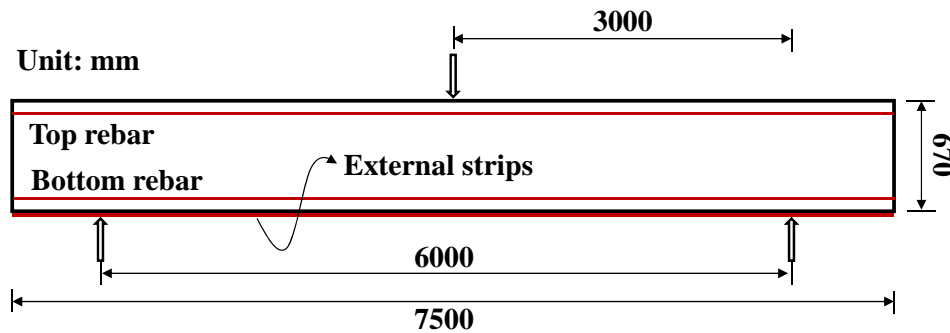

Figure 6.52: Layout of beam HS1.

6.3.1.2 Material Properties

Table 6.8 demonstrates the material properties of concrete and steel. For the properties of concrete, three different levels of properties are distinguished. Material properties at level I represent the properties of ASR unaffected concrete. Compressive strength measured from concrete cube is given in the benchmark, other properties are estimated based on Model Code 2010. Material properties at level II represent the properties of ASR affected concrete. The residual compressive and tensile strength are measured from cubes and cylinders drilled from the field, and other properties are estimated based on Model Code 2010. Material properties at level III are predicted based on the lower bond residual property curve proposed by ISE (1992). The expansion is estimated according to the reduced tensile strength, which is 0.6%. Other properties are estimated based on this expansion. Level III represents the severest property reduction that can happen in this case.

6.3.1.3 Experimental results

Figure 6.53 shows load-deflection relation of ASR affected beam HS1. For the shear capacity of ASR unaffected beam HS1, only the theoretical value is available. The shear capacity of ASR unaffected beam HS1 is 402 kN, and the shear capacity for ASR affected beam HS1 is 330 kN, which is 82% of the unaffected value.

Table 6.8: Material properties

Material properties	Steel				
	Area(In total) (mm^2)	Reinforcement ratio	Yielding stress (N/mm^2)	Hardening	Modulus of elasticity (kN/mm^2)
Top rebar	643	0.20%	220	No hardening	200**
Bottom rebar	1737	0.54%	220	No hardening	200**
External strips	4309	1.33%	410	No hardening	200**
Material properties	Concrete				
	Compression strength cube (N/mm^2)	Compression strength cylinder (N/mm^2)	Compressive fracture energy (N/mm)	Indirect tensile strength (N/mm^2)	Tensile fracture energy (N/mm)	Modulus of elasticity (kN/mm^2)
Level I (Virgin)	55	44*	36**	3.27	0.144**	34
Level II	50 (9%↓)	40* (9%↓)	32(8%↓)	1.0 (70%↓)	0.07***(51%↓)	31.5 (7%↓)
Level III	33 (40%↓)	26.4* (40%↓)	23(38%↓)	1.0 (70%↓)	0.07***(51%↓)	20.4(40%↓)

Level I: measured from ASR unaffected concrete.

Level II: measured from ASR affected concrete.

Level III: estimated based on the expansion according to the lower bond curve proposed by ISE (Details see section 3.1).

*Compressive strength of cylinder is estimted as 0.8 times compressive strength of cube

** Calculated based on Model Code 2010

***In the total strain based crack model, after the precrack, fracture energy will be reduced along the reloading stress-strain path, as illustrated below:
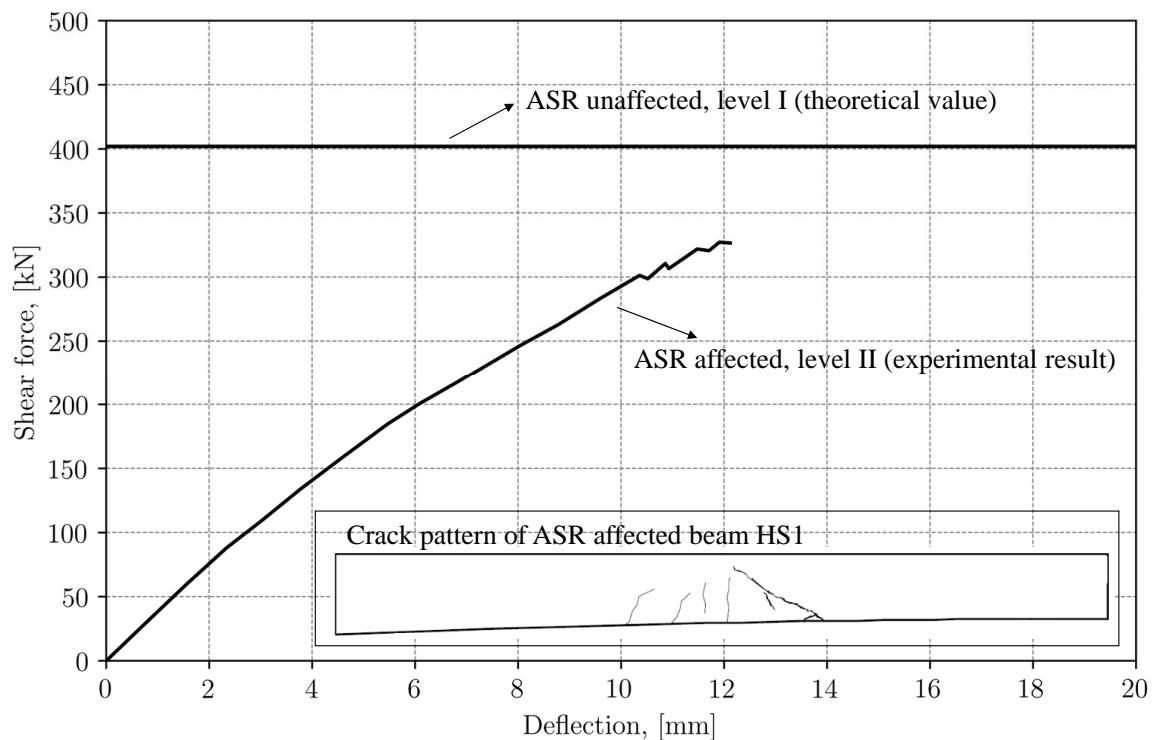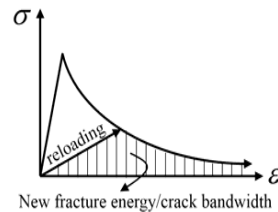

Figure 6.53: Theoretical value of ASR unaffected beam and experimental result of ASR affected beam.

6.3.2 Finite Element Analyses

Analyses of ASR affected and unaffected beam HS1 are demonstrated individually in the subdections below. Layout of the analyses is shown in Figure 6.54. For the ASR unaffected case, properties at level I is used as the input material properties, and no shadow mesh is involved in the analysis. For simulating ASR affected beam HS1, two methods are performed. In method I concrete is precrakced by shadow mesh with large stiffness, and in method II the property reductions are directly taken into account by the input material properties. In the previous benchmark, it is concluded that using shadow mesh with small stiffness did not result in a good simulation and also the expansion is not given in the original report. Therefore, shadow mesh with small stiffness is not considered in this benchmark.
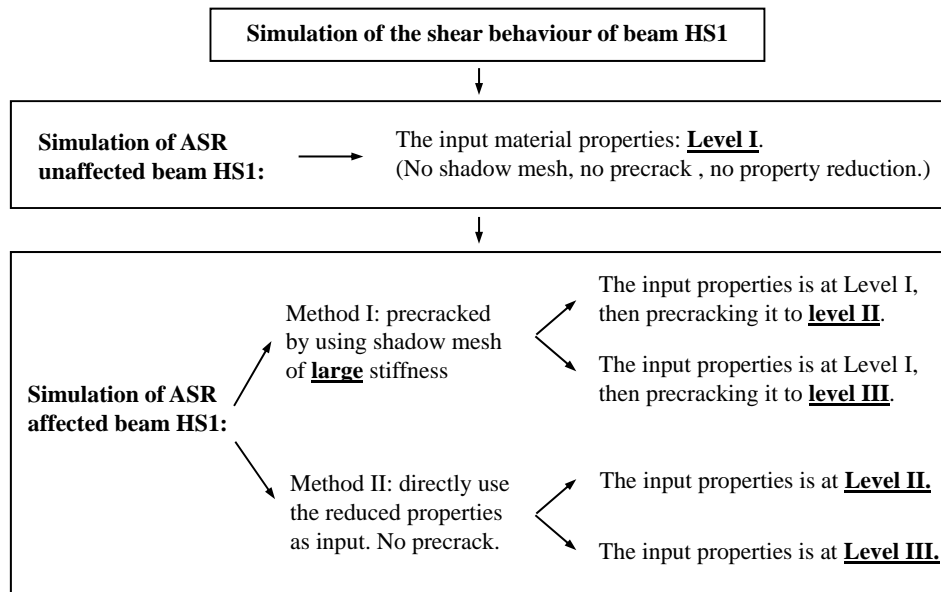

Figure 6.54: Layout of the finite element analyses.

6.3.2.1 ASR Unaffected Beam HS1

To simulate ASR unaffected beam HS1, material properties at level I are used as the input material properties. Level I represents the property of normal (unaffected) concrete, more details please check Table 6.8. The material model used in this benchmark is the same with the previous benchmark, excepting that the minimum shear retention factor β changed from 0 to 0.01, and the element size is 50 mm. Figure 6.55 shows the mesh of the finite element model.
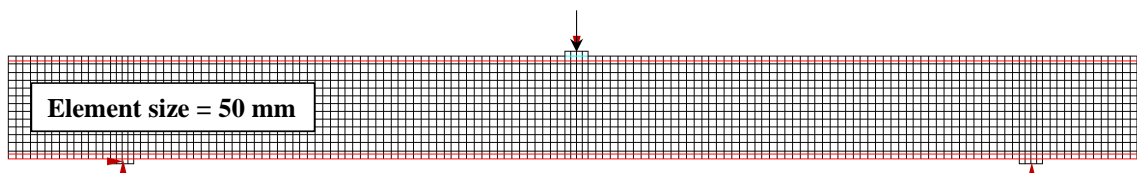

Figure 6.55: Mesh of current finite element model

Results

Figure 6.56 shows the numerical result compared with the theoretical value calculated according to the original report. A good agreement is observed between the peak load value and the theoretical value. Therefore, the material model (including the Al-Mahaidi shear behaviour, exponential tensile behaviour, parabolic compressive behaviour and element size etc.) used in this analysis is applied for the simulation of ASR affected beam HS1.

Table 6.9: Simulation of ASR unaffected beam HS1

Material properties	Compression strength cylinder (N/mm^2)	Compressive fracture energy (N/mm)	Indirect tensile strength (N/mm^2)	Tensile fracture energy (N/mm)	Modulus of elasticity (kN/mm^2)
Level I (Virgin)	44	36	3.27	0.144	34

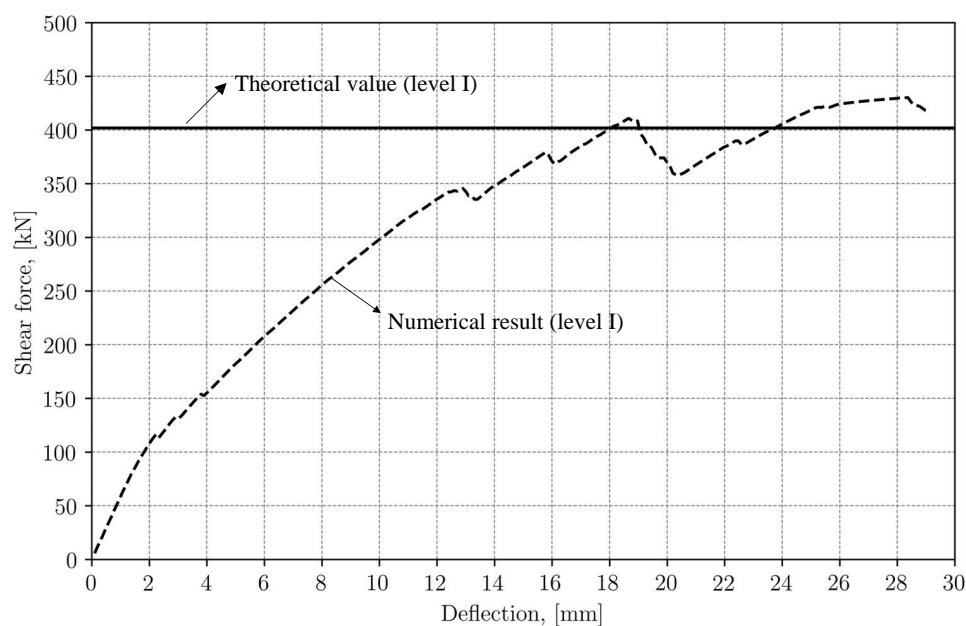|	Concrete	Steel

Input material properties	Level I	Top rebar:
		    Modulus of elasticity: 200GPa
		    Yielying stress: 220MPa
		Bottom rebar:
		    Modulus of elasticity: 200GPa
		    Yielying stress: 220MPa
		External strips:
		    Modulus of elasticity: 200GPa
		    Yielying stress: 410MPa

Material model	Total strain based crack model	Fully embedded reinforcement, Von Mises plasticity
Crack direction	Fixed	—
Tensile behaviour	Exponential	—
Compressive behaviour	Parabolic	—
Shear behaviour	Al-Mahaidi, β=0	—
Element size	50mm	—

Figure 6.56: Simulation of ASR unaffected beam HS1

95

6.3.2.2 ASR Affected Beam HS1, Precracked by Shadow Mesh of Large Stiffness

In this subsection, ASR affected beam HS1 is simulated with the involvement of shadow mesh. The input material of concrete is at level I, and then concrete is precrakced to level II and level III as demonstrated in Figure 6.57. Table 6.10 shows the material properties used in the current analyses.
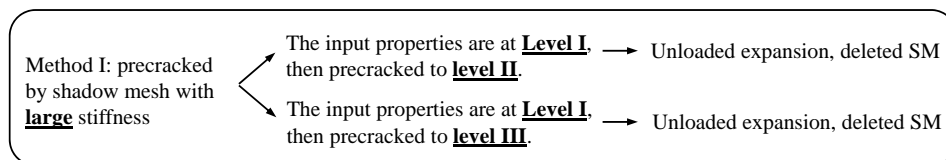

Figure 6.57: Layout of current analyses

Table 6.10: The precracking method, precracked by shadow mesh with large stiffness

Material properties	Compression strength cylinder (N/mm²)	Compressive fracture energy (N/mm)	Indirect tensile strength (N/mm²)	Tensile fracture energy (N/mm)	Modulus of elasticity (kN/mm²)
Level I (Virgin)	44	36	3.27	0.144	34
Level II	40 (9%↓)	32(8%↓)	1.0 (70%↓)	0.07(51%↓)	31.5 (7%↓)
Level III	26.4 (40%↓)	23(38%↓)	1.0 (70%↓)	0.07(51%↓)	20.4(40%↓)

	Structural mesh (Concrete)	Steel

Input material properties	Level I	Top rebar:
		    Modulus of elasticity: 200GPa
		    Yielying stress: 220MPa
		Bottom rebar:
		    Modulus of elasticity: 200GPa
		    Yielying stress: 220MPa
		External strips:
		    Modulus of elasticity: 200GPa
		    Yielying stress: 410MPa

Properties after precracking	Tensile behaviour(anisotropic):
	    In vertical direction: Level II (for case level II)
	                                       Level III (for case level III).
	    In horizontal direction: level I.
	Compressive behaviour(isotropic):
	    Level II (for case level II)
	    Level III (for case level III)
	Young's modulus(isotropic):
	    Level II (for case level II)
	    Level III (for case level III)	

Material model	Total strain based crack model	Fully embedded reinforcement, Von Mises plasticity
Crack direction	Fixed	—
Tensile behaviour	Exponential	—
Compressive behaviour	Parabolic	—
Shear behaviour	Al-Mahaidi, β=0	—
Element size	50mm	—

Shadow mesh	
Material model	isotropic elastic material
Young's modulus (MPa)	3400000
Poisson ratio	0.2

The reduction of tensile properties

Tensile properties are reduced due to precracking. Expansion is only applied in the vertical direction. Therefore, only tensile properties along the vertical direction is reduced. Properties along the horizontal direction remains at level I. The tensile behaviour is orthotropic after the precracking. Figure 6.58 demonstrates the tensile behaviour at different material property level.
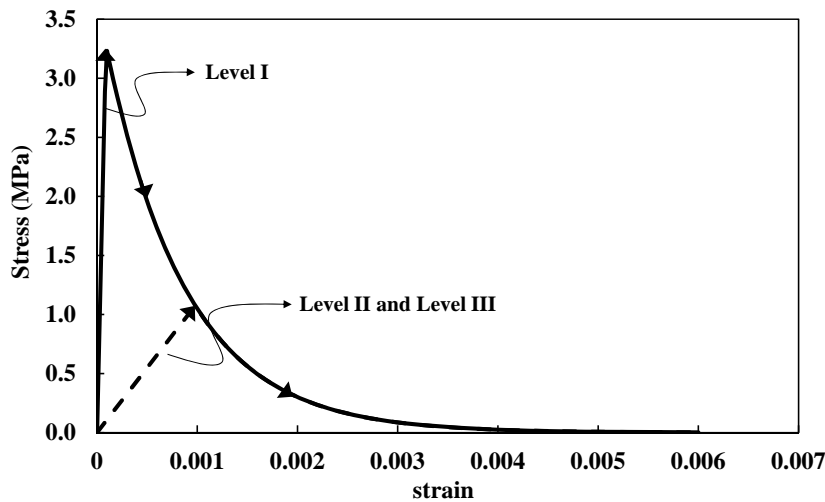

Figure 6.58: Tensile behaviour at different precracking level.(Element size =50mm)

The reduction of compressive properties

The reduction of compressive properties are taken into account by directly changing the input properties. Thus, the compressive property is isotropic. Figure 6.59 shows the compressive behaviour at different material property level.
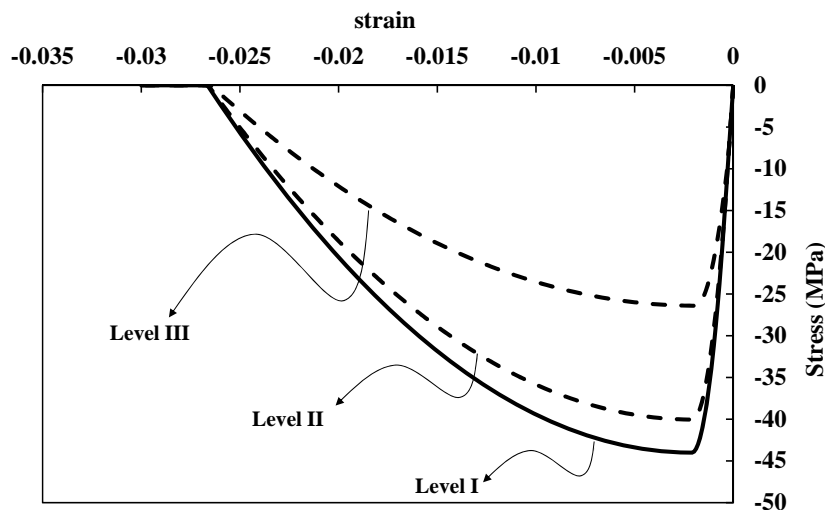

Figure 6.59: Compression behaviour at different precracking level.(Element size =50mm)

The reduction of Young's modulus

The reduction of Young's modulus is taken into account by directly using the reduced modulus as input. For the value of Young's modulus at different level please check Table 6.8.

Figure 6.60 shows the mesh of finite element model in different phase.
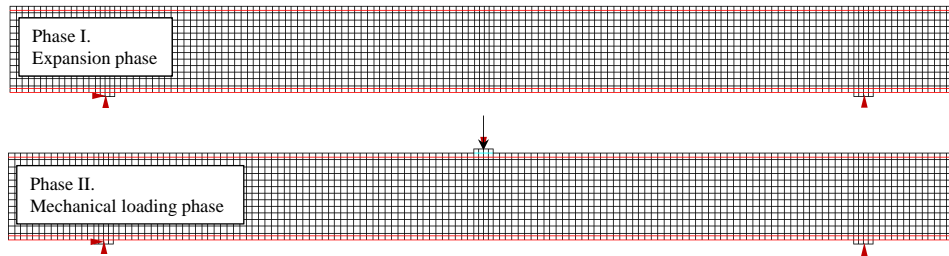
97

Figure 6.60: Mesh of current finite element models

Results

Figure 6.61 depicts the Load-deflection relation obtained from numerical results compared with the experiment. In the experiment, the residual material properties are at level II. Comparing with the numerical result at the same level, an slightly overestimation of the peak load value is observed, and the structural stiffness is simulated quite well.

It is seen that the peak load value at level II and level III are the same. The compressive properties (compressive strength and compressive fracture energy) and Young's modulus at level III is much lower than level II, but the tensile properties at level III is the same with level II. which means the tensile properties are more decisive for the load bearing capacity.

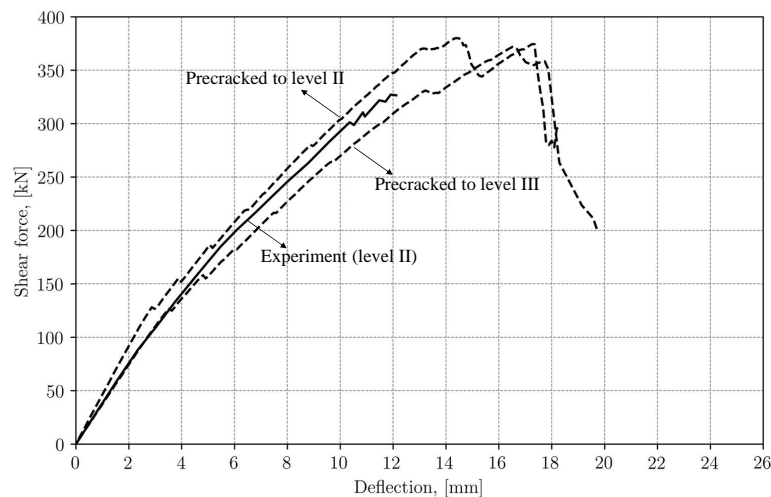Figure 6.62 shows the crack strain at the peak load step.

Figure 6.61: Simulation of ASR affected beam HS1, precracked by shadow mesh of large stiffness.
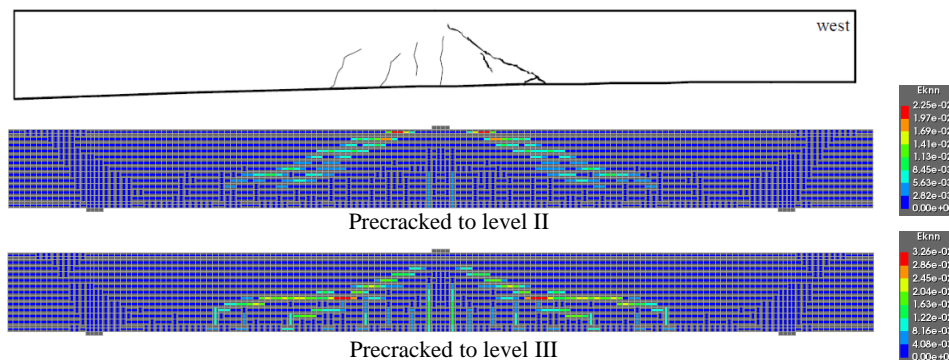

Figure 6.62: Crack strain at the peak load step

6.3.2.3 ASR Affected Beam HS1, Directly Reduce the Input Material Properties

In this subsection, the reduction due to ASR is taken into account by directly using the reduced material properties as the input properties. Comparing with the precracking method, the main difference is that no precracks are initiated in this case, so that the cracks are initiated due to shear force and can be in any direction. Another difference is that, other than the compressive properties and the Young's modulus are isotropic, the tensile properties are isotropic as well. Figure 6.63 demonstrate the layout of current analyses.
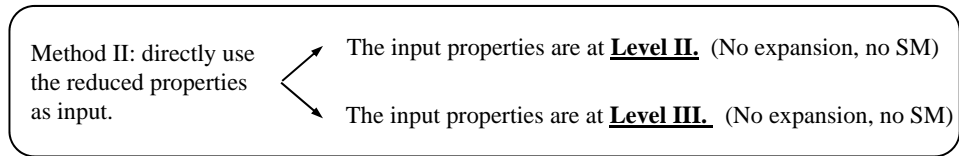
Method II: directly use the reduced properties as input.

The input properties are at **Level II.** (No expansion, no SM)

The input properties are at **Level III.** (No expansion, no SM)

Figure 6.63: Layout of current analyses

Table 6.11: The traditional method, directly reduce the input properties

Material properties	Compression strength cylinder (N/mm^2)	Compressive fracture energy (N/mm)	Indirect tensile strength (N/mm^2)	Tensile fracture energy (N/mm)	Modulus of elasticity (kN/mm^2)
Level I (Virgin)	44	36	3.27	0.144	34
Level II	40 (9%↓)	32(8%↓)	1.0 (70%↓)	0.07(51%↓)	31.5 (7%↓)
Level III	26.4 (40%↓)	23(38%↓)	1.0 (70%↓)	0.07(51%↓)	20.4(40%↓)

	Structural mesh (Concrete)	Steel

Input material properties	Tensile behaviour(isotropic):
	    Level II (for case level II)
	    Level III (for case level III)
	 Compressive behaviour(isotropic):
	    Level II (for case level II)
	    Level III (for case level III)
	 Young's modulus(isotropic):
	    Level II (for case level II)
	    Level III (for case level III)
		Top rebar:
		    Modulus of elasticity: 200GPa
		    Yielying stress: 220MPa
		 Bottom rebar:
		    Modulus of elasticity: 200GPa
		    Yielying stress: 220MPa
		 External strips:
		    Modulus of elasticity: 200GPa
		    Yielying stress: 410MPa

Material model	Total strain based crack model	Fully embedded reinforcement, Von Mises plasticity
Crack direction	Fixed	—
Tensile behaviour	Exponential	—
Compressive behaviour	Parabolic	—
Shear behaviour	Al-Mahaidi, β=0	—
Element size	50mm	—
	Shadow mesh	
Material model		
Young's modulus (MPa)	No shadow mesh	
Poisson ratio		

No phase analysis is applied. The beam is directly load by prescribed displacement. Mesh of the finite element model is shown in Figure 6.64.
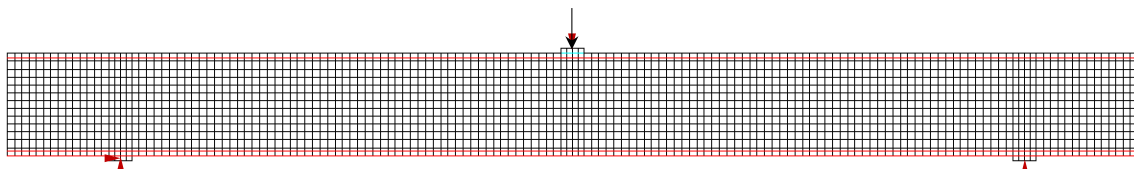

Figure 6.64: Mesh of current finite element models

Results

Figure 6.65 shows the load-deflection relation obtained from numerical results compared with the experiment. The peak load value is underestimated in both level II and level III. This is because, in this method, cracks can be initiated in any direction so that the uncoaxiality between the principal strain and crack is weaker than the previous method, therefore, the shear zone is less strengthened. Another reason is the tensile properties are reduced isotropically in all the directions in this method. In the previous method, only tensile properties along vertical direction are reduced.
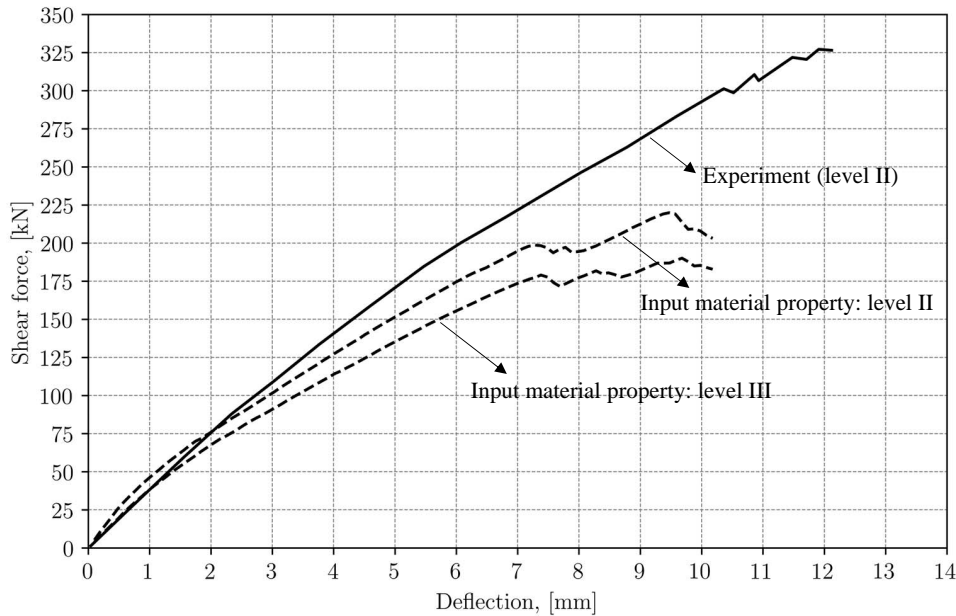

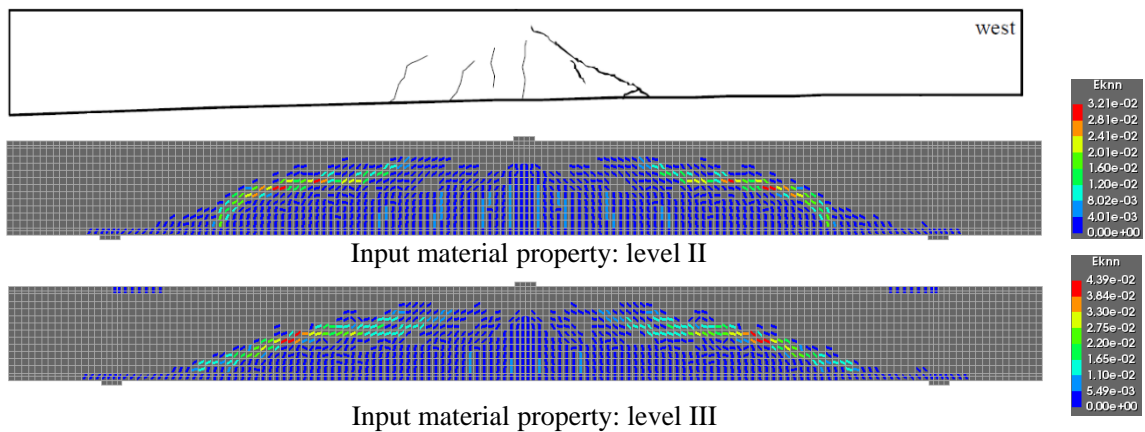Figure 6.65: Simulation of ASR affected beam HS1. Direct reduction of input material properties.

Figure 6.66: Crack strain at the peak load step

6.3.3 Conclusions

The enhancement in shear behaviour due to the initiated precracks observed in this benchmark shows agreements with the results obtained in previous benchmark. The load bearing capacity obtained from precracking is always higher than the one obtained from directly reducing the input properties. The load bearing capacity obtained from level II is always higher than the one obtained from level III. In practice, it is recommended to use the input reduction method and apply the material properties at level III to guarantee a lower bond estimation.

Chapter 7

Conclusions and Recommendations

7.1   Conclusions

In ASR affected reinforced concrete beams, due to the restrained effects of the reinforcement, the expansion in the unreinforced direction is generally larger then the expansion in the reinforced direction, leading to an non-uniform expansion cross the beams. In the first part of this thesis work, a so-called double mesh model is proposed to simulate this non-uniform ASR expansion. The input of this model is the level of free expansion, usually this free expansion is uniform. Taking into account the restrained effects of the reinforcement, the output is the non-uniform restrained ASR expansion. As its name described, the double mesh model consists of two overlapped meshes, called the structural mesh and shadow mesh. The structural mesh represents concrete and is assigned with concrete material property. The shadow mesh is a factitious mesh, and its property is found out through an extensive parametric study calibrated by experimental results reported in literature. The appropriate shadow mesh property should lead to a numerical expansion that is similar with the experiment. In total, ASR expansions in 12 different reinforced beams and cubes are simulated. It is found that when the stiffness of shadow mesh is 2% of the stiffness of structural mesh and the poisson ratio of shadow mesh is 0.3, the numerical expansion showed a good agreement with the experiments. with a relative error smaller than 8% along the unreinforced direction and 25% along the reinforced direction.

In the second part of this thesis work, the shear behaviour of ASR affected reinforced concrete beams are simulated. Traditionally, in the FE-model, the ASR damage is taken into account by directly applying the reduced material properties as the input. Because usually the applied material model is isotropic, the anisotropic residual material property cannot be reflected in this traditional method. Besides, as observed in the experiment, the failure mode in ASR affected beams may change and the capacity may increase due to the effects of ASR cracks and the induced chemical prestress. Since the ASR induced cracks and chemical prestress are completely ignored in the traditional method, the change of failure mode and the increase in shear capacity cannot be observed in the traditional model. The double mesh method introduced in this thesis is used to simulate shear failure of ASR affected beams. With the application of phase analysis, the non-uniform restrained expansion is simulated through the double mesh model by utilizing the shadow mesh property obtained from the previous study. The material properties, such as the tensile strength, the compressive strength and the Young's modulus decreases with the increase of the expansion. In this manner, the anisotropic residual material properties are achieved. Also, the ASR induced cracks are generated in a realistic way through the non-uniform expansion. The change of failure mode and the increase in shear capacity are observed from the precracking method. However, it is found that the precracking method tends to overestimate the shear capacity. This is because the simulated ASR cracks are initiated vertically and horizontally. Due to the fixed crack model, cracks cannot change its direction once initiated. This results in a situation that the coordinate axis of crack strain is not coaxial with the coordinate

axis of the total principal strain. The consequence is that the tensile stress decreases with a slower rate, and the shear resistance in shear zone is enhanced due to this uncoaxiality. The precracking method achieved an anisotropic residual material property and modelled the ASR cracks. However, the chemical prestress induced by the restrained expansion is not able to be simulated.

An additional analysis is performed in Appendix B to simulate the chemical prestress by introducing physical prestress in the reinforcement. Some prestress induced phenomena, such as the increase in stiffness and an earlier concrete crush in bending failure, are observed in this additional analysis.

7.2   Recommendations

The precracking method tends to overestimate the shear capacity due to the uncoaxiality between the crack strain and the principle strain. The applied fixed crack model allows a presence of maximum two cracks in one integration point. Those two cracks are already initiated vertically and horizontally due to the expansion. When the beam is loaded in shear, the diagonal shear crack is not able to be generated. This uncoaxiality can be mitigate if the third crack is allowed to appear.

In this thesis work, shadow mesh is assigned with elastic material property since this is the easiest way to investigate the expansion behaviour. However, it is found that even a shadow mesh with very small stiffness can have a non-negligible influence on the structural behaviour, not mention that the elastic material never fails. This is the reason that the shadow mesh has to be deleted before applying the mechanical loads. If shadow mesh is assigned with a non-elastic material property, for instance, the stiffness decreases with the increase of expansion, and at certain moment, the stiffness reaches zero. Then, the shadow mesh can stay in the model and the pracracking method has the potential to simulate the chemical prestress.

As for the shear behaviour of cracked concrete beams. Different behaviours are observed when the cracks are generated by different reasons. For beams cracked by ASR, an increase of structural stiffness is expected due to the presence of chemical prestress. Whereas, for beams cracked by the mechanical loads, a softening in structural stiffness is observed related to the crack closure. So far, it seems that the precracking method is more promising for simulating the cracks generated by mechanical loads. It is worthy to validate the precracking method through the mechanical precrakced beams.

Appendix A

Appendix: The effects of the Direction of Crack Initiation on Beam Behaviour

In this appendix, two beams are designed to validate that assumption that the overestimated result in method II is related to the direction of cracks initiation. In the normal beam, there is no precracks, and cracks can be initiated in any direction. In the precracked beam, before applying the mechanical load the beam is precracked by shadow mesh, and cracks are initiated vertically and horizontally. As illustrated in Figure A.1, the precracking is designed in a way that the residual tensile strength is just slightly lower than the original strength so that the cracking direction is initiated without reducing the material properties. Then, two beams are loaded by downwards prescribed displacements. Key informations about the finite element models are demonstrated in Table A.1.
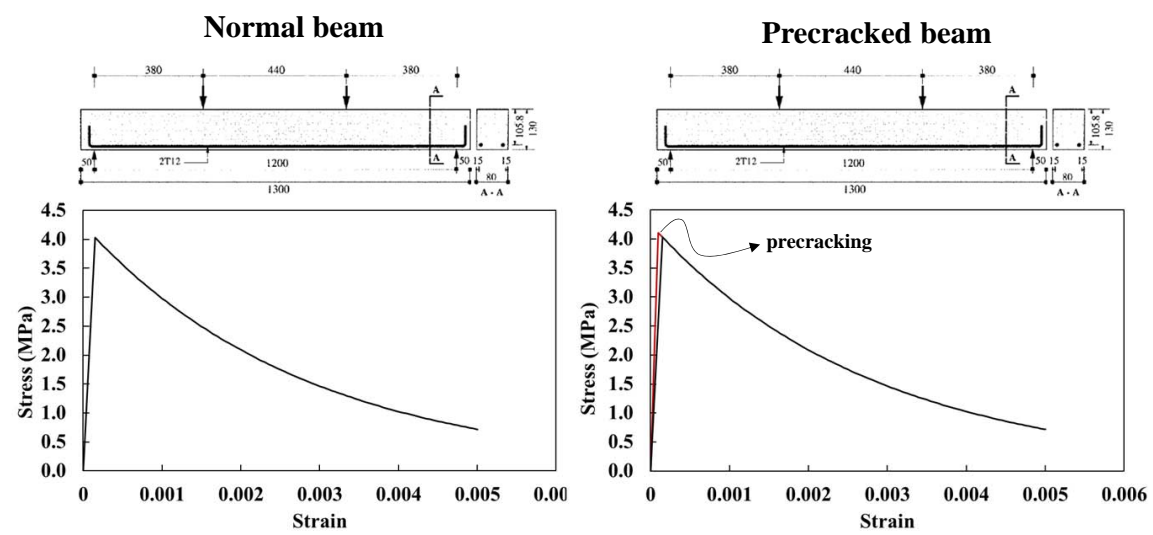

Figure A.1: The tensile behaviour of normal beam and precracked beam

Table A.1: Key information of current finite element models

	Normal beam	Precracked beam
Material model	Total strain based crack model	
Crack orientation	Fixed crack model	
Direction of cracks initiation	Cracks can be initialted in any direction.	Cracks are initiated vertically and horizontally
Young's modulus (MPa)	34000	
Poisson ratio	0.2	
Tensile strength (MPa)	4.11	
Tensile fracture energy (N/mm)	0.148	
Tensile behaviour	Exponential	
Compressive strength (MPa)	49	
Compressive fractrue energy (N/mm)	36	
Compressive behaviour	Parabolic	
Shear behaviour	Al-Mahaidi	
Minimum reteneion factor	$\beta=0$	
Element size (mm)	10	
Crack bandwidth (mm)	10	

Load-deflection relation

Figure A.2 illustrates the load-deflection relation of the normal beam and the precracked beam. The structural stiffness is the same but the normal beam failed in an earlier stage. The peak load value in precracked beam is approximately 25% higher than in the normal beam.
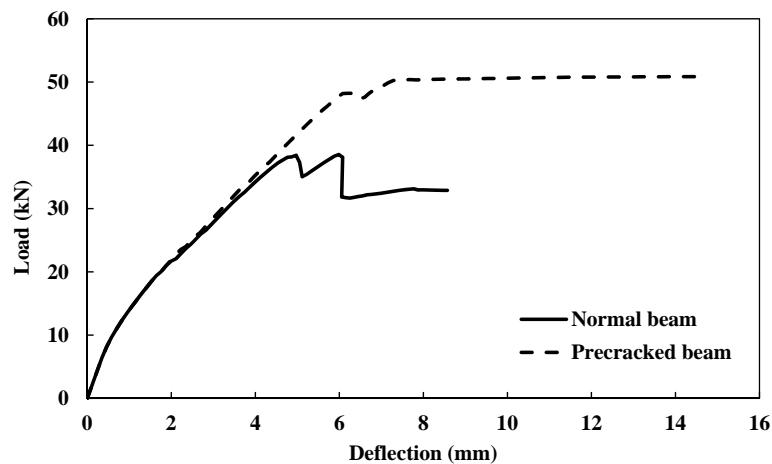

Figure A.2: The load-deflection relation of normal beam and precracked beam.

Crack pattern

Figure A.3 shows the crack pattern of two beams at the deflection of 6 mm. Cracks in the precracked beam are located vertically and horizontally. This is because in the precracked beam, the cracking direction is initiated vertically and horizontally at the precracking stage. Fixed crack model is used so that the cracks cannot change its direction and have to propagate along the initiated directions, which results in a situation that the cracking direction is not aligned with the principal strain direction. This uncoaxiality between the principal strain coordinate axis and the cracking coordinate axis leads to a slower reduction in tensile strength (see Figure), which is the reason of the overestimated numerical results.
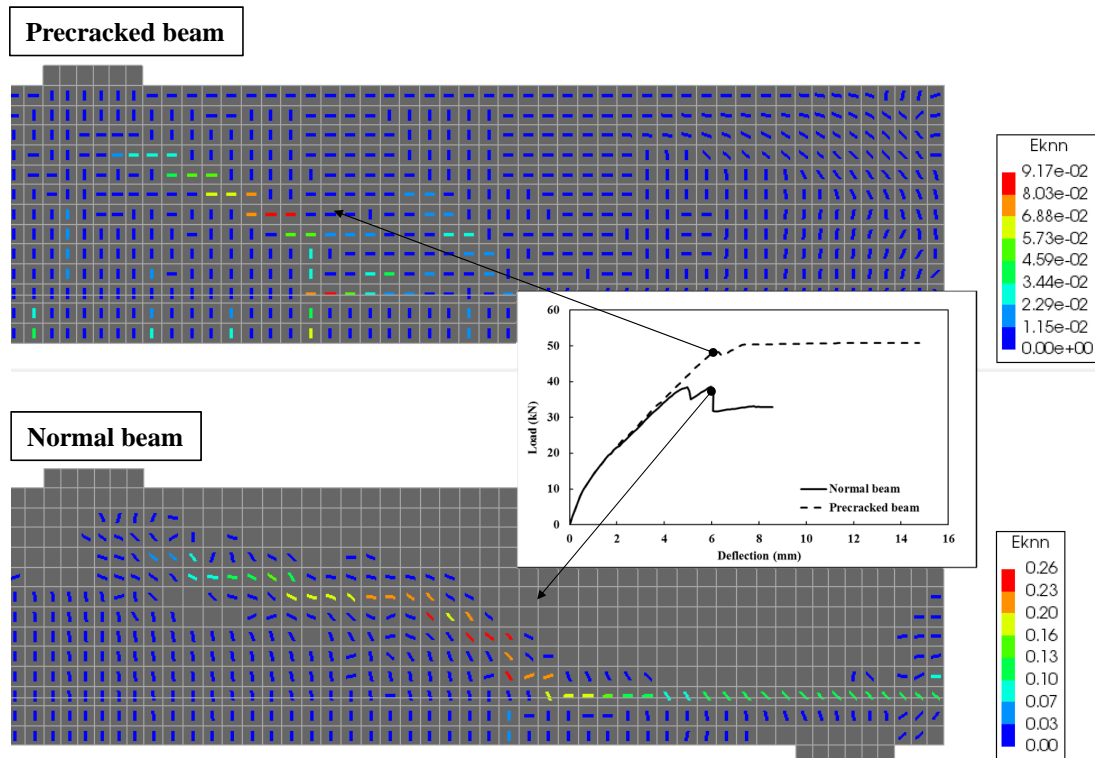

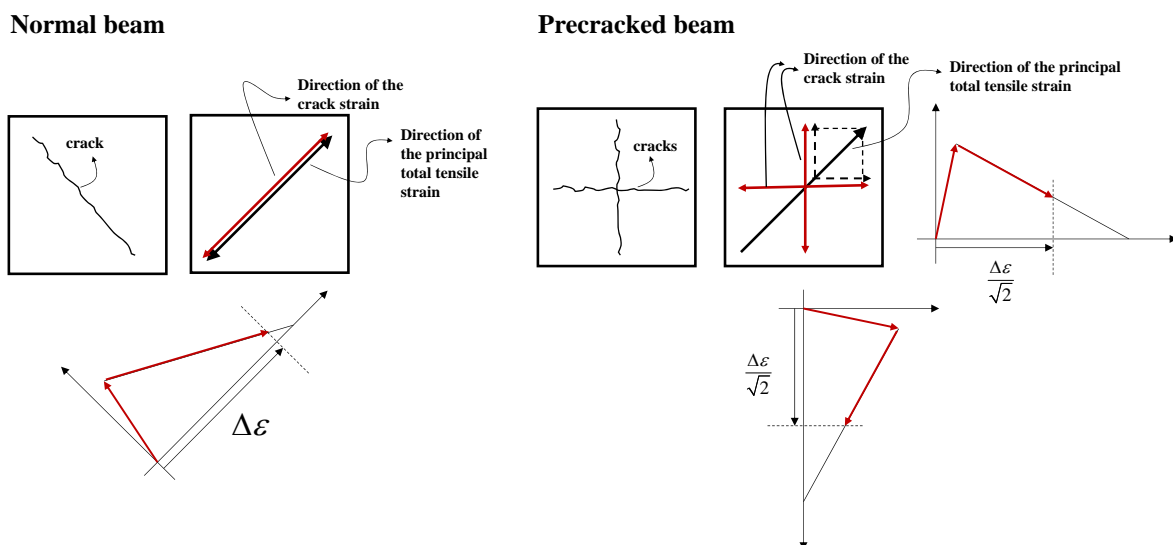Figure A.3: The crack pattern of normal beam and precracked beam.

Figure A.4: In precracked beam, tensile stress decreases with a slower rate.

Failure mode

The shear resistance in shear zone is increased due to the vertically and horizontally initiated crack direction. With the further loading of the precracked beam, it may happen that the propagation of flexural cracks become faster than the propagation of shear cracks, and in the end the beam fails in bending. In other word, the failure mode can be changed from shear failure to bending failure due to the precracking, and this is more likely to happen when the concrete is not severe precracked. This phenomenon was recorded in some experiments. According to (Ahmed et al., 1998), some ASR unaffected beam was failed in shear, and the same beam but the ASR affected one failed in bending.
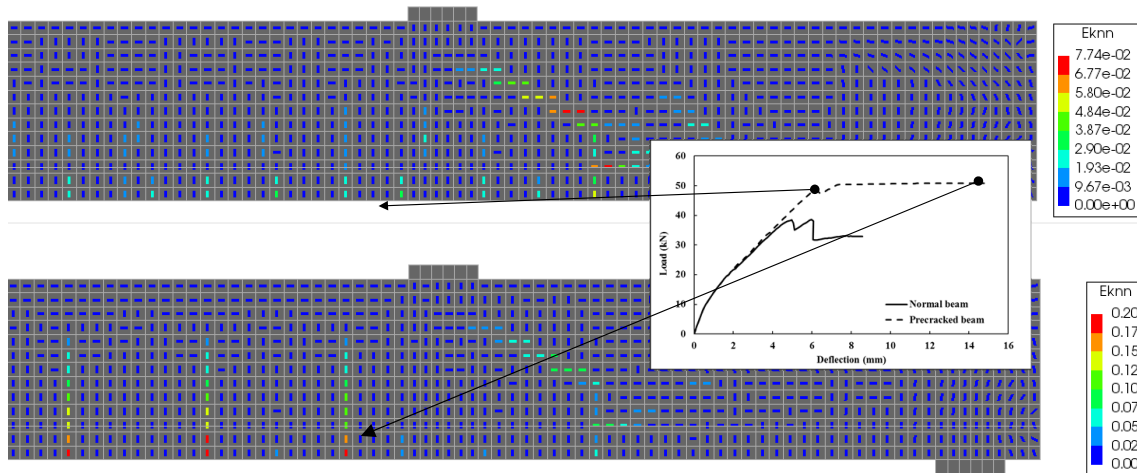

Figure A.5: The tensile behaviour of normal beam and precracked beam

Appendix: Simulation of Chemical Prestress

In the precracking method, the expansion is simulated and the ASR damage is embedded through the expansion. However, it is found that the the simulated expansion has to be unloaded before applying the shear load. Otherwise, the expansion will result in a stiffness softening at the beginning stage of the load-deflection response. According to the unloading-reloading path, the residual material properties such as tensile strength, compressive strength and Young's modulus are kept after the unloading of the expansion. However, the ASR induced chemical prestress disappears after the unloading, which means that effects of chemical prestress is not able to be simulated in the precracking method. Not mention in the traditional method, the chemical prestress is completely ignored. In this Appendix, this chemical prestress is added back by applying pretension stresses on the reinforcement. The reason that the chemical prestress can be simulated by pretension in reinforcement is both of them lead to the same consequences: the reinforcement loaded in tension and the the surrounding concrete loaded in compression.

This appendix is an additional analysis of benchmark (Ahmed et al., 1998). According to the benchmark, the mean steel strain after the expansion is measure, which is 1300×10^{-6}. The stress in reinforcement is calculated as: $1300 \times 10^{-6} \times 200 \times 10^3 = 260 MPa$. This is the value of pretension stress that is applied in the reinforcement. The applied pretension stress is constant along the reinforcement and assuming no prestress loss.

The pretension is first applied within the frame of the traditional method. In the traditional method, ASR damage is taken into account by directly applying the reduced material properties as the input values. Phased analysis is used. Figure B.1 shows the layout of the phase analysis. The material properties are illustrated in Table B.1.
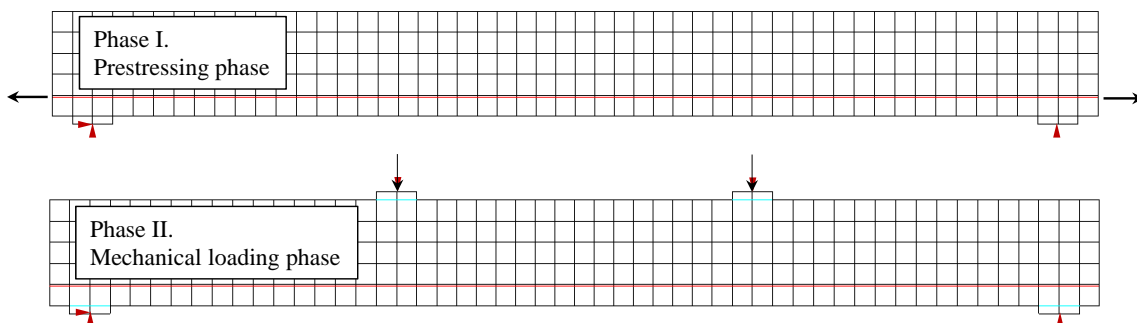

Figure B.1: Phase analysis: applying prestress within the frame of the traditional method

Table B.1: Material properties: applying prestress within the frame of the traditional method

Material properties	Compression strength cylinder (N/mm^2)	Compressive fracture energy (N/mm)	Indirect tensile strength (N/mm^2)	Tensile fracture energy (N/mm)	Modulus of elasticity (kN/mm^2)
Level I (Virgin)	50	37	4.11	0.148	34
Level II (Residual)	44 (11%↓)	34(8%↓)	3.9 (5%↓)	0.14(5%↓)	27 (20%↓)

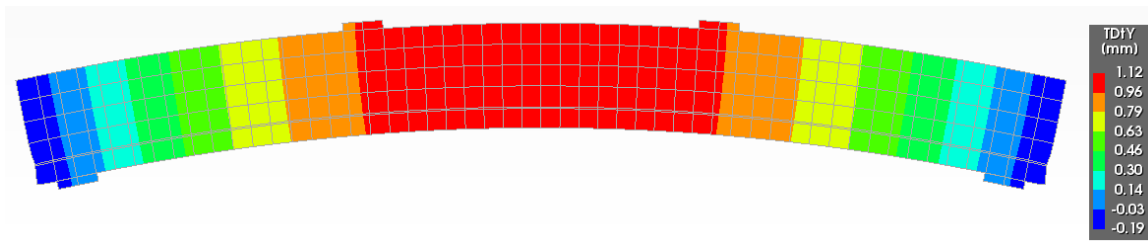|	Structural mesh (Concrete)	Steel
Input material properties	Tensile behaviour(isotropic): Level II Compressive behaviour(isotropic): Level II Young's modulus(isotropic): Level II	Modulus of elasticity: 200GPa Yielying stress: 460MPa
Material model	Total strain based crack model	Fully embedded reinforcement, Von Mises plasticity
Crack direction	Fixed	—
Tensile behaviour	Exponential	—
Compressive behaviour	Parabolic	—
Shear behaviour	Al-Mahaidi, β=0	—
Element size	25mm	—
Pretension stress	—	260 MPa
	Shadow mesh	
Material model		
Young's modulus (MPa)	No shadow mesh	
Poisson ratio		

Figure B.2: Deformation after applying prestress

The deformation after applying prestress is shown in Figure B.2. Due to the asymmetric distribution of the reinforcement, a hogging with maximum deflection of 1.12 mm is observed.

The load-deflection response is depicted in Figure B.3, marked as curve ③. The numerical result of the traditional method without applying prestress performed in chapter 6 is also shown in this Figure, marked as curve ②. The experimental result is marked as ①. Due to the presence of prestress, the stiffness is increased. An overestimation of stiffness is observed in curve ③. The peak load value is increase as well. The peak load value after applying prestress is 50 kN, and the peak load from experiment is only 30 kN. The presence of prestress changes the failure mode. According to the experiment the beam failed in shear, however, with the prestress, now the beam failed in bending. The numerical result obtained from the traditional method without prestress, marked as ②, gives a better prediction of the peak load value and a correct failure mode.
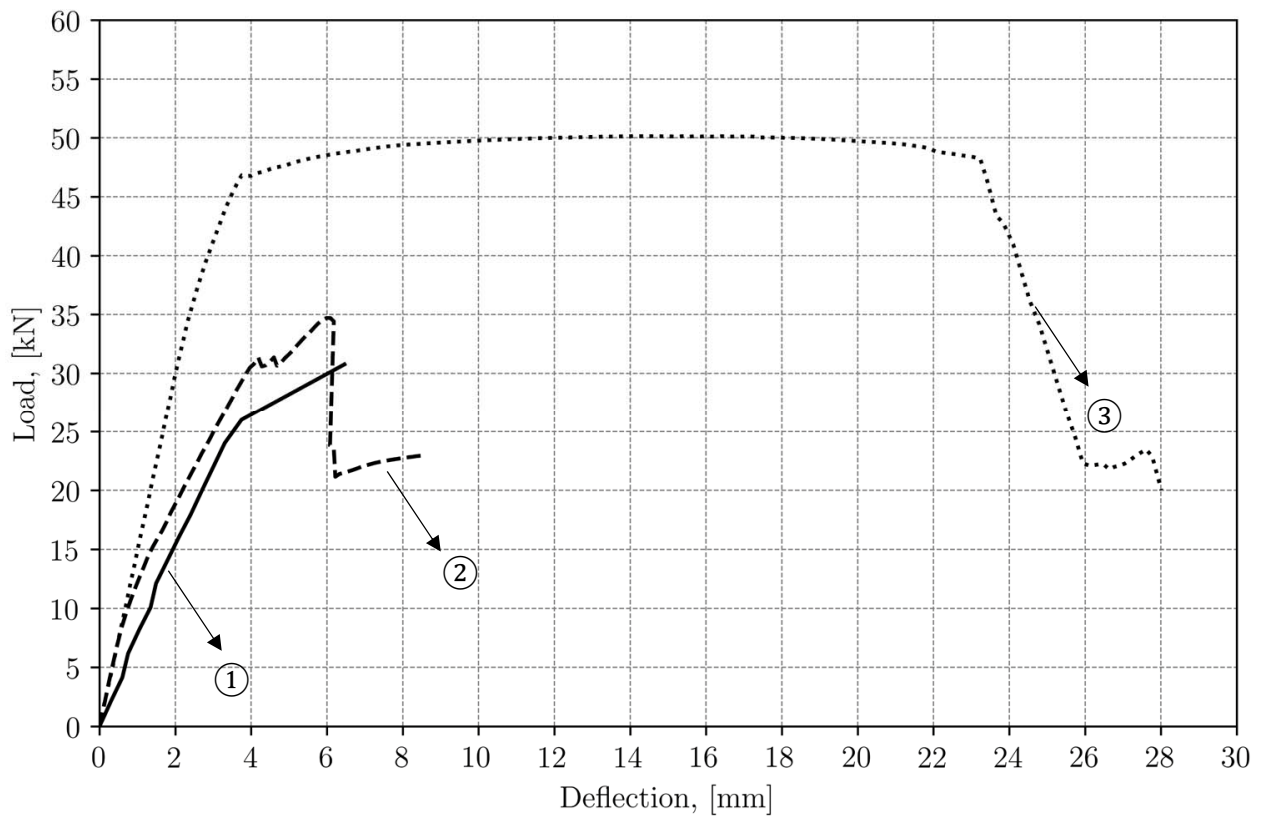
① Experimental results of ASR affected beam.

② The traditional method: ASR damage is taken into account by directly reducing the input material properties.

③ The traditional method + prestress: ASR damage is taken into account by directly reducing the input material properties. Pretension is applied on rebar to simulate the chemical prestress.
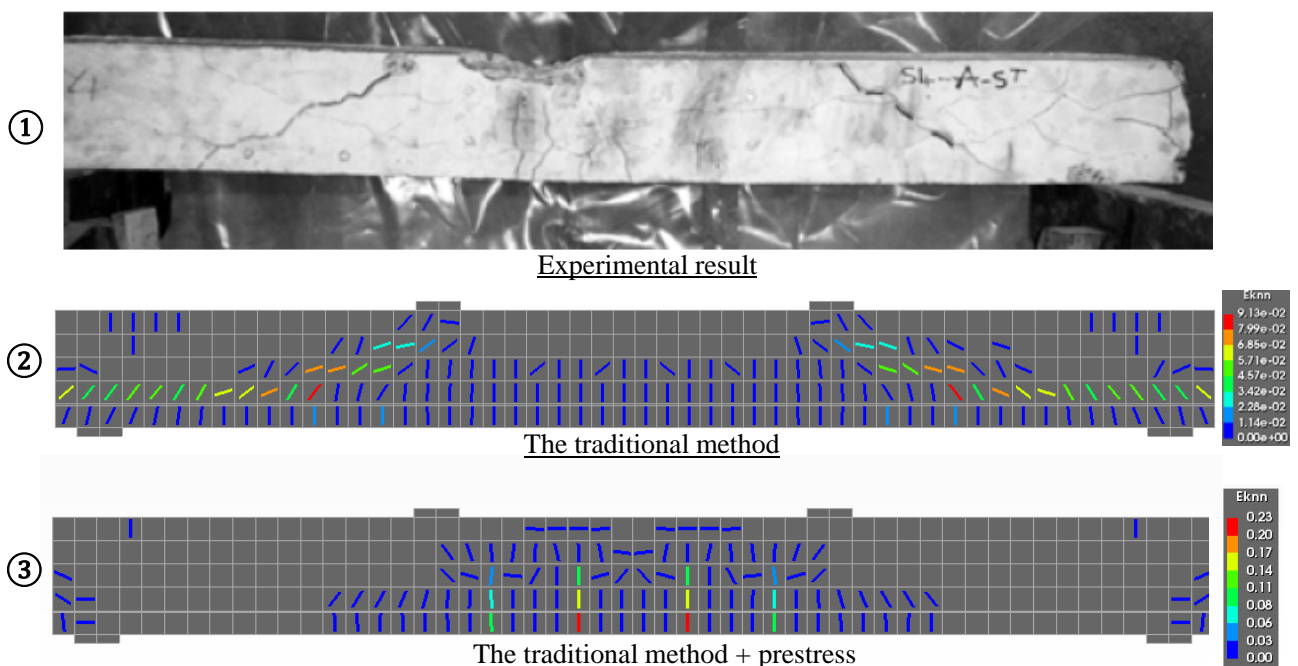
①

Experimental result

②

The traditional method

③

The traditional method + prestress

Figure B.3: The load-deflection response and crack pattern at failure load

After the traditional method, the pretress is applied within the frame of the precracking method. Now, all the ASR effects: the degradation on mechanical properties, ASR induced cracks, ASR induced chemical prestress, are included in this FE-model. Phase analysis is applied. In Phase I, expansion is simulated to embed ASR cracks and material degradation. Then, the expansion is unloaded. Prestress is applied in Phase II. After the prestressing, the mechanical load is acted on the beam in Phase III. The layout of the phase analysis is shown in Figure B.4. Table B.2 demonstrates the material properties used in the model.
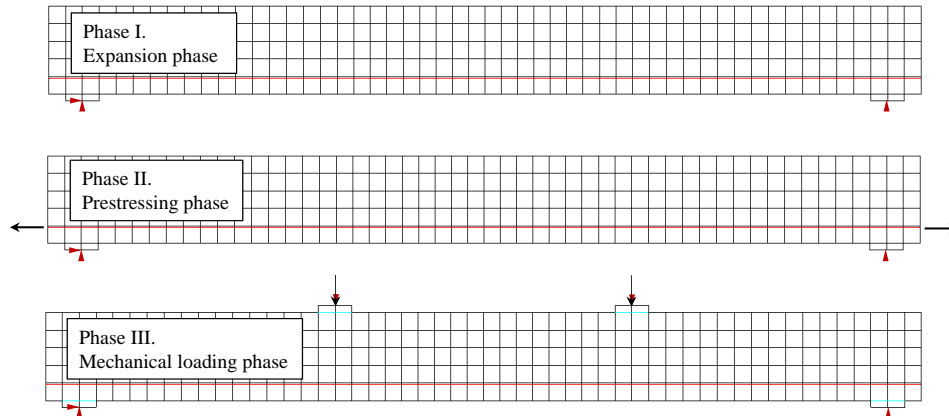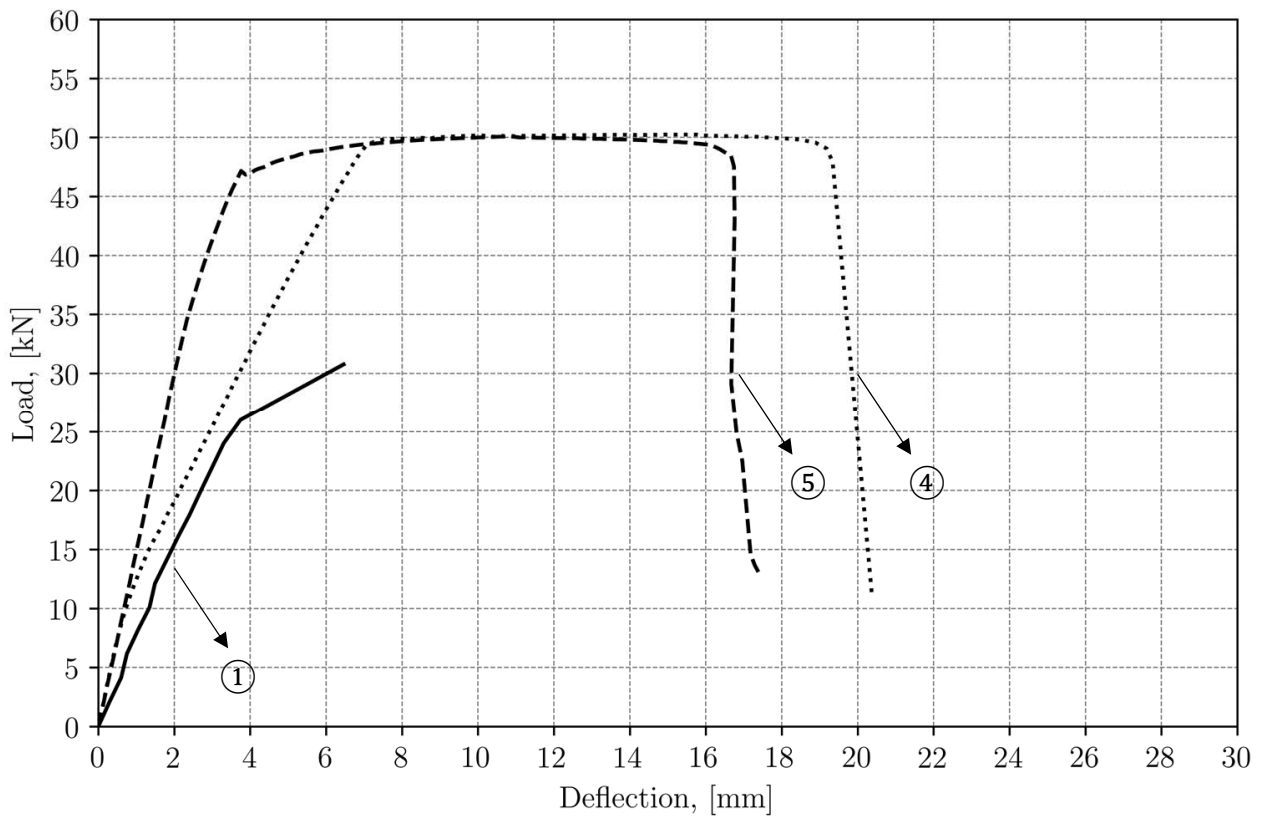

Figure B.4: Phase analysis: applying prestress within the frame of the precracking method

Table B.2: Material properties: applying prestress within the frame of the pracracking method

Material properties	Compression strength cylinder (N/mm^2)	Compressive fracture energy (N/mm)	Indirect tensile strength (N/mm^2)	Tensile fracture energy (N/mm)	Modulus of elasticity (kN/mm^2)
Level I (Virgin)	50	37	4.11	0.148	34
Level II (Residual)	44 (11%↓)	34(8%↓)	3.9 (5%↓)	0.14(5%↓)	27 (20%↓)

	Structural mesh (Concrete)		Steel	
Input material properties	Level I		Modulus of elasticity: 200GPa Yielying stress: 460MPa	
Properties after precracking	Tensile behaviour(anisotropic): In vertical direction: Level II In horizontal direction: level I. Compressive behaviour(isotropic): Level II Young's modulus(isotropic): Level II		—	
Material model	Total strain based crack model		Fully embedded reinforcement, Von Mises plasticity	
Crack direction	Fixed		—	
Tensile behaviour	Exponential		—	
Compressive behaviour	Parabolic		—	
Shear behaviour	Al-Mahaidi, β=0		—	
Element size	25mm		—	
Pretension stress	—		260 MPa	

|	Shadow mesh	
Material model	isotropic elastic material	
Young's modulus (MPa)	3400000	
Poisson ratio	0.2	

① Experimental results of ASR affected beam.

④ <u>The precracking method:</u> ASR damage is embedded through simulating ASR expansion.
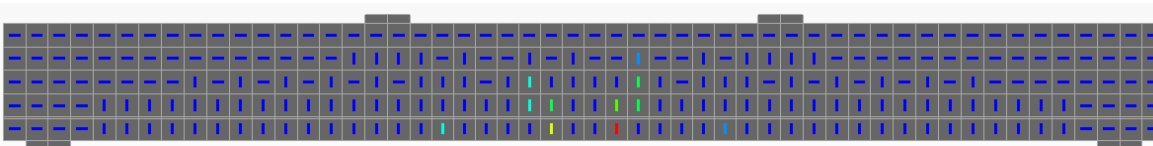
⑤ <u>The precracking method + prestress:</u> ASR damage is embedded through simulating ASR expansion. Pretension is applied on rebar to simulate the chemical prestress.
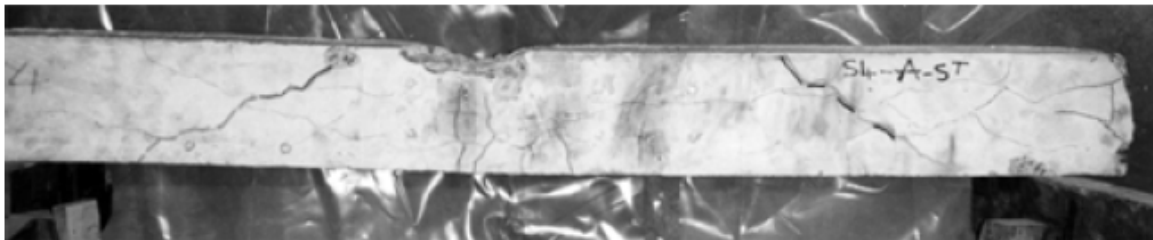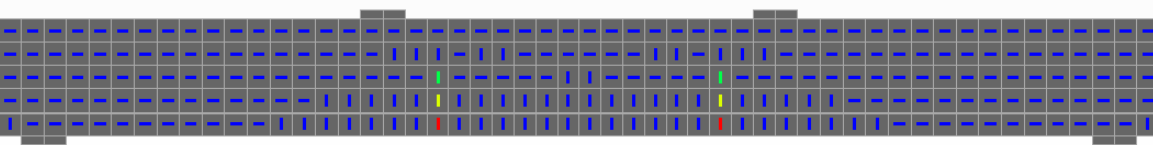

Experimental result

The precracking method

The precracking method + prestress

Figure B.5: The load-deflection response and crack pattern at failure load

The load-deflection response of this analysis is marked as curve ⑤ shown in Figure B.5. The precracking method performed in chapter 6 without prestress is marked as curve ④. An overestimation in stiffness is observed with the presence of prestress as is seen in curve ⑤. The peak load values are the same in case with and without prestress. In both cases, the beams are failed in bending, so it seems that the presence of prestress will not increase the bending capacity in the precracking method. It is observed that the prestressed beam failed earlier than the unprestressed one. This is because both beams are failed due to the crush of concrete, the prestressed one is already loaded in compression during the pretension process, thus, it will reach the crush strength earlier comparing with the unprestressed beam.

Conclusions

In this additional analysis, the chemical prestress is simulated by applying the physical prestress in the reinforcement. The reason behind this equivalent is that the chemical prestress has the same consequence comparing with the physical prestress: reinforcement loaded in tension and the surrounding concrete loaded in compression. Despite the fact that the behaviour is not able to be simulated quantitatively well. Whereas, qualitatively, some meaningful observations are obtained. For instance, an increase of stiffness is observed in some experiments such as Abe et al. (1989), Ohno et al. (1989) and Inoue et al. (1989). Most of the researchers contributes stated that the increase of stiffness is due to the chemical prestress, and this is verified numerically in this additional analysis. In paper Fan and Hanson (1998), the author found that the presence of chemical prestress results in an earlier concrete cruch for beam failed in bending, and this is observed in this analysis as well. According to the obtained numerical results, it is found that the chemical prestress can also change the failure mode. From the numerical point of view, both ASR cracks and chemical prestress are able to change the failure mode. From the experimental point of view, it is still not clear that the change of failure mode is because of the ASR cracks or the induced chemical prestress or a combination of both.

Bibliography

Abe, M., Kikuta, S., Masuda, Y., and Tomozawa, F. Experimental study on mechanical behavior of reinforced concrete members affetced by alkali-aggregate reaction. *In Proceedings of the 8th International Conference on Alkali-Aggregate Reaction in Concrete*, pages 691–696, 1989.

Ahmed, T., Burley, E., and Rigden, S. The static and fatigue strength of reinforced concrete beams affected by alkali-silica reaction. *ACI Materials Journal*, 95:356–368, 1998.

Capra, B. and Sellier, A. Orthotropic modelling of alkali aggregate reaction in concrete structures: numerical simulations. *Mechanics of Materials*, 35:817–830, 2002.

Chana, P.S. and Korobokis, G.A. *Structural performance of reinforced concrete affected by alkali silica reaction: phase 2*. Transport and Road Research Laboratory, Crowthorne, 1991.

Clayton, N., Currie, R.J., and Moss, R.M. The effects of alkali silica reaction on the strength of prestressed concrete beams. *The Structural Engineer*, 68:287–292, 1990.

Cope, R.J. *The prediction of stress distributions in reinforced concrete affected by alkali aggregate reaction.* Transport Research Laboratory, Crowthorne, 1993.

Den Uijl, J.A. and Kaptijn, N. Structural consequences of asr: An example on shear capacity. *Heron*, 47:125–139, 2002.

Esposito, R., Anac, C., Hendriks, M.A.N., and O., Copuroglu. Influence of the alkali-silica reaction on the mechanical degradation of concrete. *Journal of Materials in Civil Engineering*, 28, 2016.

Fairbairn, M.R.E., Ribeiro, L.B.F., Lopes, E.L., Toledo Filho, R.D., and Silvoso, M.M. Modelling the structural behaviour of a dam affected by alkalicsilica reaction. *Communications in Numerical Methods in Engineering*, 22:1–12, 2005.

Fan, S.F. and Hanson, J.M. Effect of alkali silica reaction expansion and cracking on structural behavior of reinforced concrete beams. *Structural Journal*, 95:498–505, 1998.

Farage, M.C.R., Alves, J.L.D., and Fairbairn, E.M.R. Macroscopic model of concrete subjected to alkalicaggregate reaction. *Cement and Concrete Research*, 34:495–505, 2004.

Ferche, A.C., D.K., Panesar, Sheikh, S.A., and Vecchio, F.J. Toward macro-modeling of alkali-silica reaction-affected structures. *ACI Structural Journal*, 114:1121–1129, 2017.

Hanshin. *Report of investigation of alkali-aggregate reaction.* Committee on AAR of the Hanshin Expressway Company, Osaka, Japan, 1986.

Hendriks, M.A.N., Boer, D.A., and Belletti, B. *Guidelines for Nonlinear Finite Element Analysis of Concrete Structures*. Rijkswaterstaat Centre for Infrastructure, Report RTD:1016-1:2017, 2017.

Hobbs, D.W. *Alkali silica reaction in concrete.* Thomas Telford Ltd, 1988. ISBN 0727713175.

Inoue, S., Fujii, M., Kobayashi, K., and Nakano, K. Structural behaviour of reinforced concrete beams affected by alkali-silika reaction. *In Proceedings of the 8th International Conference on Alkali-Aggregate Reaction in Concrete*, pages 727–732, 1989.

ISE. *Structural effects of alkali-silica reaction - Technical guidance on the appraisal of existing structures.* The Institution of Structural Engineers, London, UK, 1992.

Kobayashi, K., Fukushima, T., and Rokugo, K. Shear strength of asr-deteriorated rc members and shear reinforcing effect of repair by adding rebar. *VIII International Conference on Fracture Mechanics of Concrete and Concrete Structures*, 2013.

Koyanagi, W., Rokugo, K., and Uchida, Y. Mechanical properties of concrete deteriorated by alkali aggregate reaction under various of reinforcement ratios. *In Proceedings of the 9th International Conference on Alkali-Aggregate Reaction in Concrete*, pages 556–563, 1992.

Larive, C., Joly, M., and Coussy, O. Heterogeneity and anisotropy in asr affcted concrete consequences for structural assessment. *In Proceedings of the 11th International Conference on Alkali-Aggregate Reaction in Concrete*, pages 969–978, 2000.

Li, K and Coussy, O. Concrete asr degradation: from material modeling to structure assessment. *Concrete Science and Engineering*, 4:35–46, 2002.

Mohammed, T.K., Hamada, H., and Yamaji, T. Alkali-silica reaction-induced strains over concrete surface and steel bars in concrete. *ACI Materials Journal*, 100:134–142, 2003.

Ng, K.E. *Effect of alkali silica reaction on the punching shear capacity of reinforced concrete slab.* PhD thesis, University of Birmingham, 1991.

Ohno, S., Yoshioka, Y., Shinozaki, Y., and Morikawa, T. The mechanical behaviour of beams coated after alkali-silica reaction damage. *In Proceedings of the 8th International Conference on Alkali-Aggregate Reaction in Concrete*, pages 697–702, 1989.

Smaoui, N., Brub, M., Fournier, B., and Bissonnette, B. Influence of specimen geometry, orientation of casting plane, and mode of concrete consolidation on expansion due to asr. *Cement, Concrete and Aggregatese*, 26:1–13, 2004.

Smaoui, N., Bissonnette, B, Brub, M.A., and Fournier, B. Stresses induced by alkalicsilica reactivity in prototypes of reinforced concrete columns incorporating various types of reactive aggregates. *Canadian Journal of Civil Engineering*, 34(12):1554–1566, 2007. doi: 10.1139/L07-063. URL https://doi.org/10.1139/L07-063.

Takemura, K., Tazawa, E., Yonekura, A., and Abe, Y. Mechanical characteristics of reinforced concrete column affected by alkali aggregate reaction. *In Proceedings of the 8th International Conference on Alkali-Aggregate Reaction in Concrete*, pages 665–670, 1989.

Ulm, F.J., Coussy, O., K.F., Li, and C., Larive. Thermo-chemo-mechanics of asr expansion in concrete structures. *Journal of Engineering Mechanics*, 126:233–242, 2000.

Vecchio, F. J. and Collins, M. P. Compression response of cracked reinforced concrete. *Journal of Structural Engineering*, 119:3590–3610, 1993.

Vecchio, F. J. and Shim, W. Experimental and analytical reexamination of classic concrete beam tests. *Journal of Structural Engineering*, 130:460–469, 2004.

Wald, D.M., Allford, M.T., Bayrak, O., and Hrynyk, T.D. Development and multiaxial distribution of expansions in reinforced concrete elements affected by alkalicsilica reaction. *Struct Concrete*, 18: 914–928, 2017.

Yang, Y.G. *Shear behaviour of reinforced concrete members without shear reinforcement*. PhD thesis, Delft University of Technology, 2014.